RW B | RESEARCH

ELECTRONICS | PHYSICS

DEVELOPMENT OF NON-DESTRUCTIVE METHODS FOR DETERMINING RESIDUAL STRESS AND FATIGUE DAMAGE IN METALS

FINAL REPORT

PREPARED UNDER CONTRACT NO. NAS8-20208 BY

ROBERT W. BENSON AND ASSOCIATES, INC.

633 Thompson Lane

NASHVILLE, TENNESSEE 37204

March 8, 1963

ROBERT W. BENSON & ASSOCIATES, INC.
633 THOMPSON LANE • NASHVILLE, TENNESSEE 37204

DEVELOPMENT OF NON-DESTRUCTIVE METHODS FOR DETERMINING RESIDUAL STRESS AND FATIGUE DAMAGE IN METALS

FINAL REPORT

PREPARED UNDER CONTRACT NO. NAS8-20208 BY

ROBERT W. BENSON AND ASSOCIATES, INC.

633 Thompson Lane

NASHVILLE, TENNESSEE 37204

March 8, 1968

PREFACE

The Development of Nondestructive Methods for Determining Residual Stress and Fatigue Damage in Metals, Contract No. NAS8-20208, was conducted under the supervision of Mr. Wayman Clotfelter of Propulsion and Vehicle Engineering Laboratory, George C. Marshall Space Flight Center, Huntsville, Alabama. The project consisted of the development of techniques for the measurement of stress, the development of an instrument for measuring stress and the study of methods for measuring fatigue damage. A practical application of ultrasonic stress analysis was the study of aluminum plates containing weldments. The project was under the general supervision of Dr. Robert W. Benson with Dr. J. Ronald Chapman being responsible for the development of instrumentation, Mr. Harold F. Huffman being responsible for ultrasonic surface wave measurements and Mr. Samuel H. Pearsall being responsible for microwave measurements of fatigue damage. Technical assistance was provided by Messrs. Jimmie L. Holladay, Harold Hagar, Robert Fay and Samuel H. Pearsall, III.

ABSTRACT

Methods of measuring stress within various alloy of aluminum using both shear and surface waves have been developed. Transducers were designed which allow for the determination of the relative ultrasonic velocities along the principal axes of stress. Relationships have been established for a number of aluminum alloys between the ultrasonic velocity and stress. From the relationships, it is possible to determine the magnitude of stress that exists within a particular portion of a metallic structure. A special instrument has been designed and constructed which allows for the measurement of ultrasonic frequency differences which are also related to stress.

The techniques, which have been developed, have been applied to the measurement of stress in aluminum plates containing weldments. It has been found necessary to provide methods of determining the orientation of the principal axes of stress and to determine the effect of material properties such as grain orientation. The accuracy of measurements obtained ultrasonically compare favorably with destructive tests of specimens.

An investigation was undertaken to establish relationships between electrical surface resistance and fatigue damage. Microwave frequencies and techniques were used in order to take advantage of small, high "Q" resonators, and to confine the resistance measurements to a few millionths of an inch of the surface. Aluminum plates subjected to flexural fatigue damage were investigated at wave lengths of 3 centimeters. An increase in surface resistance was found to preceed any visual evidence of fatigue damage and impending fatigue.

TABLE OF CONTENTS

LIST OF FIGURES

Cont.

FIGURE Page

FIGURE PAGE

LIST OF TABLES

Cont.

CONTRACT NO. NAS8-20208

CONTROL NO. 1-6-54-01018(IF)

FINAL REPORT

I. INTRODUCTION

The measurement of stress has been the object of many studies over a long period of time. Early experiments were concerned with the determination of the elastic properties of metals and the distribution of loads within various configurations. Designs utilized safety factors which assured adequate performance under all conditions of use. Modern technology, especially for airborne or space application, requires designs which give adequate strength with minimum weight. Concurrent with the development of materials which have superior strength to weight ratios, was the development of techniques of stress analysis which allowed the maximum utilization of materials.

Stress analysis has developed through a number of useful stages including full scale destructive testing, the use of optically transparent models, and more recently the extensive use of sensitive strain gages. Destructive testing is always a necessary part of a non-destructive testing program to assure that the measurements obtained predict the actual state of the material. The final structure, however, must be tested in some non-destructive manner to assure adequate performance of a specific structure. The use of optical models, observed by photoelastic methods has been invaluable as a method to determine stress concentrations which analytically are difficult to predict.

The strain gage has been developed as a most useful tool for the examination of stresses in actual metallic structures.

Limitations of the strain gage include the lack of methods for the measurement of residual stress, limited spatial resolution and problems associated with the bonding of the gages to the structure. The strain gage does allow for dynamic, as well as static, measurement of stress and has numerous applications for stress analysis.

Ultrasonic methods of stress analysis were first demonstrated in 1957, when it was shown that ultrasonic shear waves may be used in a manner similar to the photoelastic method using polarized light beams with optically transparent models. Exploratory work demonstrated that the change of shear wave velocity was proportional to the applied stress even beyond the elastic limit of certain materials. Later studies demonstrated that the velocity of ultrasonic surface waves was also affected by stress, indicating that the stress near the surface may be measured independently. Further work showed the possible application of ultrasonic methods to dynamic stress analysis.

While all of the above cited programs were conducted on a laboratory basis, sufficient evidence had been obtained to warrant the development of methods for use of the ultrasonic stress analysis in the field. This report describes the development of techniques which are suitable for the measurement of both bulk and surfaces stresses in metallic structures. It further describes a particular instrument that has been developed with specific transducers for the application of these techniques. The use of the techniques to study the stress distribution in aluminum plates containing weldments is given as a practical application. These measurements have been supplemented by destructive tests which confirm the validity of the measurements.

II. ULTRASONIC STRESS MEASURING TECHNIQUES

A basic factor in measuring stress by ultrasonic techniques is the system utilized to perform the actual measurement. The study conducted in this project used two types of

systems. These are the modified time of flight system and the frequency null system. Each of these systems are designed to measure changes in ultrasonic velocity.

A. Modified Time of Flight System

A block diagram of the modified time of flight system is shown in Figure 1. The RF pulse generator used in the system shown has an output voltage of 400 volts peak-to-peak fed from a link couple. With appropriate plug-in coils the output frequency covers a range from 1 to 50 MHz. The duration of the RF pulse is variable from 1 to 10 microseconds at a repetition rate of 1 KHz. Generally speaking, the pulse width is 4 microseconds which gives sufficient time for the vibrational build-up of the crystal transducer to occur. Although the particular RF pulse generator was constructed in the laboratory, similar equipment can be obtained commercially.

The RF amplification of the received signals is achieved by commercially produced RF amplifiers especially designed for pulsed systems. In some cases, specifically with shear crystals bonded with wax, no amplification is needed since the voltage generated at the receiving crystal is of the order of tenths of a volt. However, amplification is necessary for measurements conducted on surface waves generated by lucite wedges at frequencies above 5 MHz where the received signal at the crystal is only at the millivolt level. Lower frequency surface wave signals are strong enough so that no amplification other than the oscilloscope is needed. The RF amplification system when used consists of a tunable preamplifier designed to operate from 5 to 60 MHz with a typical gain of 20 to 40 db over the above frequency range. The preamplifier is followed by a wideband amplifier with an adjustable gain of 0 to 65 db from 5 to 60 MHz.

The variable trigger delay is basically a single shot multivibrator triggered at the initiation of a pulse by the RF pulse generator. Triggering of the oscilloscope occurs when the single shot returns to its normal state. The delay

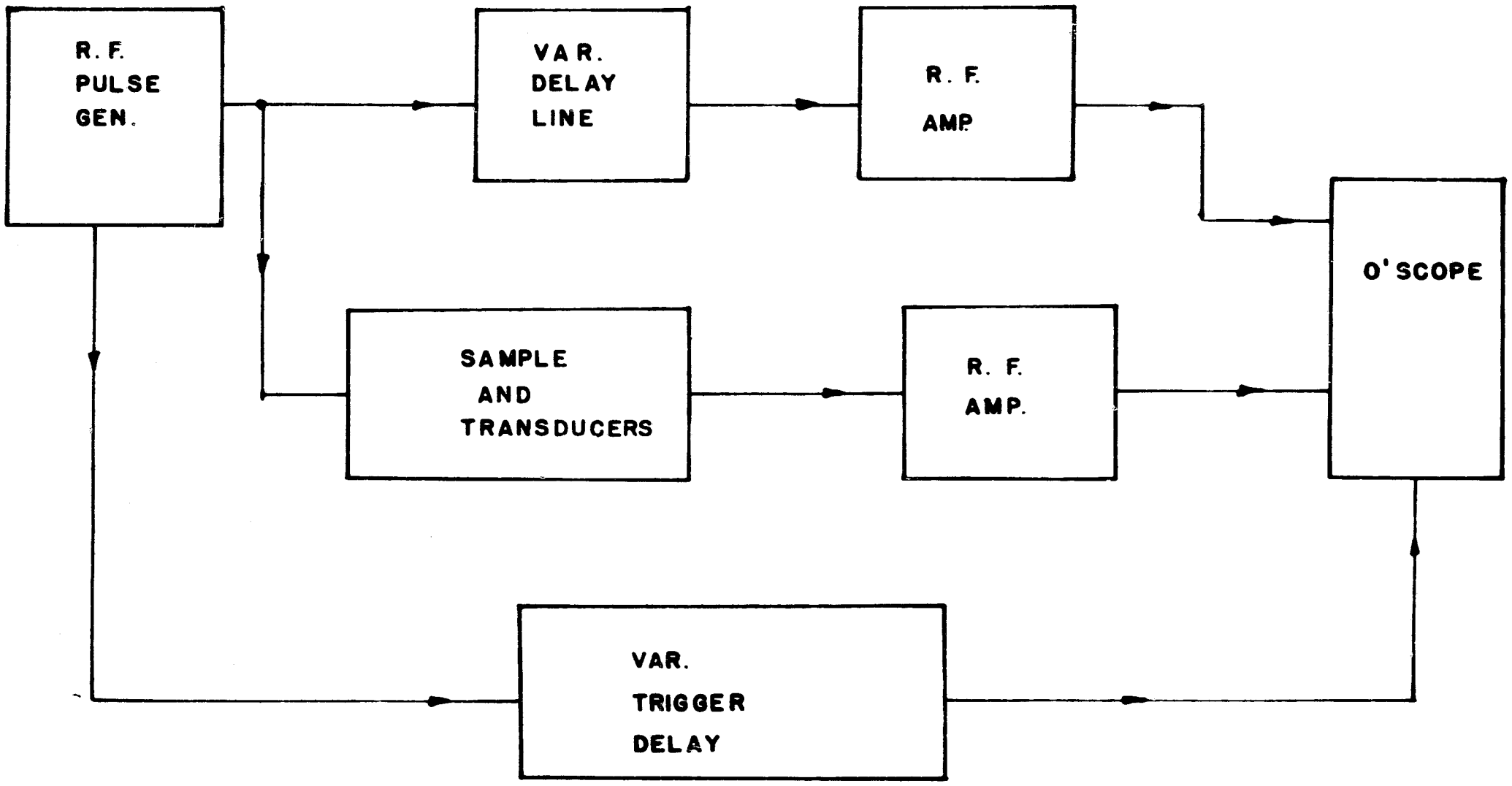

Figure 1. Block Diagram Showing the Modified Time of Flight System Used in Measuring the Change in Velocity of Ultrasonic Surface Waves.

time of the trigger is continuously variable from 1 to 100 microseconds with a positive output voltage spike of 3 volts.

The output of the RF pulse generator is applied to the sending transducer attached to the sample as well as to the transducer on a variable delay line. Some applications require that a single crystal transducer be used as both the sender and the receiver. When this is the case, the RF pulse generator is connected to the sample transducer through a diode switch as shown in Figure 2. A circuit diagram of the diode switch is shown in Figure 3.

The operation of the switch can be understood if it is recalled that the output of the RF pulse generator comes from a low impedance link couple. During the time the generator is supplying the RF driving pulse, diodes D_1 and D_2 are alternately conducting as the RF swings positively and negatively. Also note that diodes D_3, D_4 and D_6 are conducting during this time. This fact enables the high voltage driving pulse to be attenuated before reaching the preamplifier so that the amplifier will not overload. When the RF driving voltage ceases, the crystal is then ready to receive. Since the voltage generated by the crystal upon the reception of an ultrasonic pulse is low (usually below 0.5 volts, none of the diode pairs are driven into forward conduction. Under these conditions, the link couple of the generator is essentially disconnected from the crystal and the received signal is directed to the preamplifier through the two 100 ohm resistors.

For measurements utilizing the modified time of flight technique, a delay line is required. The delay line used employs a pair of surface wave transducers whose path length can be changed with a traversing mechanism. By changing the path length, the time necessary for the surface wave pulse to reach the receiver can be changed. Therefore, the received pulse from the delay line can be adjusted to occur at any reasonable time after the RF pulse is applied to the sender. In some cases the measurements taken with the shear waves did not utilize the delay line as will be explained later. In any case, the delay line or reference signal provides a

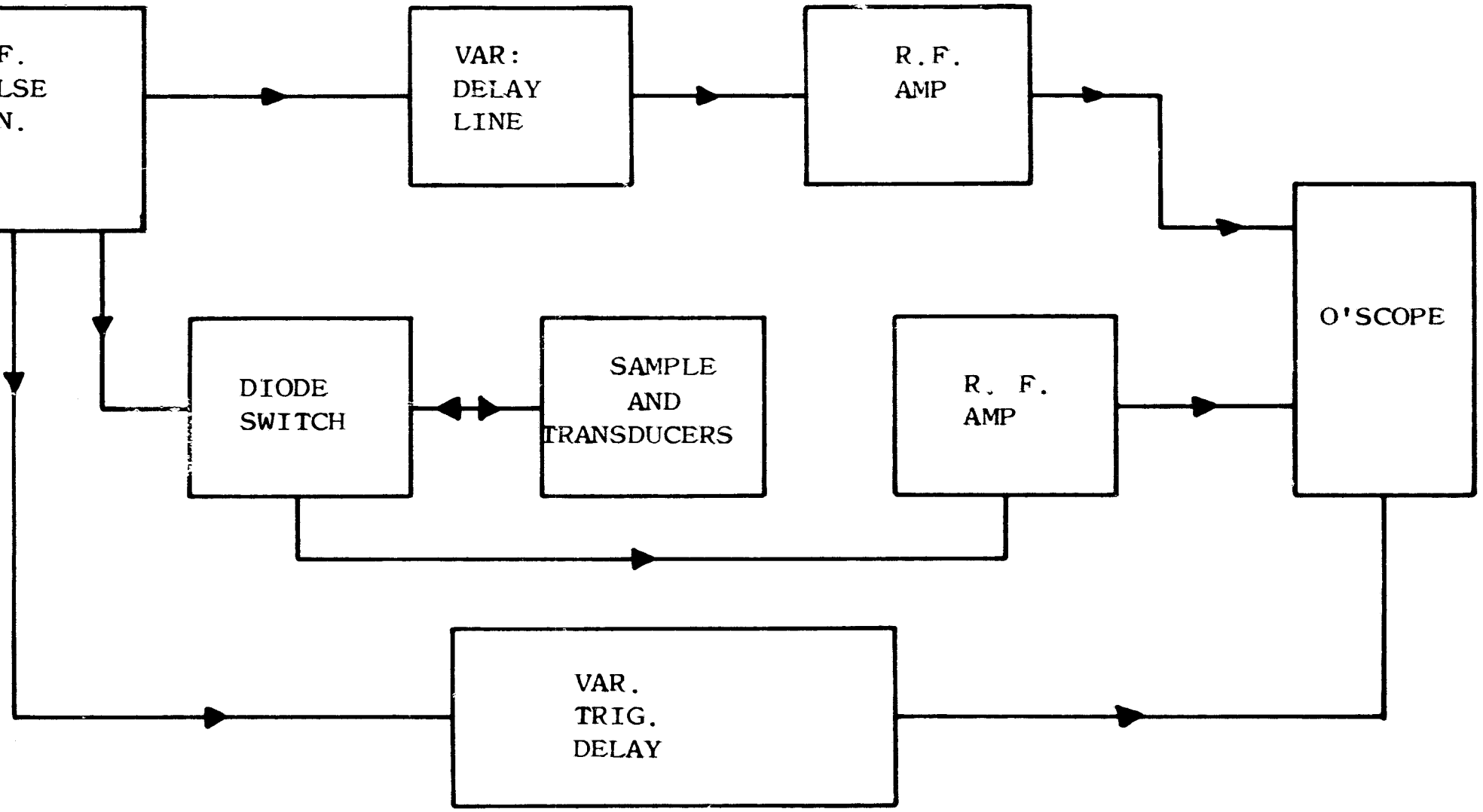

Figure 2. Block Diagram Showing the Connection of the R.F. Pulse Generator to the Sample Transducer through a Diode Switch.

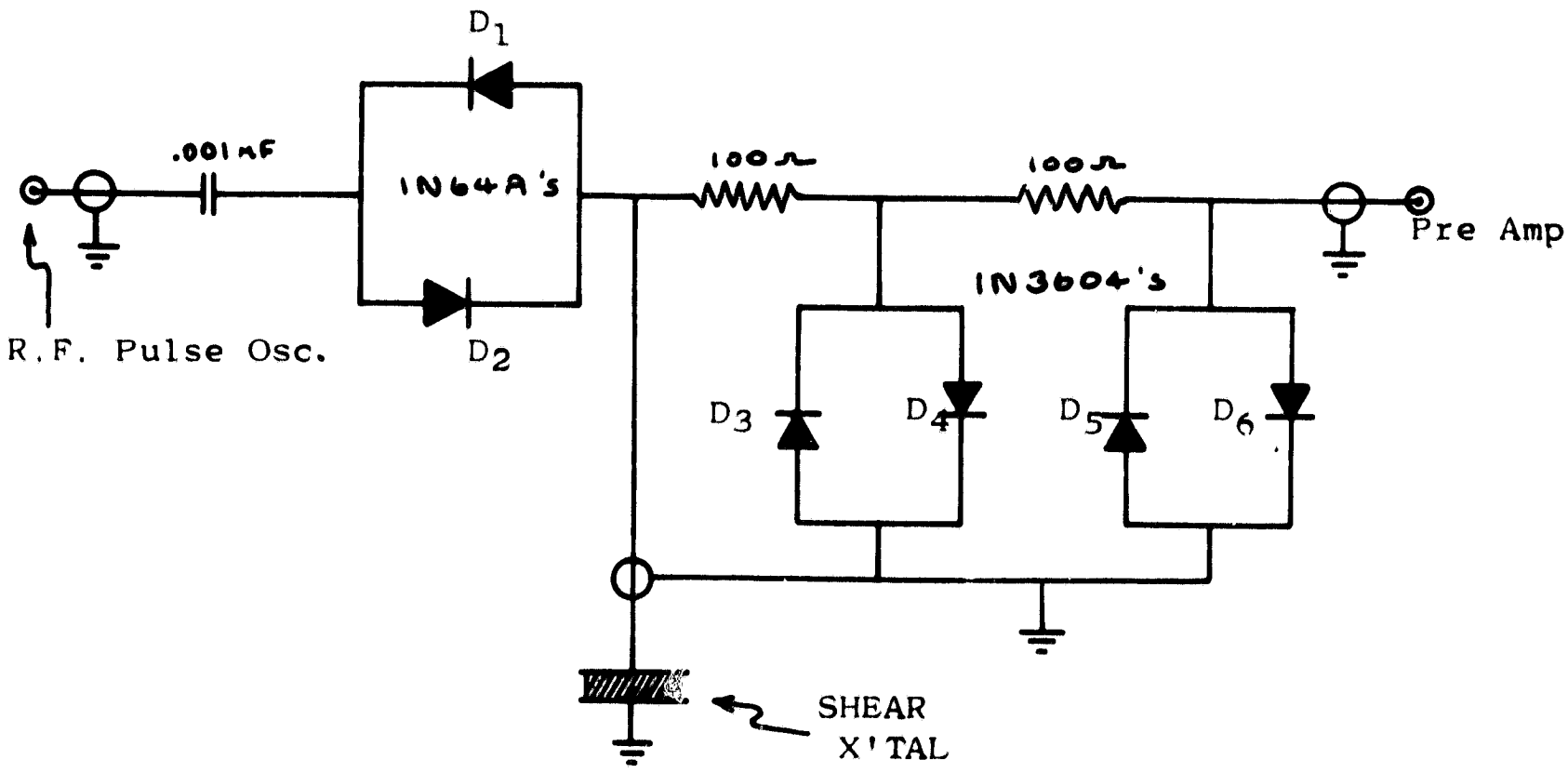

Figure 3. Diode Switch circuit for shear x'tal operation.

RF pulse that can be placed in time so that it coincides with the received pulse from the sample. The delayed trigger, shown in the diagram, is then used to start the oscilloscope trace at the time of arrival of the first received pulse.

The particular oscilloscope shown in Figures 1 and 2 has a dual channel plug-in amplifier with a bandwidth from 0 to 25 MHz and a sensitivity of 0.005 volts per centimeter. It is possible to display each of the inputs of the oscilloscope amplifier alternately so that signals from the delay line and sample could be viewed simultaneously on the two traces. Furthermore, the oscilloscope is equipped with an internal delay trigger. By this means it is possible to delay the time of initiation of one of the traces.

The actual procedure involved in making the modified time of flight measurements is not very complicated. For example, suppose a sample is to be investigated and it takes 20 microseconds for the signal to traverse the specimen. The variable delay trigger is turned to its minimum delay time of 1 microsecond. With the time base of the oscilloscope set at 5 microseconds per centimeter, the trace displaying the received signal from the sample would show the received RF pulse at approximately the middle of the oscilloscope screen. The received delay line signal, which is viewed on the other oscilloscope trace, is made to coincide in time with the signal from the transducers of the delay line by an adjustment of the spacing of the delay line transducers. Once the delay line has been adjusted properly, the variable delay trigger is then adjusted so that the oscilloscope traces are initiated at approximately 20 microseconds after the RF voltage was initially applied to each of the senders. After this adjustment the received signals appear at the beginning of the oscilloscope trace.

The time base is then changed to 0.1 microsecond per centimeter. With this setting and the RF frequency of the pulses in the region of 3 to 10 MHz, the pulses on each trace appear as if they were continuous sine waves. Also it is important to point out that it is possible to visually observe a phase shift between the two signals. Before any

stress is applied to the sample the two signals are brought in phase with each other by adjusting a calibrated 10 turn potentiometer which controls the internal delay trigger of the oscilloscope. The amount of delay time necessary to visually bring the signals in phase can then be read directly from this calibrated potentiometer. It is possible to read change in delay times of 10^{-9} seconds.

As stress is applied to the sample the velocity of the ultrasonic wave changes. This means that the time it takes the wave to traverse the sample is changed. When this change occurs a phase shift between the sample signal and the delay line signal is visually noted on the oscilloscope. The internal oscilloscope trigger can then be adjusted to bring the signals in phase. The change in time of travel through the sample then corresponds directly to the time necessary to change the internal trigger for phase alignment. In other words, if the delayed triggers show a delay of 150×10^{-9} seconds and the two signals are in phase, application of stress makes the signals slip in phase. To bring the signals in phase again requires, for example, the internal trigger to be further delayed by 20×10^{-9} seconds. Therefore, the applied stress produced a 20×10^{-9} second change in the travel time for the ultrasonic wave.

Normally, the oscilloscope connections are made so that the trace displaying the sample signal is the one affected by the internal trigger...As a result, if the signal from the sample is delayed, i.e., the velocity decreases, the internal delay trigger is adjusted so that the initiation of the trace showing the sample pulse occurs earlier.

B. Frequency Null System

The second type of system used to make measurements of ultrasonic velocity changes is the frequency null system. A block diagram of this system is shown in Figure 4. The RF oscillator operating between 6 and 8 MHz is a variable frequency, continuous wave oscillator. From the diagram it is seen that the oscillator output is connected to the driving

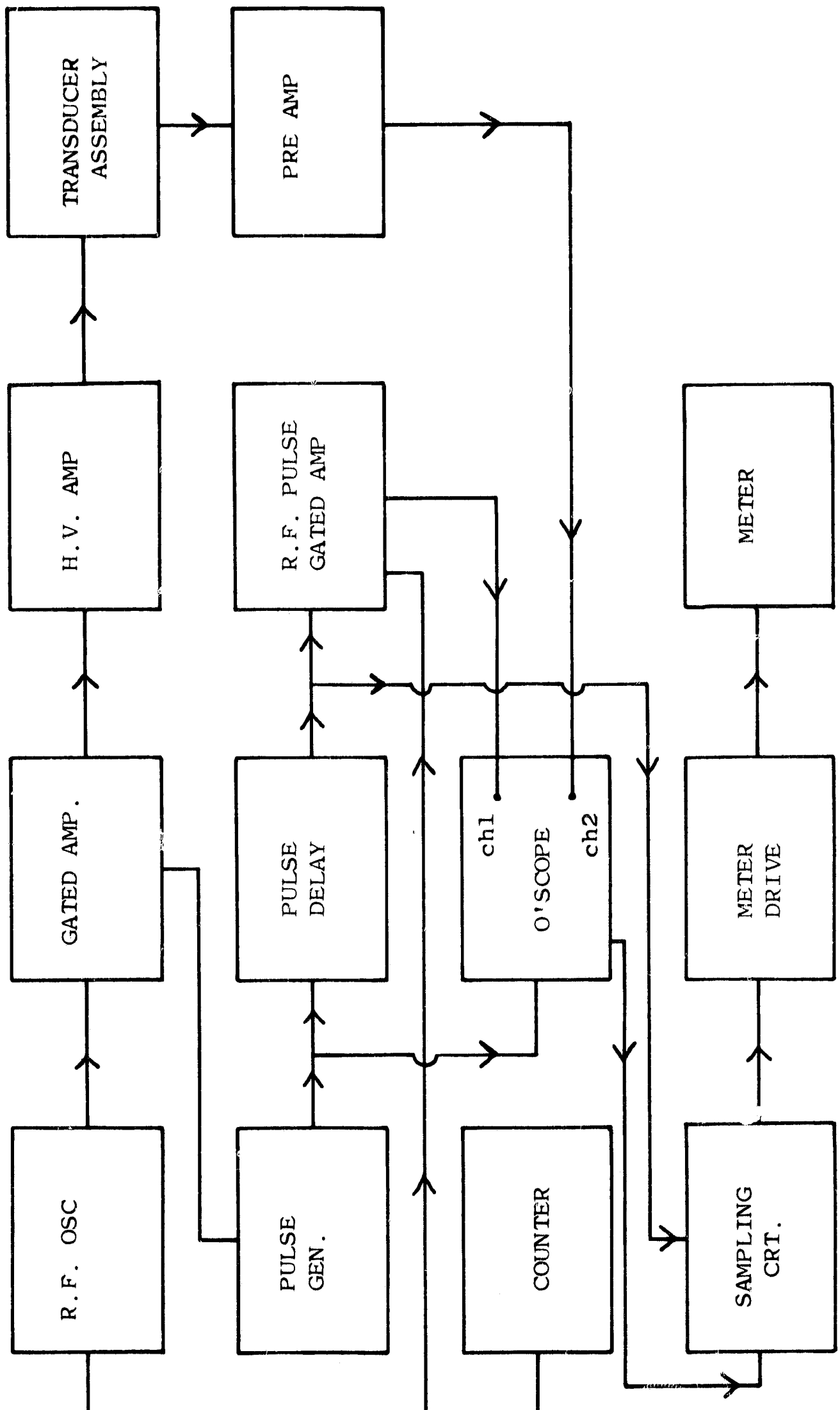

Figure 4. Block Diagram of the Frequency Null System.

pulse gated amplifier, the reference pulse gated amplifier, and the counter. The counter continuously monitors the frequency of the RF oscillator whereas the two gated amplifiers are controlled from an off to an on state in order to pass the RF signal of the oscillator.

The driving pulse gated amplifier is controlled by the pulse generator which has a square wave output. This output pulse has an adjustable repetition rate between 300 and 1200 Hz and a width that can be varied from 2 to 10 microseconds. Therefore, the width and repetition rate of the RF pulse passed by the driving pulse gated amplifier corresponds to the width and repetition rate of the pulse generator. Needless to say, the frequency of the RF driving pulse is that of the oscillator.

The pulse generator output is also connected to the oscilloscope external sync terminal in addition to the pulse delay unit. The purpose of the pulse delay unit is to deliver a second control pulse with a fixed duration of 1.5 microseconds. This pulse occurs at an adjustable time between 5 and 30 microseconds after the initiation of the RF driving pulse and allows the reference pulse gated amplifier to pass an RF pulse to one channel of a dual channel oscilloscope.

The signal received from the transducer assembly and sample is amplified by a preamplifier having a 60 db gain. Once the received RF signal is amplified it is directed to the other channel of the dual channel oscilloscope. It is possible to algebraically add the two signals of channels 1 and 2. It should be pointed out that the oscilloscope starts its trace at the time of initiation of the RF driving pulse since it is synchronized by the pulse generator. Therefore, by properly adjusting the time of the reference pulse, the received signal and reference pulse can be added. Time relationships of the driving, reference and received pulses are shown in Figure 5.

Conditions necessary for the reference pulse to cancel or null a portion of the received pulse are that they be 180^{o} out of phase and have equal amplitudes. The phase condition can be brought about by frequency adjustment of the RF

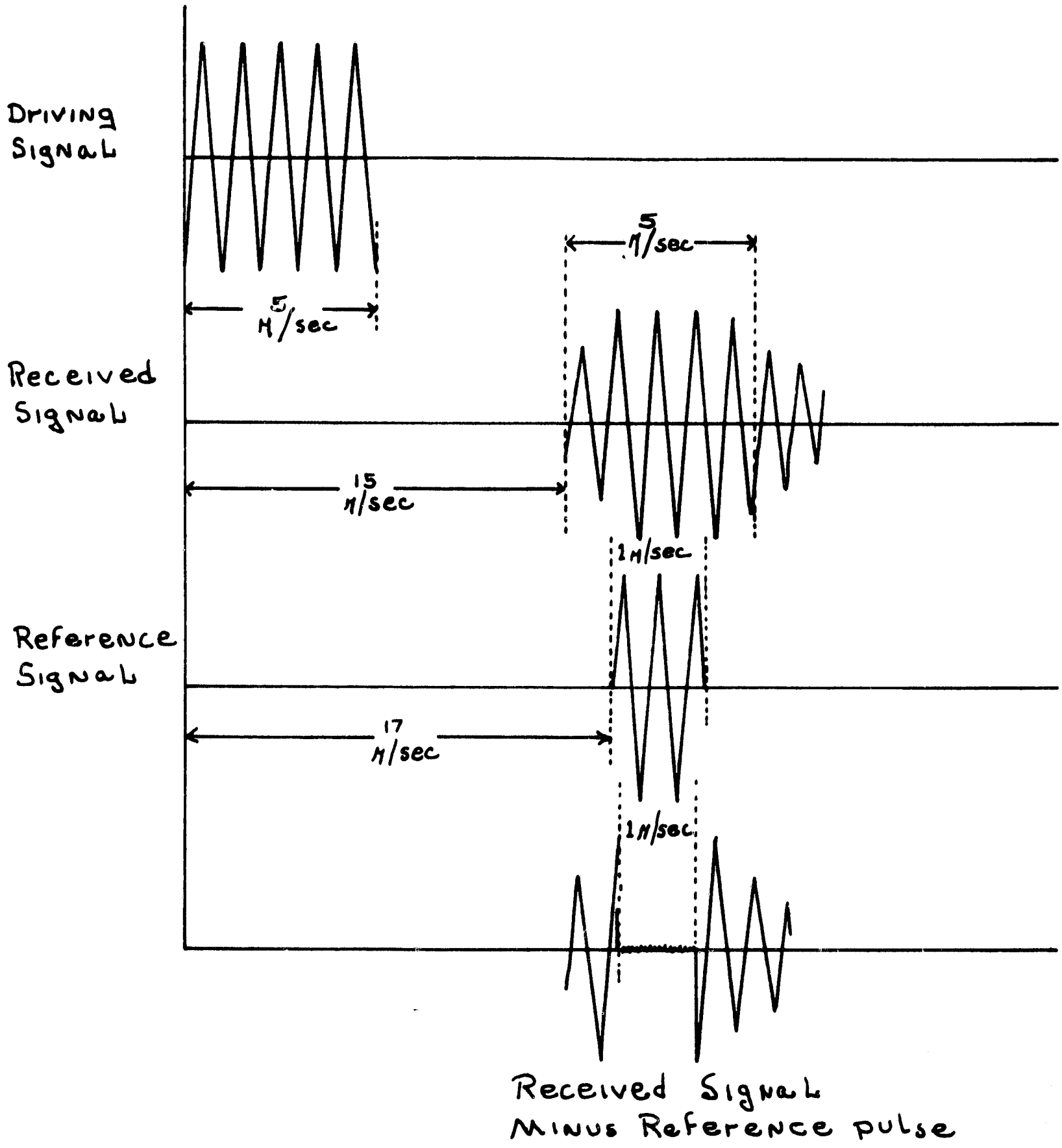

Figure 5. Time Relationships Between the Driving Signal, Received Signal, and the Reference Pulse.

oscillator while the amplitude condition is obtained by varying the gain in one channel of the oscilloscope. In order to aid in determining the frequency at which the null occurs, the output of the vertical amplifier section of the oscilloscope is fed to a sampling circuit. This circuit samples the added received and reference pulses during the time the reference pulse occurs. The block diagram shows that the same control pulse that operates the reference pulse gated amplifier also operates the sampling circuit. The sampling circuit is actually another gated amplifier. In this case, however, the amplitude of the added signal present in the vertical amplifier is converted to a DC voltage. The DC voltage is then amplified to a level necessary to drive an ammeter. The meter then reads a minimum value when the addition of the received and reference pulses is a minimum.

The modified time of flight system directly measures the percentage change in velocity of an ultrasonic wave by comparing the change in travel time to the total travel time. A similar measure is obtained by the use of the frequency null system so long as there is a fixed path length provided by a transducer. In order to utilize the system to measure a change in the ultrasonic velocity, the following relationship exists:

$$N_\lambda = \frac{L}{V} f \qquad (1)$$

where N_λ is the number of wave lengths, L the path length of the surface wave, V is the velocity of the surface wave, and f is the frequency of the driving signal. The equation shows that N_λ is directly proportional to the driving frequency and inversely proportional to the surface wave velocity. Therefore, if any of these parameters change the number of wave lengths will also change accordingly. Consider the plot of Figure 6 where N_λ is plotted versus frequency. The dashed line represents the result when the velocity increases as would be the case when a sample is put into compression. It is seen that for the same number of wave lengths to occur in a path of length L, the frequency has to be increased from f_o to a new value f_1.

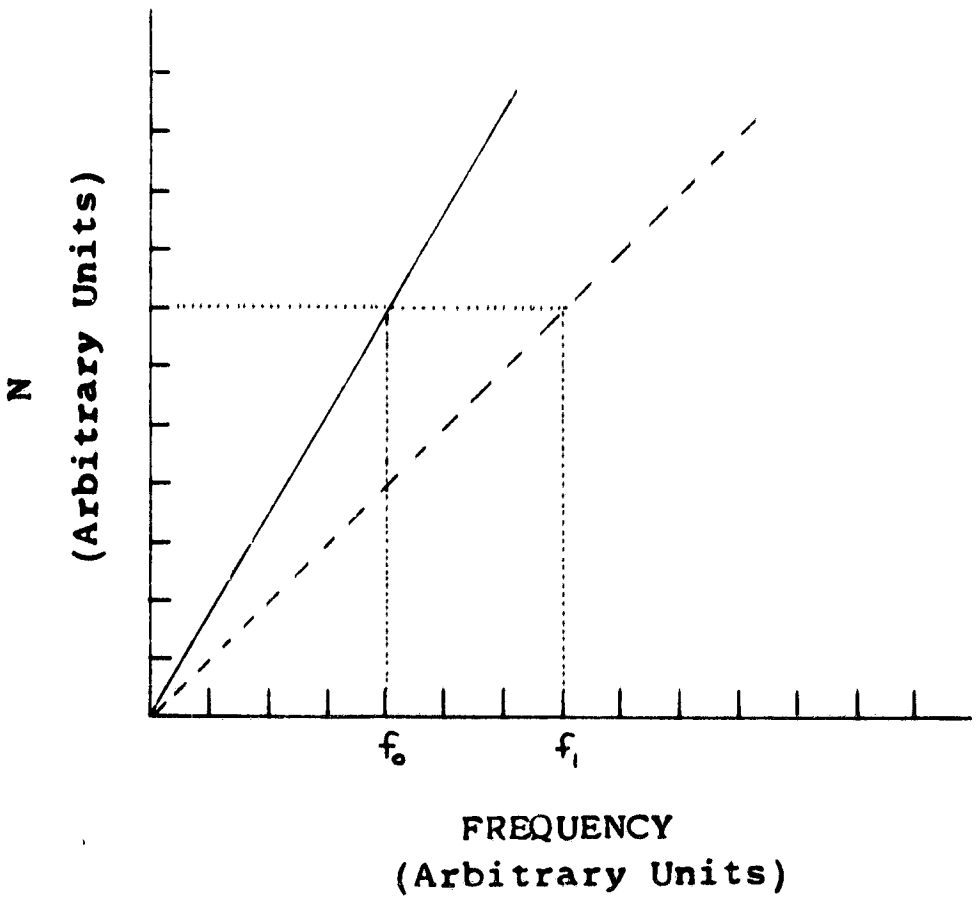

Fig. 6. The Relationship Between Frequency and Wave Lengths for Materials With Different Velocities.

The relationship between the change in frequency Δf, and the change in travel time Δt, can be obtained by a comparison under stressed and unstressed conditions as follows:

$$N_\lambda = \frac{L}{V_o} f_o = \frac{L}{V_o + \Delta V} (f_o + \Delta f)$$

$$\frac{\Delta f}{f_o} = \frac{\Delta V}{V_o} \qquad (2)$$

$$\Delta f = \frac{L \Delta V}{L V_o} f_o = \frac{T \Delta V}{L} \qquad (3)$$

The quantity L/V_o is the travel time for the surface wave in the unstressed condition and is represented by T. The travel time for the stressed conditions is:

$$\frac{L}{V_o + \Delta V} = T - \Delta t \qquad (4)$$

This equation can be rearranged to give

$$\frac{\Delta V}{L} = \frac{\Delta t}{T(T - \Delta t)} \qquad (5)$$

Substituting equation (5) into equation (3) results in

$$\Delta f = \frac{\Delta t f_o}{T - \Delta t} \approx \frac{\Delta t f_o}{T}$$

where the last approximation is valid since Δt is much less than T. As an example, suppose that f_o is 10 MHz, Δt is 10^{-8} seconds and R is 10^{-5} seconds. With these values Δf would be 10 KHz. It is seen from equation (2) that this Δf would correspond to 0.1 per cent change in the surface wave velocity. Therefore, this technique has a high sensitivity to a velocity change while maintaining simplicity from the standpoint of physically making a field type of measurement.

It should also be pointed out that the technique can be used to make absolute velocity measurements. Consider the case where the transducer assembly is placed on a sample and the received and reference signals are phase aligned by adjusting the driving frequency. The driving frequency is then

increased to a new value in order to bring the two signals in phase again. This frequency change corresponds to that necessary to increase the number of wave lengths in the path length by one. From equation (1) the following relationship can be found:

$$\frac{V_0}{L} = \Delta f' \qquad (7)$$

Since the path length L is known, the absolute velocity can be determined.

III. STRESS ANALYSIS USING SHEAR WAVES

A. Determination of Particle Motion of a Y-cut Quartz Crystal

The actual measurement of stress using the above described equipment involves the generation of the proper type of ultrasonic wave. For the measurement of the bulk stress through the thickness of a sample, shear waves are used. The shear wave is generated by the use of a Y-cut quartz crystal coupled to the output of the pulsed RF generator. The measurement of stress is dependent upon the bi-refringence property of the metallic sample being studied. In order to make absolute measurements, it is therefore necessary to know the polarization of the particle motion generated by the crystal in the metallic sample. The Y-cut quartz crystal produces a plane polarized ultrasonic wave where the particle motion is usually along a major axis of the crystal. The illustration of Figure 7 shows the apparatus used to determine which of the axes is the direction of particle motion. Two mediums, water and aluminum, are used. The Y-cut quartz crystal is mounted on the aluminum as shown in the Figure and oriented in such a fashion that the sides of the transducer are parallel to the sides of the aluminum block.

It should be pointed out that by arbitrarily mounting the crystal in this fashion, the particle motion can be as indicated in the Figure or it can be into the plane of the

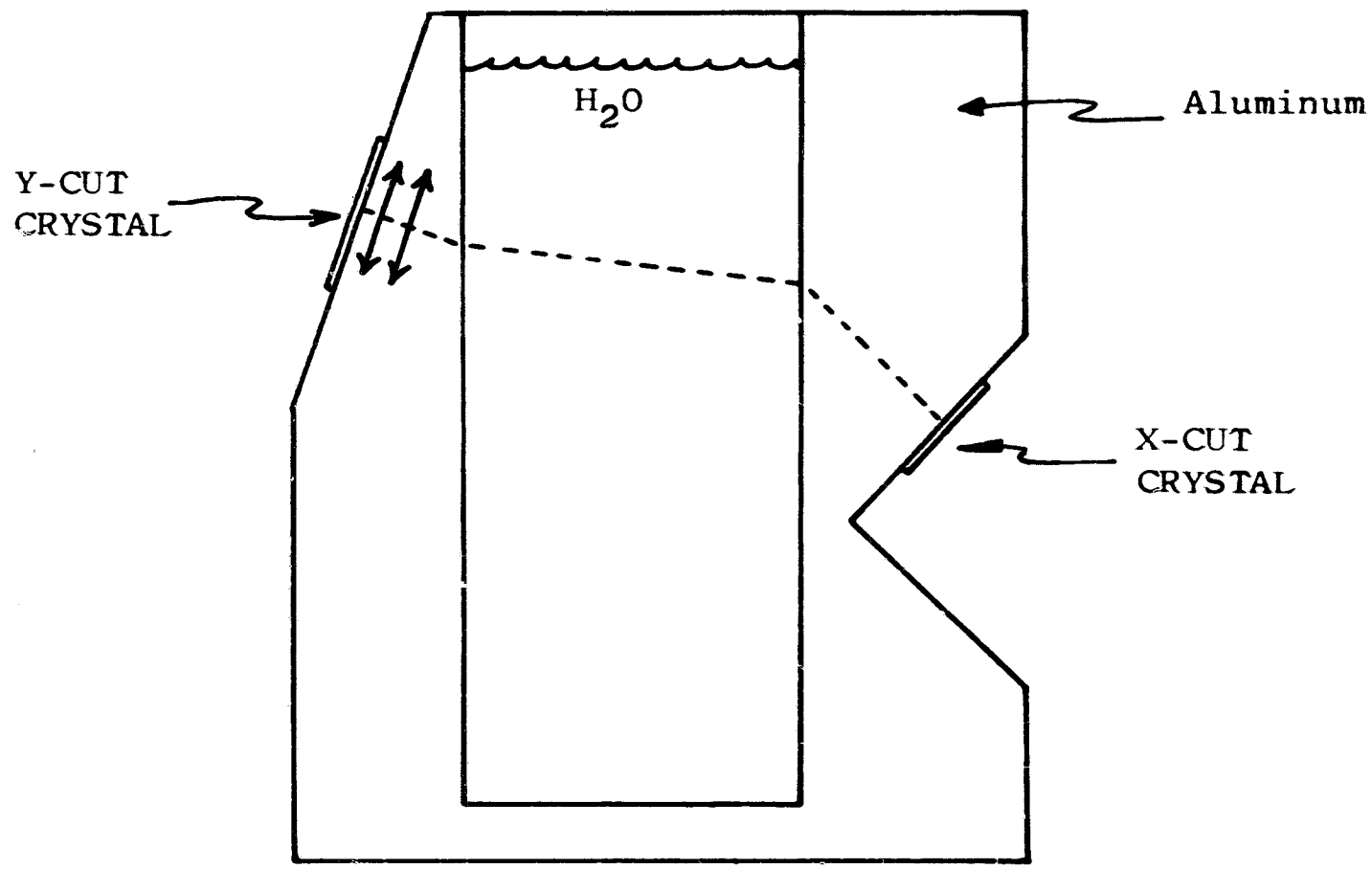

Figure 7. Apparatus Used to Determine the Direction of Particle Motion.

paper. If the particle motion of the crystal is in the direction shown in the Figure, then there will be a component of motion perpendicular to the first aluminum-water interface and a longitudinal wave will be generated in the water. Liquids have a very low shear modulus which does not permit the propagation of a shear wave so that all of the energy transmitted across the boundary propagates as a longitudinal wave. As the wave travels through the water, it is refracted at the water-aluminum boundary and is received by an X-cut quartz crystal. When the particle motion is into the plane of the paper, note that there would no longer be a normal component of motion at the aluminum-water interface resulting in all of the incident energy being reflected. This case is achieved by rotating the Y-cut crystal by 90°.

To make the actual determination of particle motion, the rays of the sound beams were traced through the system using Snell's law of refraction. For convenience, the angle of the incident shear wave with the normal at the aluminum-water interface was chosen so that the wave front of the received longitudinal waves would make a 45 degree angle with respect to the normal at the water-aluminum boundary. A 45 degree notch was then machined in the aluminum to mount the receiving crystal.

For each of the two orientations of the Y-cut crystal, a 7 MHz pulse was used to drive the crystal. It is found that the received pulse varies by at least a 10 to 1 ratio in amplitude for the two orientations. Therefore, the larger amplitude indicates a particle motion in the direction shown in the Figure for which there is a normal component at the aluminum-water interface.

The Y-cut crystals are attached to the aluminum with a red wax whose melting point is not much above room temperature. In many instances the red wax coupling agent is used when making stress measurements. This type of coupling is very efficient; however, it is not a convenient way to couple the transducer in any type of field measurement. Another couplant which has a good coupling efficiency and is a liquid was found. This couplant is the part "A" of epoxy cement. Since it is a liquid it lends itself more readily for field measurements.

B. Lucite Backed Quarts Crystal Transducer Assembly

The Y-cut quartz transducer was also incorporated into a transducer assembly with a lucite backing as shown in Figure 8. As can be seen from the illustration, a 7 MHz crystal is bonded to the lucite with silver epoxy. This thin layer of epoxy also serves as one electrode for the crystal. The other electrode is formed when the transducer assembly is placed on a metallic surface such as a sample. It is noted that this sample material is an electrical ground.

The lucite backed transducer assembly along with the epoxy A coupling yield a convenient way to generate shear waves in metals such as aluminum. An advantage of the lucite backing is that it sufficiently damps the Y-cut crystal so that there is no excess ringing when it is excited by an electrical RF pulse. This particular transducer assembly has been used effectively with the modified time of flight system. In this application it was employed in a single crystal operation where one crystal serves as both the sender and receiver. The block diagram of Figure 2 shows how the modified time of flight system was changed with the addition of the diode switch in order to enhance single crystal operation. An explanation of the operation of the system was given beginning on page 4.

C. Determination of the Principle Axes of Bulk Stress

The mounting of the Y-cut quartz crystal and the determination of its axis of polarization are preliminary to the measurement of a bulk stress. The ultrasonic shear wave is used to measure the amount of bi-refringence which is caused in a material due to the presence of stress. The bi-refringence being a variation of velocity with orientation of the sample under study. If a plane polarized ultrasonic wave is passed through a material whose velocity varies with the orientation of the sample, then the state of polarization, in general, will change from linearly polarized to elliptically polarized, to circularly polarized and so on back to plane polarization at an angle of 90^{o} to the original axis of polarization.

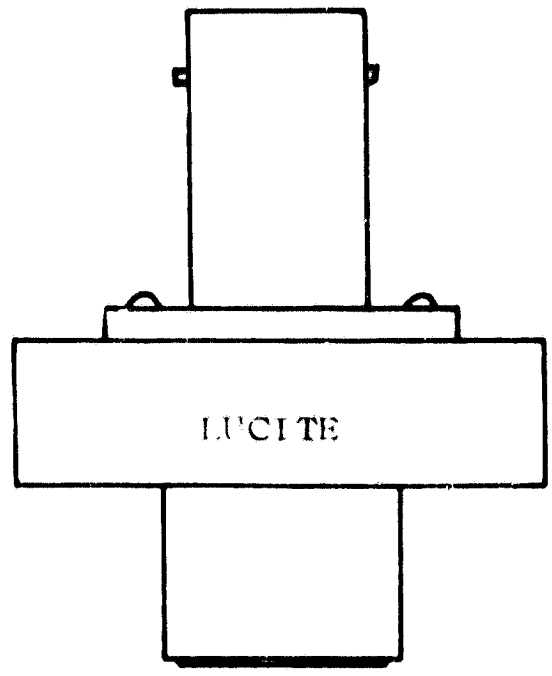

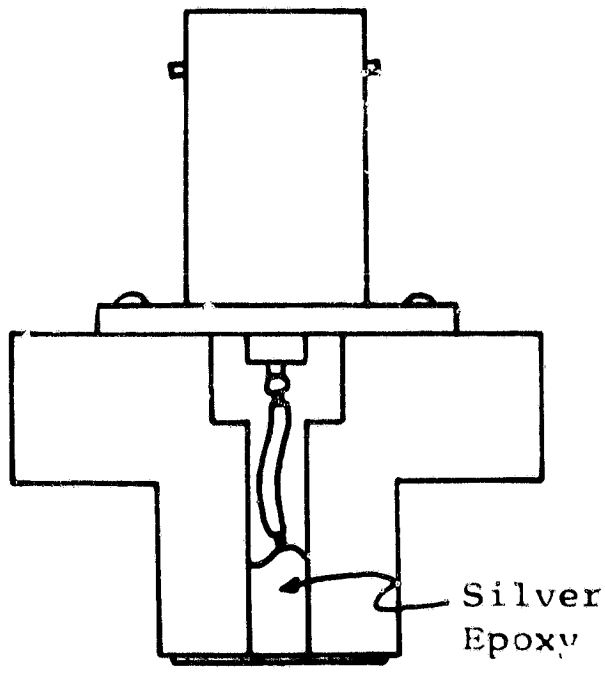

CUT-AWAY

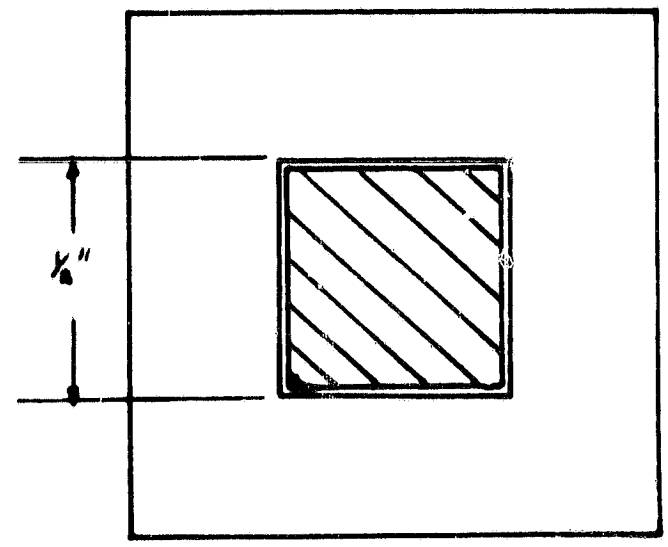

BOTTOM VIEW

Figure 8. Configuration of the Lucite-Backed Shear Wave Transducer.

In order to illustrate the use of bi-refringence for the measurement of stress using ultrasonic shear waves, consider the diagram of Figure 9. Suppose that the sample has an applied stress in the direction shown. The velocity for a shear wave will be dependent upon the particle motion and its relationship to the principal axes of stress. If the lucite-backed transducer is applied as in position 1, then the shear wave will propagate to the back side of the sample, be reflected, and then received. Since the shear wave propagates perpendicular to the major axis of the applied stress the polarization of the wave will not undergo a change. In other words, the wave will traverse the sample as a linearly polarized wave at a velocity V_1. Now suppose the transducer assembly is oriented parallel to the applied stress as shown at position 2. Here again the shear wave will traverse the sample linearly polarized but at velocity V_2. For an orientation of the transducer assembly other than parallel or perpendicular to the major axis of stress, the shear wave will change its state of polarization, such as the orientation at position 3. This fact can be easily seen if the amplitude of the particle motion generated by the transducer is broken down into two components. Let one of the components be parallel to the axis of the applied stress while the other is perpendicular. Since the velocities for the two components are different, V_1 and V_2, it is seen that there will be a time of travel difference developing between the wave with particle motion parallel and the wave with particle motion perpendicular to the applied stress. As the wave propagates, this time difference yields a phase change between the two components of the transverse particle motion. It can be seen that such a phase shift would give rise to a constantly changing state of polarization. The special case of a circularly polarized wave occurs when the two components are 90^o out of time-phase and when the amplitudes of the two components are equal. In Figure 10 an illustration of the above discussion is shown. The Y-cut transducers is shown placed arbitrarily with respect to the applied stress. A trace of the particle motion as the wave progresses through the sample is illustrated. Note that it is possible to have the wave linearly polarized in a direction which is 90^o to the original wave generated by the transducer.

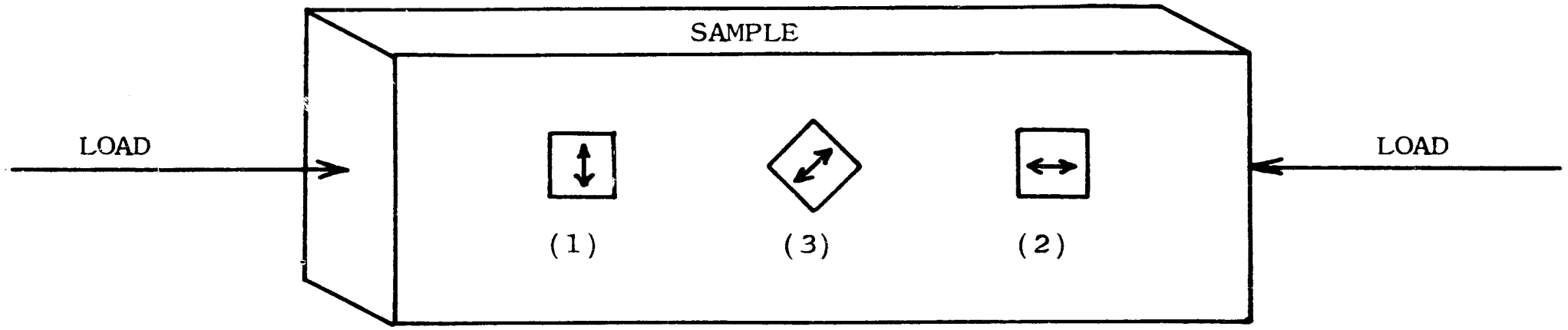

Figure 9. Diagram Illustrating Possible Directions of Shear Crystal Placement on a Sample.

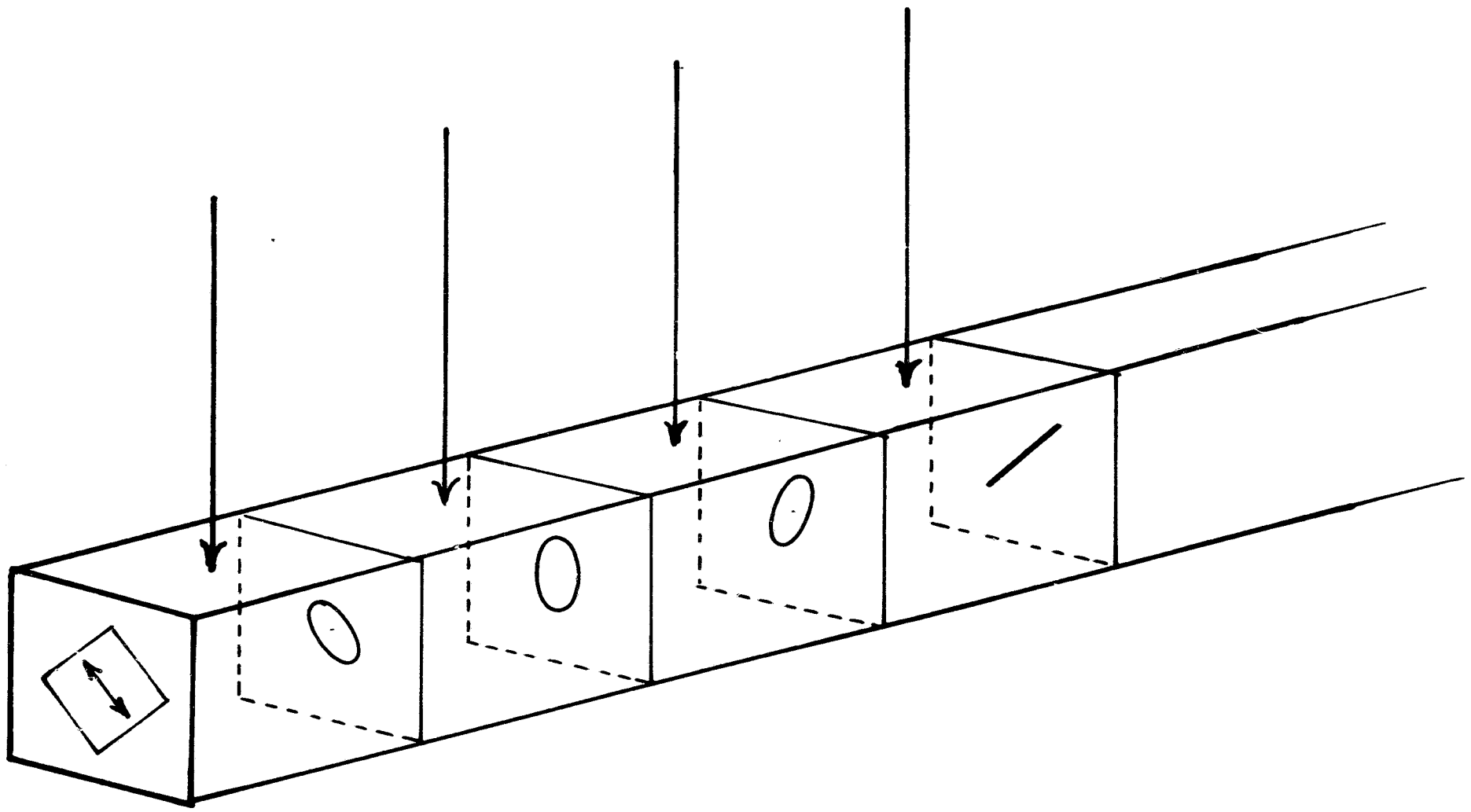

Figure 10. Diagram Showing Polarization of a Shear Wave as it Passes Through a Medium.

Suppose that it is now desirable to measure the stress in a sample of metal, for example, aluminum. The first problem is to determine the orientation of the major axis of stress. The lucite-backed transducer is coupled to the surface of the sample and excited by a pulsed RF source. The oscilloscope used for the modified time of flight system is adjusted so that the sweep speed is sufficient for the observation of several received reflections of the shear wave as it traverses the thickness of the sample. If the orientation of the transducer is askew to the major axes of stress, then the polarization of the wave changes as the wave travels back and forth in the sample. The Y-cut crystal of the transducer assembly is only sensitive to the component of particle motion parallel to its axis of polarization. Therefore, when the reflected pulses received have changed their polarization, the received signal amplitude is affected. If, for example, a received pulse has a linearly polarized particle motion that is 90° to the polarization of the crystal receiver, the pulse will be absent. On the other hand, if the transducer assembly is placed parallel to a major axis of the stress, no change of polarization of the wave will occur. Therefore, the amplitude of the received pulses will exhibit no effects due to polarization.

The picture in Figure 11 shows two oscilloscope traces. The upper trace is the reception of shear wave pulses as they have traversed a 1 inch sample with the transducer assembly oriented parallel to the principal axis of stress. Note that the decay pattern with this orientation is exponential. The amplitude of the received pulses is effected only by the attenuation characteristic of their material. However, as the transducer assembly is rotated a few degrees the decay pattern departs from exponential as illustrated in the second trace of Figure 11. In this trace it is evident that the third received pulse has the majority of its particle motion perpendicular to the polarization of the Y-cut crystal. Once a major axis of stress is found by observing the exponential decay pattern, the transducer assembly can be rotated 90° and a similar decay pattern will also be found. This would then clearly locate the major stress axes as was illustrated for positions 1 and 2 of Figure 9. The modified time of flight system can now be used in the usual fashion to determine the difference in velocity of the shear wave along the directions of the orthogonal major stress axes.

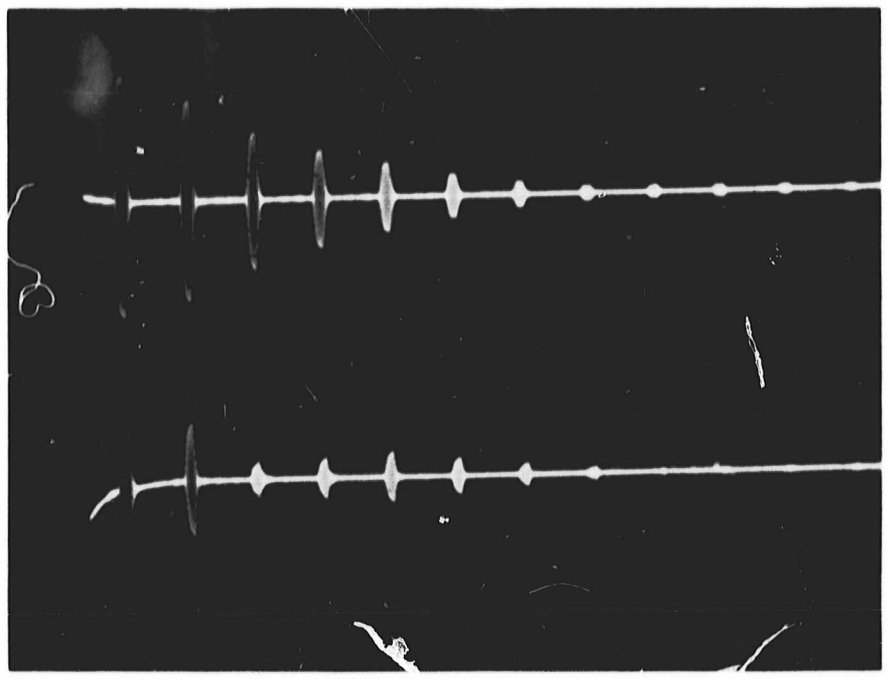

Figure 11. Oscilloscope Photograph Showing the Decay Pattern of a Shear Wave in 0.5 Inch Plate.

D. Shear Wave Velocity Change Versus Stress

Before making an actual stress measurement it is necessary to determine the relationship between the change in velocity of the ultrasonic shear wave and stress. In general, the relationship will be dependent upon the material and most likely upon the particular alloy of the material. Tests were therefore conducted on five different aluminum alloys in order to determine the stress-acoustical coefficients which relate the change in velocity to stress. The alloys which were studied were 2014-T6, 2024-T351, 2219-T87, 6061-T651 and 7075-Y651. The tests were conducted on samples which had dimensions of 4.75 by 1 by 1.5 inches. The samples were placed in a press as shown in Figure 12. The shear wave was propagated through the sample along its 1 inch dimension. A uniaxial compressive load was applied. As the load was increased, the change in velocity of a shear wave propagated with particle motion parallel to the applied load versus a wave propagated with particle motion perpendicular to the applied load was recorded. The graph of Figure 13 shows a plot of the parallel velocity change minus the perpendicular velocity change versus stress. For all aluminum alloys it was found that the shear wave with particle motion parallel to the direction of the applied compressive load increased with stress while the velocity of the perpendicular wave decreased. The reason that this latter wave decreases in velocity is due to the fact that there is a tensile stress created in this direction as a result of Poisson's ratio. A listing of the stress-acoustic coefficients is given in Table I.

The Table also gives the absolute velocity of the shear wave for the various alloys. The velocities were determined by the time of flight system. The lucite-backed transducer assembly was placed on a sample of known thickness and the multiple reflections were observed as shown in Figure 11. By using a beam intensifier incorporated in the oscilloscope, the time between successive reflections could be measured to within 0.1 microsecond. Note that for single crystal operation, the time between the reflected pulses represents the time necessary for the wave to traverse twice the thickness of the sample. The measured thickness of the sample was then divided by one-half the time measured between reflections to yield the shear wave velocity of the material.

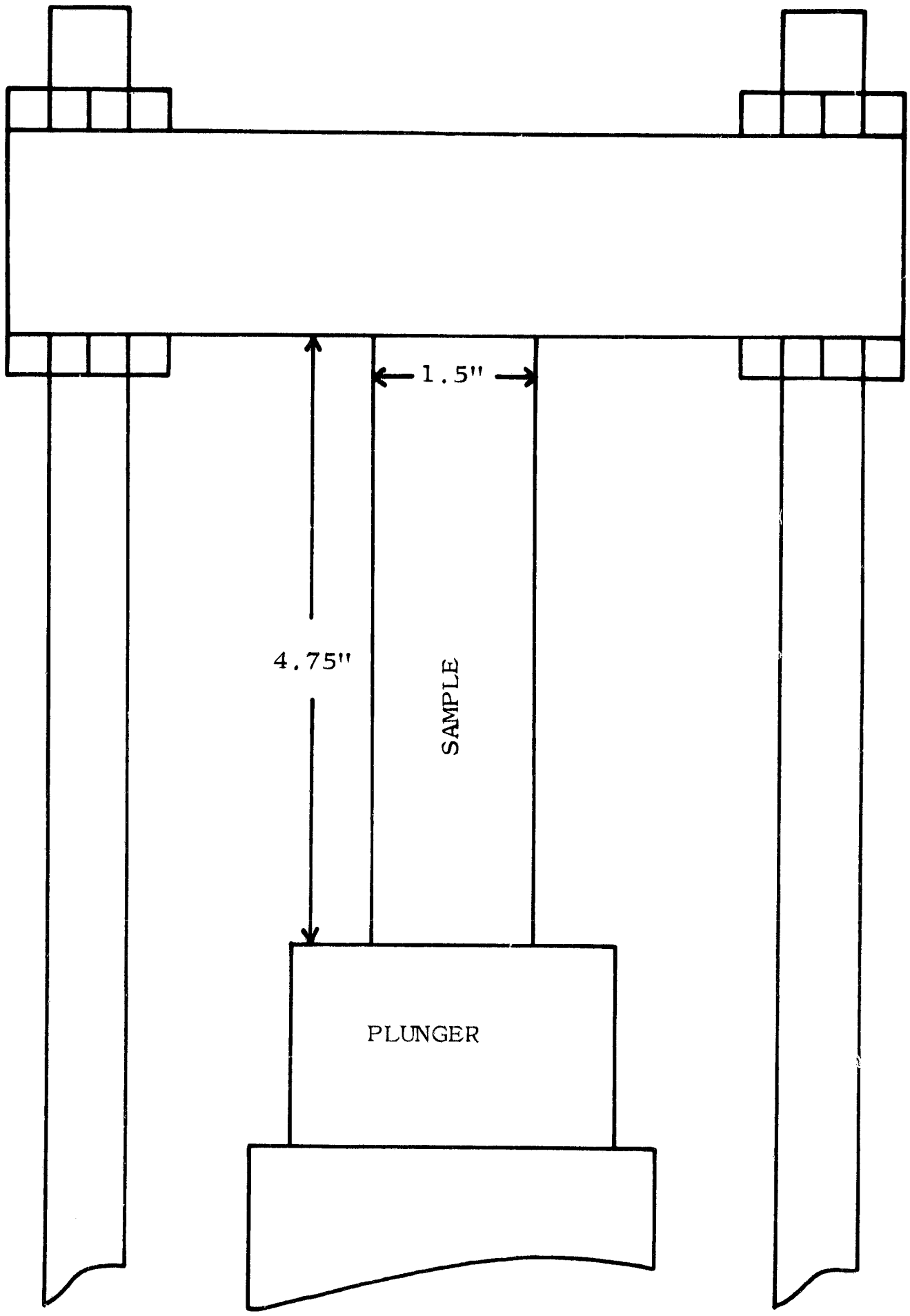

Figure 12. Illustration Showing How Samples were Placed in the Press.

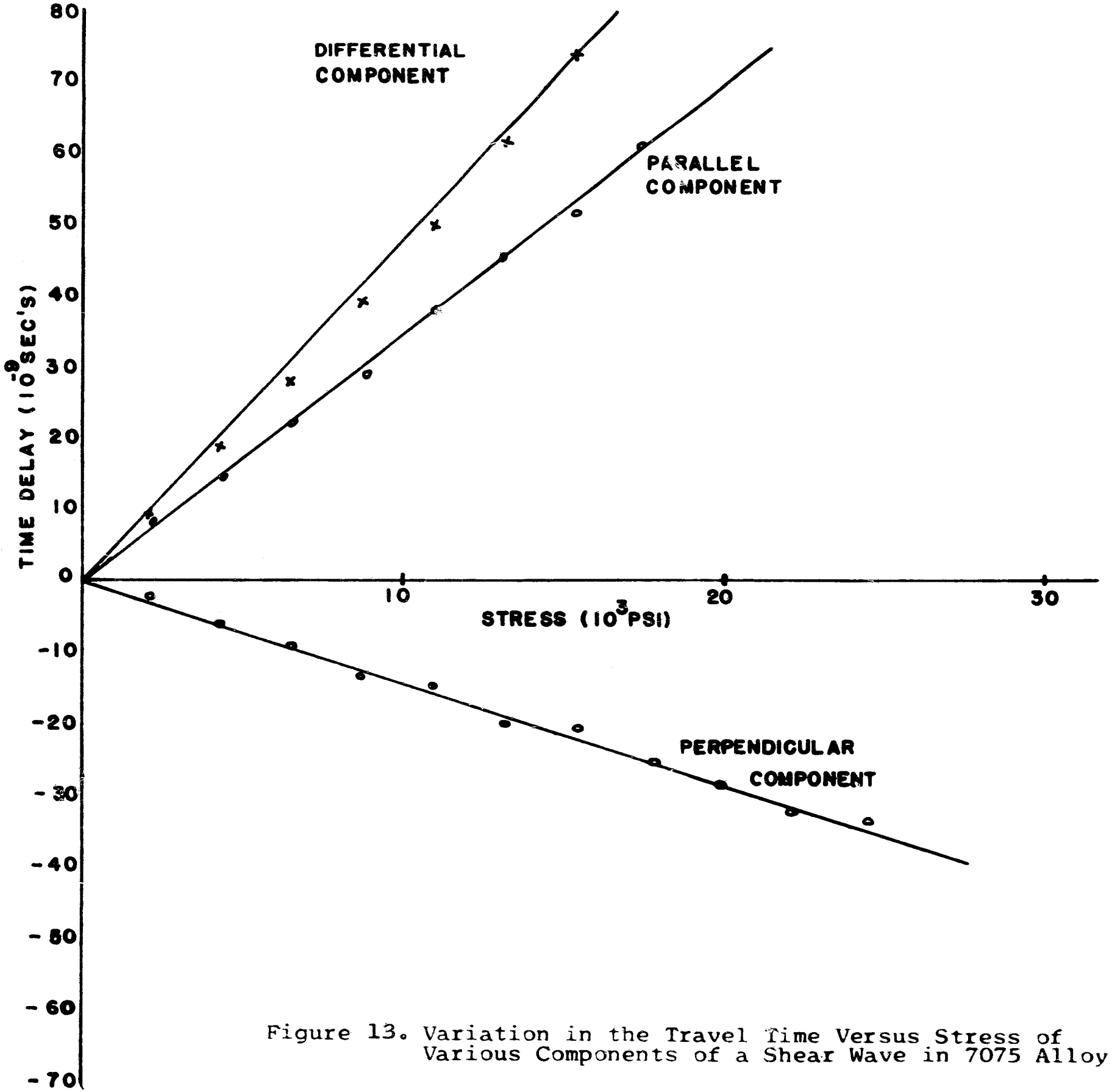

Figure 13. Variation in the Travel Time Versus Stress of Various Components of a Shear Wave in 7075 Alloy.

TABLE I

Acoustical Velocity Data*

Characteristic	Alloys					
	2014	2024	2219	6061	7075	
Temper	T6	T351	T87	T651	T651	
Modulus ($ksi \times 10^3$)	10.6	10.6	10.6	10.0	10.0	
Yield (ksi)	63	47	56	40	73	
Delay Time for 1" Path Length at 1 ksi (10^{-9} sec.)	1.11 1.22	1.93 .78	1.09 1.15	3.32 0.417	3.61 .179	(Shear Wave) (Surface Wave)
Delay Time at Yield for 1" Path Length	69.9 76.9	90.7 36.6	61.0 64.5	133 16.8	263 13.1	(Shear Wave) (Surface Wave)
Absolute Velocity Shear Wave -- (Meters/Sec.)	3130	3300	3120	3045	3480	
Absolute Velocity Surface Wave - (Meters/Sec.)	2920	3030	2880	2905	3030	
Frequency-Null Constant for 2" Double Lucite Wedge Surface Wave Transducer ($KHz/10^3 psi$)	1.00	0.640	0.950	0.342	0.106	

* Measurements were made at 7 megacycles per second with the exception of Surface Wave Data for 7075 which were made at 5 megacycles.

To summarize, a lucite backed transducer assembly was constructed that can be coupled to a surface with the aid of a suitable couplant. It was found that the "A" part of epoxy cement provides the necessary coupling to generate and detect satisfactory shear waves. The transducer assembly along with the couplant gives the ability to make bulk stress measurements of a solid material such as aluminum. It was found that the major axes of stress in an unknown sample could be found by observing the decay pattern of the multiple reflections. As the transducer is rotated on a given location, there will be two orthogonal directions where the decay pattern becomes exponential. These two directions then determine the major stress axes. Using the modified time of flight system, the difference in shear wave velocity along these two directions can be determined. The magnitude of stress in the material at this location can be found by referring to the stress-acoustic coefficients for the particular alloy under consideration as given in Table I. These coefficients were determined by applying a load to a sample and noting the velocity change as stress was introduced. It should be noted that the computed stress is dependent upon the thickness of material as well as the delay per unit path length.

E. Limitations of Shear Wave Analysis

Although the shear wave is extremely useful in making measurements of stress in the bulk of a material, it should be remembered that stress is a three dimensional quantity. In order to completely analyze a given sample the stress measurements have to be made accordingly. To better understand this problem consider making stress measurements on a large plate subjected to load. Normally in this case the measurement would be made through the thickness of the plate which has a much smaller dimension than its length or width. Furthermore, assume that the surfaces of the plate are in tension while the bulk of the plate is in compression. (This situation can be encountered with residual stresses due to rolling of the plate.) As the shear wave traverses the thickness dimension it will measure only the net stress along its path length. If the wave goes through an equal amount of compression and tension while traversing the sample, then it would

appear that the sample was in a condition of zero residual stress even though the equal amounts of tensile and compressive stresses may be of very high magnitude. This dilemma can be solved if it is possible to propagate the wave at right angles to the thickness dimension. In this manner layers of tension and compression could be detected and measured. However, in many practical applications it is impossible to make this measurement due to physical limitations such as inaccessibility or the fact that the dimensions are too large. If the path length the wave travels is greater than one foot, attenuation and beam spreading are only a few factors which arise to produce inaccuracy of measurement. It should be pointed out that the transducer assembly discussed above covers an area of 1/2 by 1/2 inch. The stress measurement then gives the average stress present within this area.

IV. STRESS ANALYSIS USING SURFACE WAVES

An alternate method of examining the stress distribution throughout the thickness of a material utilizes ultrasonic surface waves. The surface wave propagates in the material near the surface and penetrates to a depth of approximately one wave length. The particle motion of the surface wave is similar to that of a shear wave inasmuch as the motion is essentially transverse to the direction of propagation. Although in general, the particle motion is elliptical, the major axis of the ellipse is perpendicular to the surface of the material.

A. Transducer Development Studies

Various means of measuring the ultrasonic velocity of surface waves are available. For the purposes of stress analysis, it was decided that a system of measurement similar to that used for the measurement of bulk stress with shear waves would be most desirable. For this purpose, it was anticipated that the velocity variation would be dependent upon the orientation of the direction of propagation of the surface wave with the direction of principal axes of stress. For experimental purposes, a velocity dependence upon stress for surface waves was verified by the use of a pair of surface

wave transducers rigidly fixed to a sample with a constant spacing. An observation of the change in velocity with stress could be made, but in addition a change in the propagation time was observed due to the strain in the sample.

The use of two separate transducers, one for the generation and one for the detection of surface waves, for actual measurements of stress on samples leads to a problem in the measurement of frequency and path length. Frequency can, of course, be measured accurately with electronic counters providing that a continuous oscillator is used in conjunction with a gated amplifier. These circuits have been described in the frequency null section of instrumentation. The measurement of path length is a much more difficult task. For most surface wave transducers, those using a lucite wedge, the point of generation and detection of the surface wave is difficult to define and certainly difficult to measure.

A series of studies was therefore undertaken to determine methods for the accurate measurement of the change in velocity of surface waves versus orientation on the sample. had been established that the measurement of the velocity along the two principal axes of stress would be sufficient. The first study therefore consisted of the construction of n interferometer which was placed on the surface to be stud d. The interferometer was geometrically equivalent to a typ al optical interferometer in which a single source was use with two receivers and a beam splitter. The beam splitter n- sisted of a knife edge of aluminum placed at 45° with espect to the generated surface wave. A portion of the sur ce wave propagated under the knife edge to the first receiv and the remainder was reflected at 90° to a second receive The same surface wave was therefore caused to propaga along two orthogonal paths on the same surface.

Although this arrangement looked promisin an absolute measurement of the relative velocities was st l dependent upon the accurate measurement of at least one dis nce. Through experimentation with the beam splitter, tha is an aluminum knife edge, it was discovered that a port n of the surface wave energy was converted to a longitudin wave which propagated up through the knife edge body. F ther observations

showed that a wedge type structure which contacted the surface along a well defined sharp edge was a relatively efficient receiver as well as generator of ultrasonic surface waves. The most important feature was that it was unnecessary to use a couplant with the knife edge providing that a force was used to couple the edge to the surface.

B. The Knife Edge Surface Wave Transducer Assembly

As a result of these studies, various configurations were tried using a pair of knife edges to generate and detect ultrasonic surface waves. The major problem arises from the fact that when two knife edge segments are constructed in a single piece so that the distance between the segments is held constant, considerable energy is transmitted directly through the structure from one crystal to the second crystal. The final configuration is as shown in Figure 14 where the path between the sending crystal and the receiving crystal has been increased sufficiently so that the surface wave arrives at the receiving crystal before the arrival of any interfering energy transmitted through the body of the transducer.

The operation of the transducer consists of an X-cut quartz crystal that generates longitudinal waves which propagate down a wedge structure to a well defined edge that contacts the surface. The partical motion at the ultrasonic frequency is normal to the surface along the line of the knife edge and generates a surface wave which travels out in both directions normal to the knife edge. The second knife edge contacts the sample surface at a fixed distance from and parallel to the first knife edge. As the surface wave travels under the second knife edge, a longitudinal wave is generated which propagates up the receiving wedge and is detected by the second X-cut quartz crystal. In order to assure uniform contact of the knife edge to the surface, the knife edge is flattened so that its width is approximately one half wave length of the surface wave which is generated. Furthermore, a force is applied normal to the surface along the axes of the two knife edges to obtain contact. The total force required is of the order of 50 pounds and is applied by the loading frame shown in Figure 15.

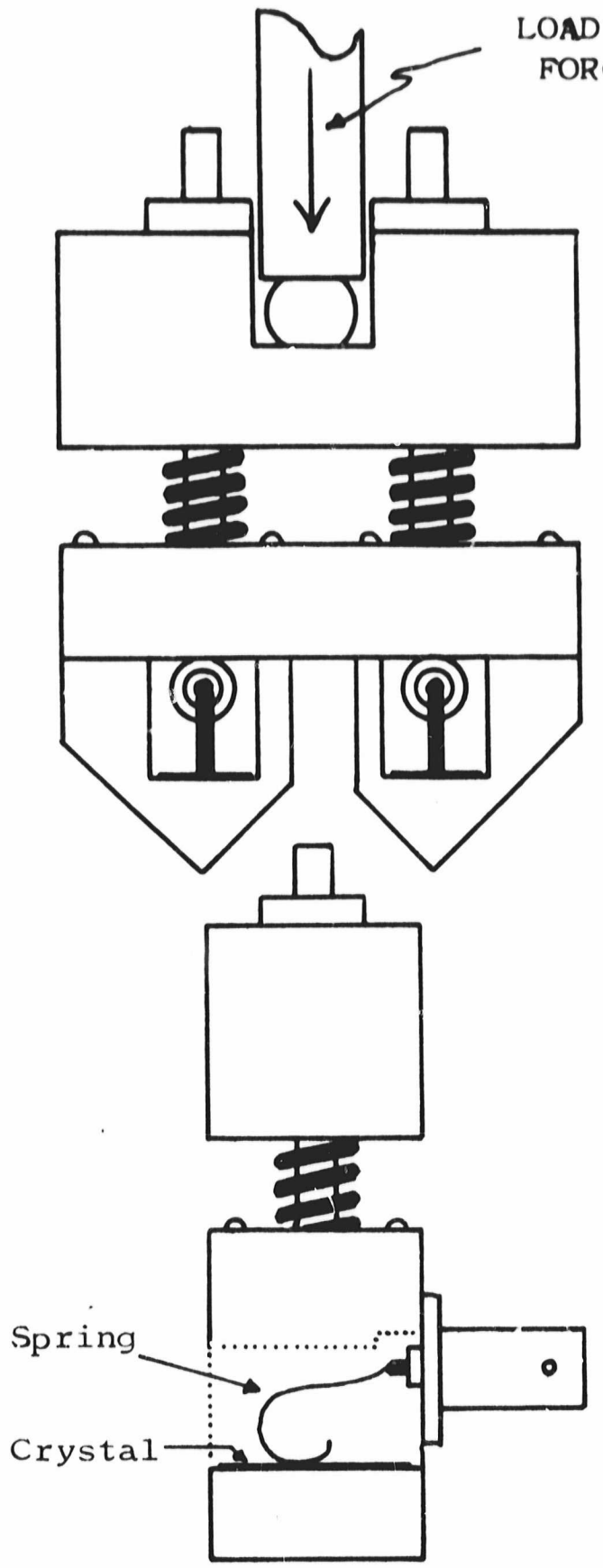

Figure 14. Configuration of the Knife Edge Surface Wave Transducer Assembly.

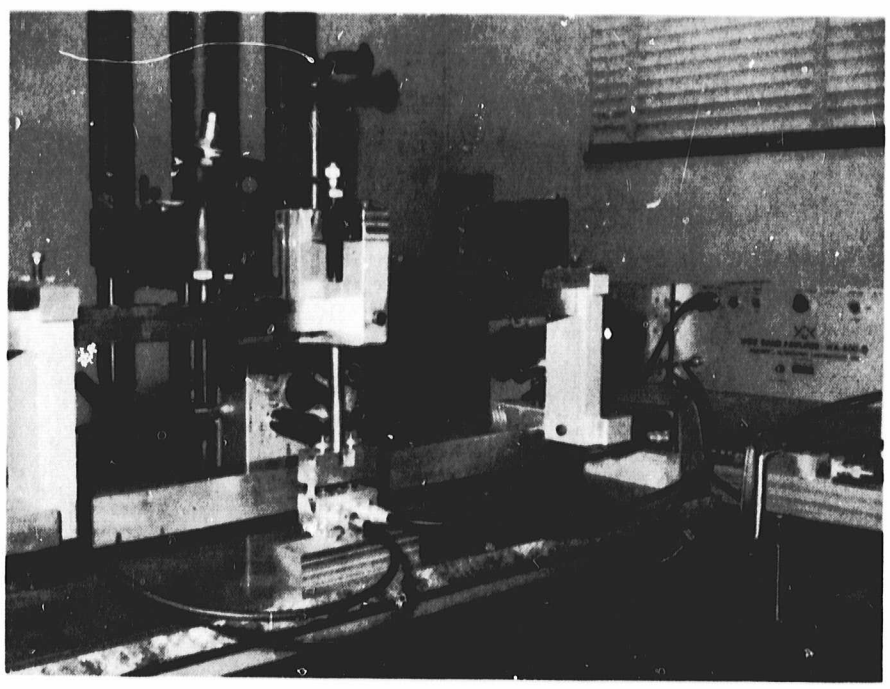

Figure 15. Photograph Showing the System Used to Apply Force to the Transducer.

C. The Double Lucite Wedge Surface Wave Transducer

Another type of transducer assembly that is used for the generation and detection of surface waves is illustrated in Figure 16. This particular assembly was constructed especially for use with the frequency null system. It is seen that both the sending and receiving quartz crystals are mounted on a single piece of lucite. The 7 MHz, X-cut crystals are mounted at the critical angle with respect to the sample surface so that all the energy entering into the sample propagates as a surface wave. This angle is determined by Snell's Law and it is found that for the combination of lucite and aluminum an angle of 67.5^{o} is appropriate.

Because of the fact that all the ultrasonic energy propagates as a surface wave, this type of transducer is more efficient than the knife edge transducer. As a result this assembly was used with the transistorized frequency null system which has a lower RF output pulse than the vacuum tube pulser. It is noted that the lucite portion of the transducer assembly is surrounded by an aluminum cover. This cover acts to give additional strength to the lucite as well as serving as a connector mounting. The reason the lucite needs added strength arises from the fact that this transducer assembly operates with no couplant other than a force couple. The force necessary for proper operation is of the order of 100 pounds. With this much force it is seen from the shape of the lucite that the path length between sender and receiver would change significantly without the aid of the aluminum. Here again, as with the knife edge transducer assembly, a constant path length is essential for the measurement of surface wave velocity changes.

It has been found that the velocity of surface waves in aluminum changes with stress. As a result of this fact surface waves can be used as a measure of stress that are present near the surface of a sample. The depth of penetration of such a wave is approximately one wave length. Typically speaking, this corresponds to a depth of the order of 1 millimeter at a frequency of 3 MHz. It is of importance to be able to measure this type of stress since a high tensile surface stress can greatly accelerate the stress-corrosion process.

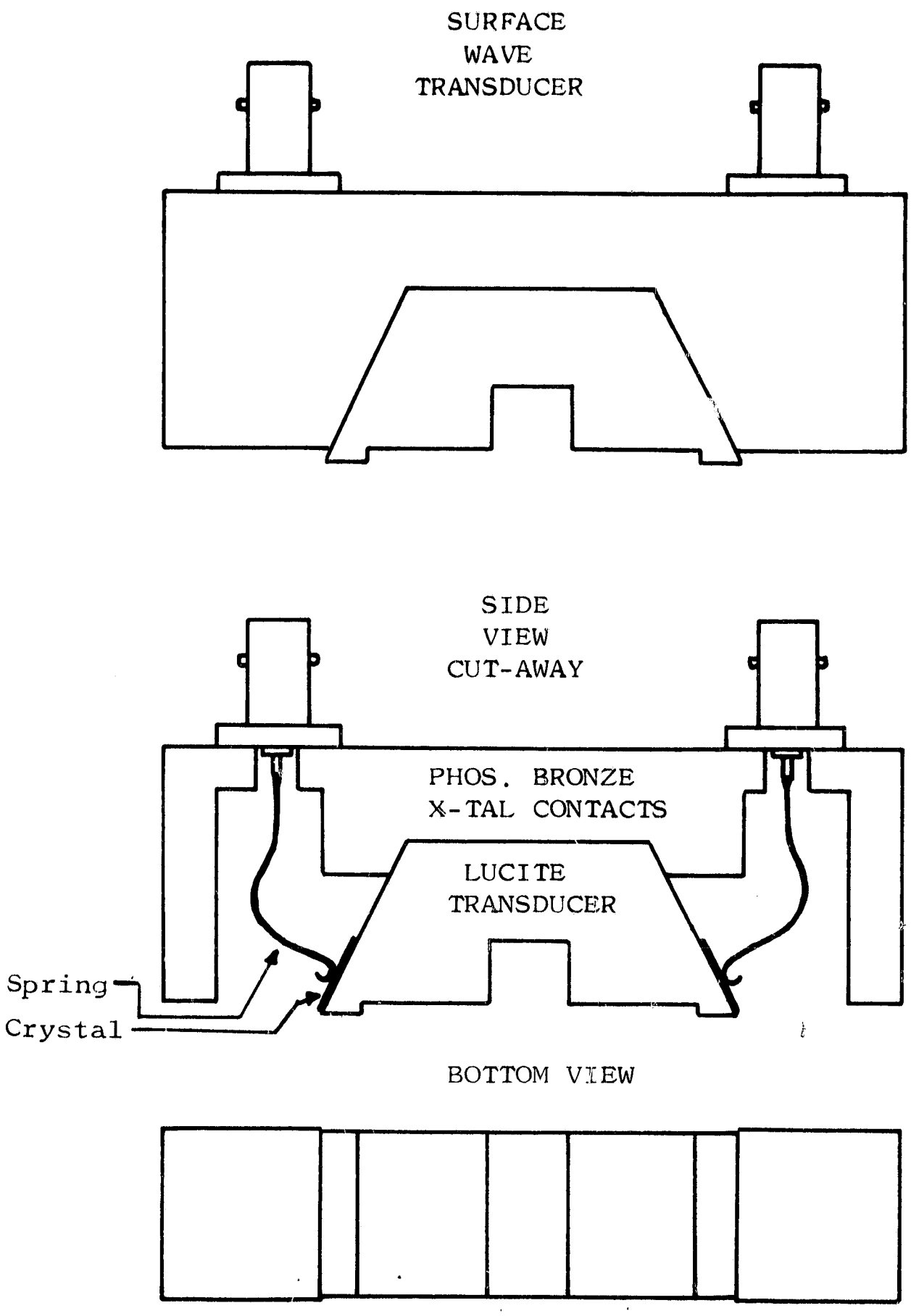

Figure 16. Configuration of Lucite Surface Wave Transducer Assembly.

D. Determination of Principle Axes of Surface Stress

Just as with the shear wave, it is necessary to determine the direction of orientation of the major axis of stress appear on the surface before a measurement can be made. Although both measuring systems could be used for such a determination, the frequency null system has been used during this program. The lucite transducer assembly is placed on the surface of a sample at a particular location using a loading frame to give the force couple. The frequency of the continuous wave oscillator is adjusted so that a null is found. Once the frequency for the null is recorded, the transducer assembly is rotated 10^{o} and the null frequency is again recorded. Figure 17 shows a typical plot on polar paper of the change in frequency versus transducer orientation. In this particular case, it was found that the frequency change, maximum minus minimum frequency, was 15.5K hertz.

From the previous discussion on measuring systems, it is remembered that the higher frequency corresponds to a compressive stress. Therefore, position 10 on the graph is in a compressive state as compared to position 1 or 19. It should be pointed out that the plot of Figure 17 not only shows the direction of the major axes of stress, but also since the shape of the curve is a smooth function, it shows that the surface stress is unidirectional over the area of the sample the transducer assembly covers. That is to say, the surface stress does not have any curvature between the sender and the receiver.

The magnitude of the stress present at the surface can be found in a similar manner as in the measurement of bulk stresses. Once the orientation of the stress is found by the frequency null system, the difference between the maximum and minimum frequencies corresponds to the stress magnitude. It should be remembered at this time that not only can the stress magnitude be measured by the frequency null system, but also by the time of flight system. In the latter case, the knife edge transducer assembly is placed along the two major axes of stress. The change in time of flight along the two major axes of stress can then be measured in nanoseconds for a known travel time over a fixed path length.

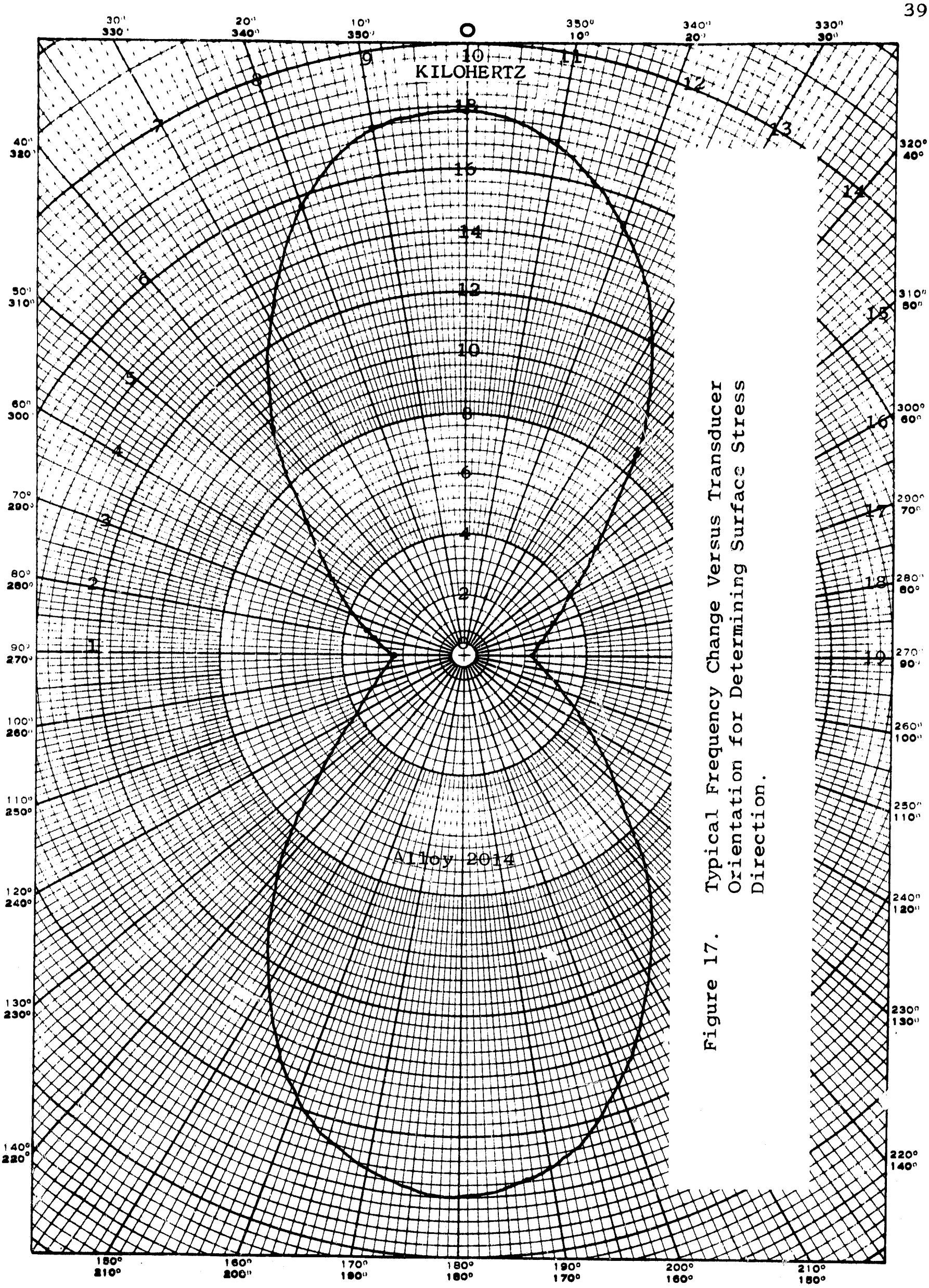

Figure 17. Typical Frequency Change Versus Transducer Orientation for Determining Surface Stress Direction.

E. Surface Wave Velocity Change Versus Stress

To determine the amount that the surface wave velocity changes with stress, samples of various aluminum alloys were placed in a press. These samples were compressively loaded in the same fashion as was done when the stress-acoustic constants for shear waves were determined. Initially, a transducer assembly, either lucite or knife edge, was placed on the 1.5 inch side of the sample. As the load was increased, the change in surface wave velocity was noted using the modified time of flight system at a frequency of 7 MHz. This procedure was followed for the five alloys of aluminum listed in Table I. From this Table it can be seen that there is a wide variation in the stress-acoustic constants for the aluminum alloys tested. The graph of Figure 18 shows a typical travel time change of surface wave over a constant path length versus stress for Alloy 6061. Note that the time variation is linear with stress and that the graph shows that the velocity increases with increasing compressive stress.

The absolute velocity of the surface wave was measured in all of the alloys that were investigated. This measurement was conducted in the following manner. Two lucite wedges were constructed having the proper angle for surface wave generation. The receiving wedge was moved along the surface of the sample toward the sending wedge. The time of travel of the received wave was measured as the receiving transducer was moved toward the sender in increments of 0.1 inches over a total path length of 2 inches. The change in the time of travel is plotted versus path length change as shown in Figure 19. By graphically taking the reciprocal of the slope of this curve the velocity can be determined.

F. Stress Gradient Studies Using Surface Waves

Another experiment in stress analysis using surface waves was conducted. This experiment was concerned with the determination of stress gradient. Since the penetration depth of a surface wave can be controlled by changing frequency, it is possible then to measure the average stress in a given sample at various depths. To make such a measurement using

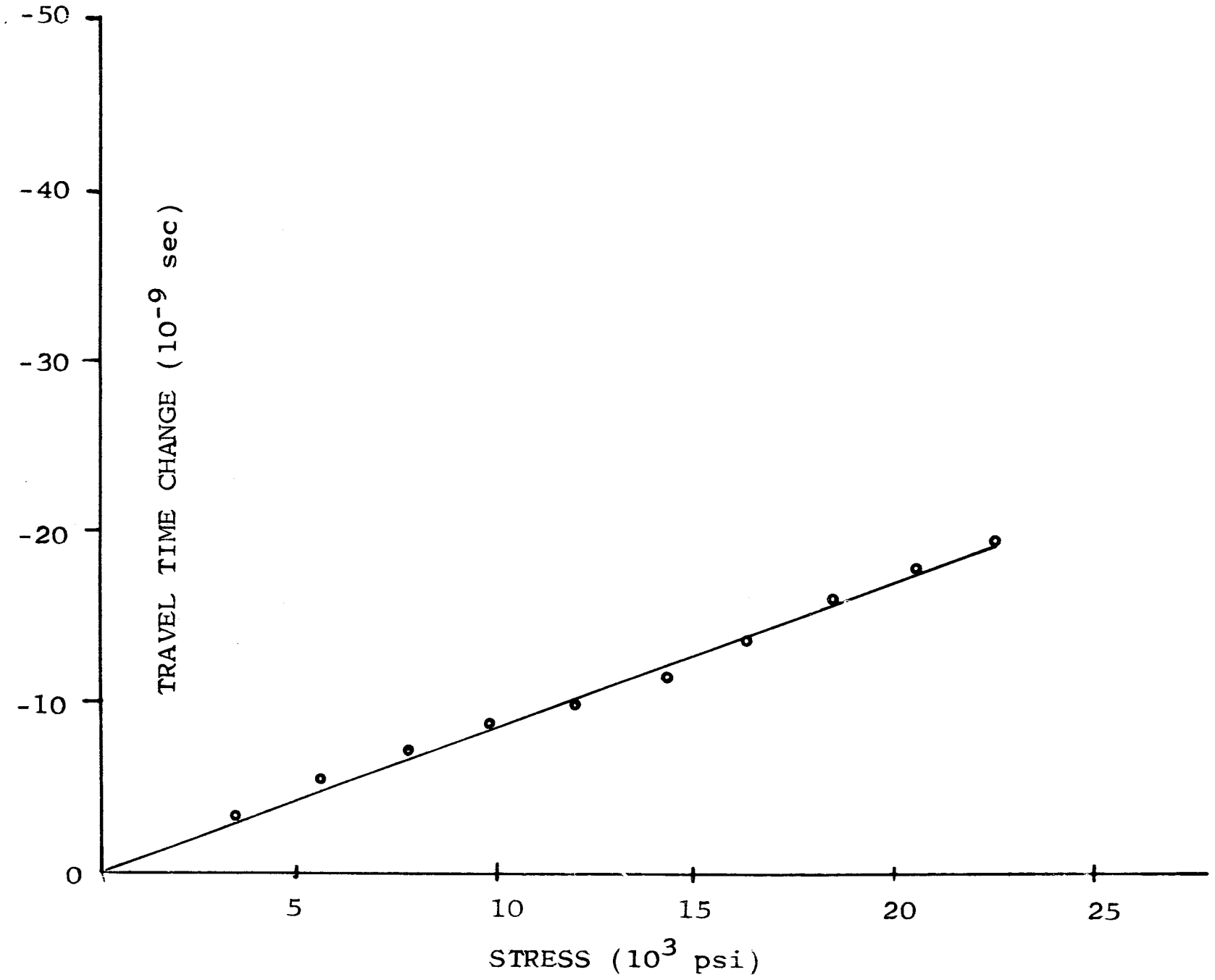

Figure 18. Change in Time of Travel (over a 1.5" Path length) of Surface Waves vs. Stress in a Uniaxially Loaded Sample of 6061 Alloy.

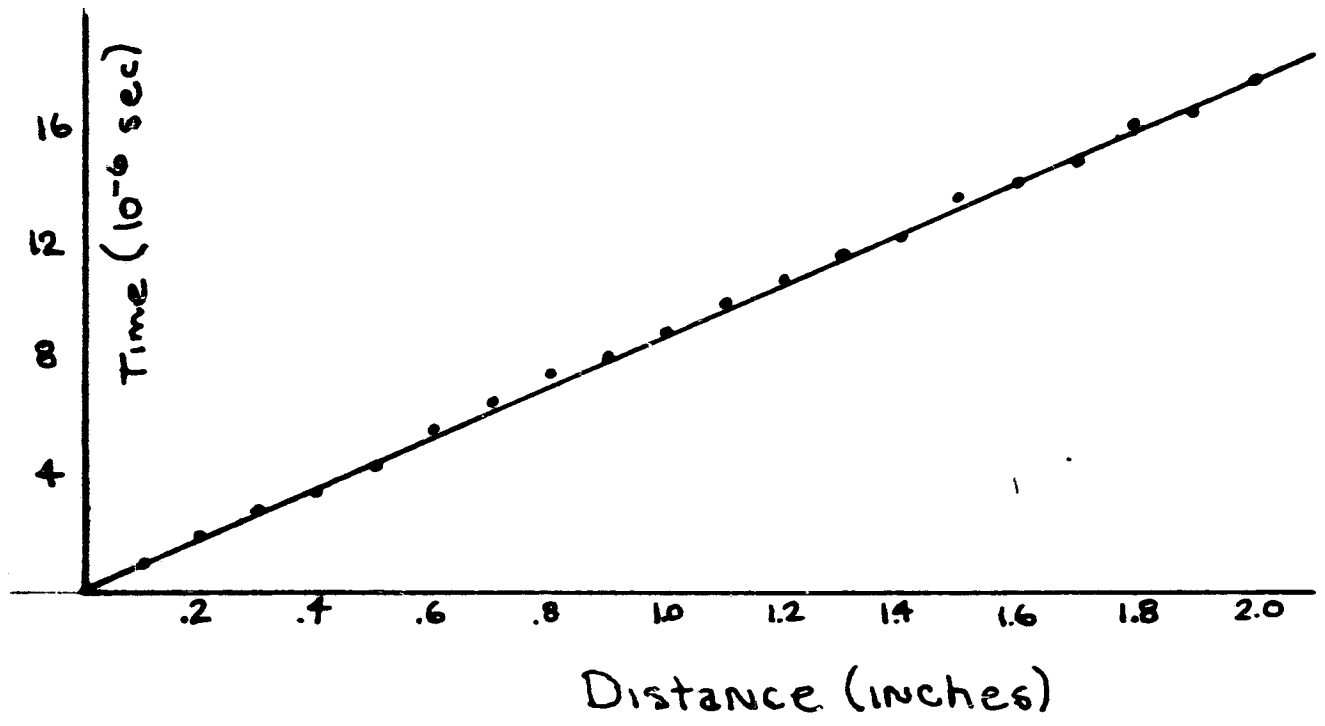

Figure 19. Change in Time of Travel versus Pathlength Change for Surface Waves in Alloy 6061. Velocity is equal to 2905 Meters per Second.

an applied stress gradient, the loading apparatus shown in Figure 20 was employed. This type of loading scheme introduces a constant bending moment in the sample within the region of the innermost supports. The introduced stress varies linearly with distance from the neutral fiber. The top portion of the sample of Figure 20 is in tension while the fibers of the sample below the neutral fiber are in compression. Surface waves were generated using 1 MHz quartz crystal at frequencies of 1, 3, 5, and 7 MHz. For each of these four frequencies, velocity changes were noted using the modified time of flight system as the bar was stressed.

The average stress in a sample when subjected to a constant bending moment can be calculated. A simple formula is derived in Figure 21 expressing the average stress from the surface into the sample. Note that if the penetration depth of the wave is to the neutral fiber, the average stress would be one half the stress present at the surface since the stress increases linearly from the neutral fiber (See Figure 21). If the penetration of the wave is the thickness of the sample, the average stress would be zero. This results since the wave would theoretically see an equal amount of compression and tension.

Figure 22 shows a plot of the average calculated stress in percentage of S_{max} that would be present as a function of frequency i.e., depth of penetration for a sample having a thickness of 0.5 inch (a equals 0.25 inch). The assumption was made that the surface wave penetrated one wave length into the sample and travels at a velocity of 3000 meters per second. Under these conditions, complete penetration would occur at a frequency of 236 KHz, in which case the average stress would be zero. Plotted also on the graph of Figure 22 are the actual data points obtained at 1, 3, 5, and 7 MHz using a sample of 2014-T651 aluminum Alloy, 0.5 by 2 inches in cross section. For a given deflection of the sample in the loading frame, the velocity changes were determined at the above frequencies. The velocity changes at 1, 3, 5, and 7 MHz were converted to a percentage of the change noted at 7 MHz. It is seen that the agreement between the calculated average stress and the actual measured stress is good.

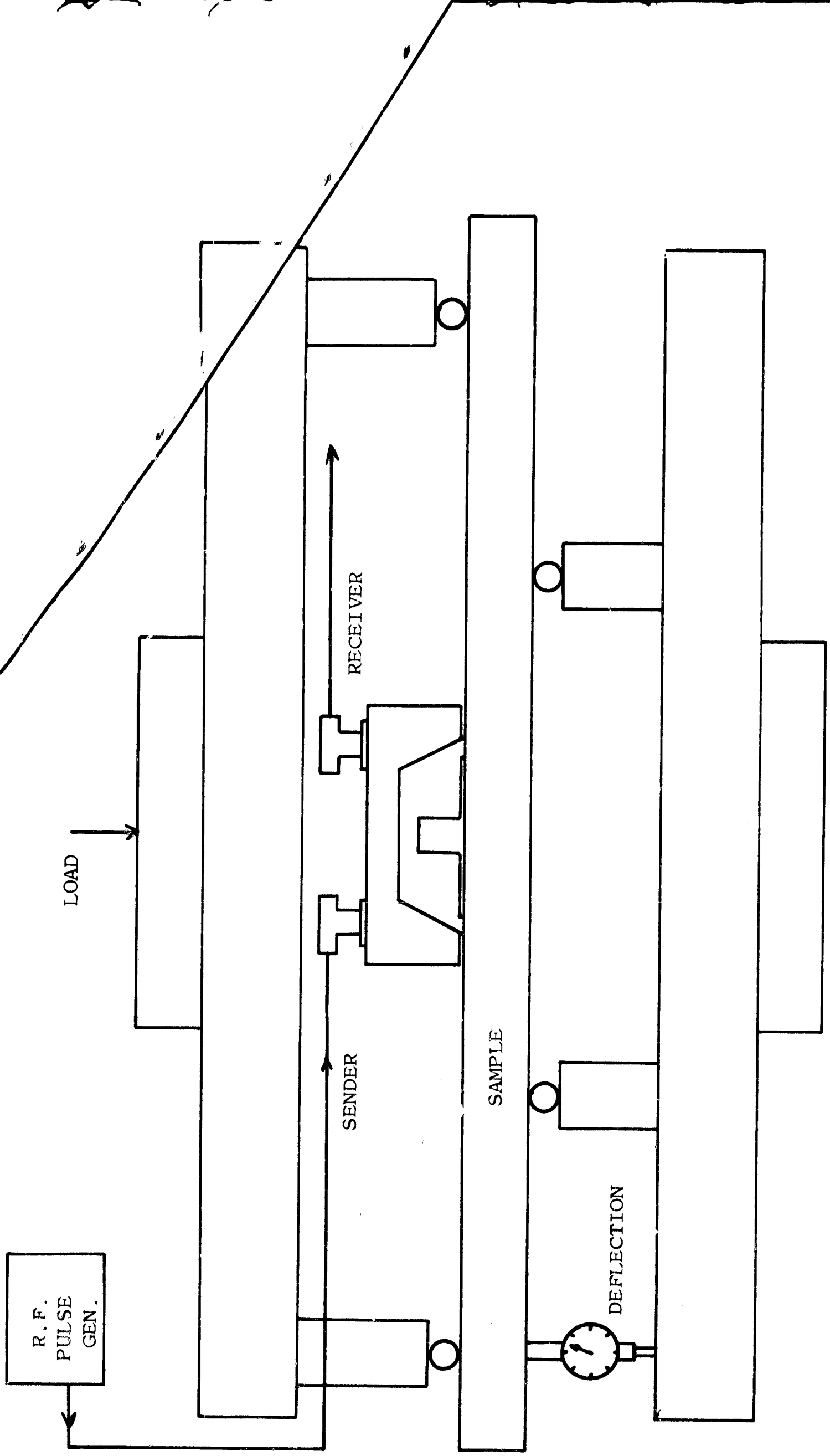

Figure 20. Loading Frame Used for Producing a Bending Moment in a Sample.

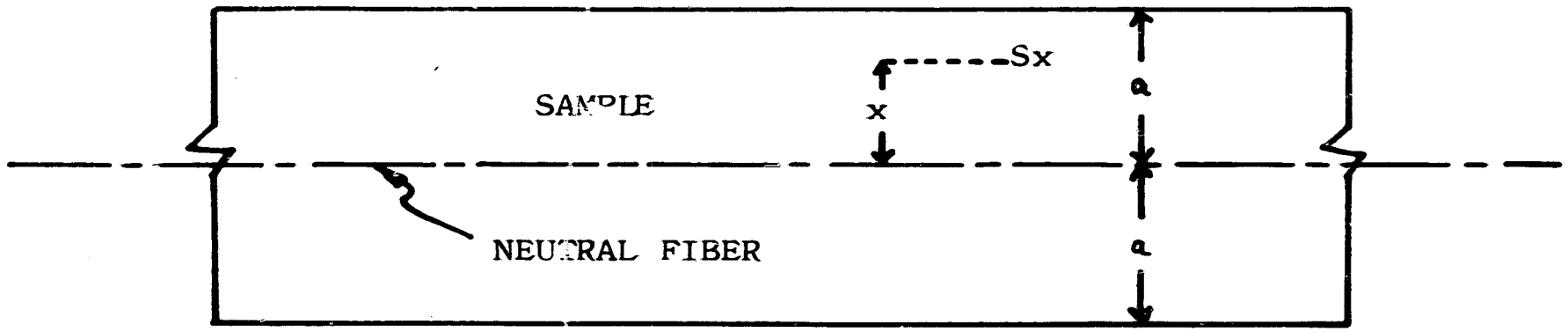

$$Sx = (\text{Constant})\ X$$

$$Sa = (\text{Constant})\ a = Smax$$

$$Savg = \frac{Smax + S}{2} = \frac{Smax\ (1+x/a)}{2}$$

Figure 21. Sample Subjected to Constant Bending Moment Defining Fiber Location for Calculating Average Stress Versus Depth.

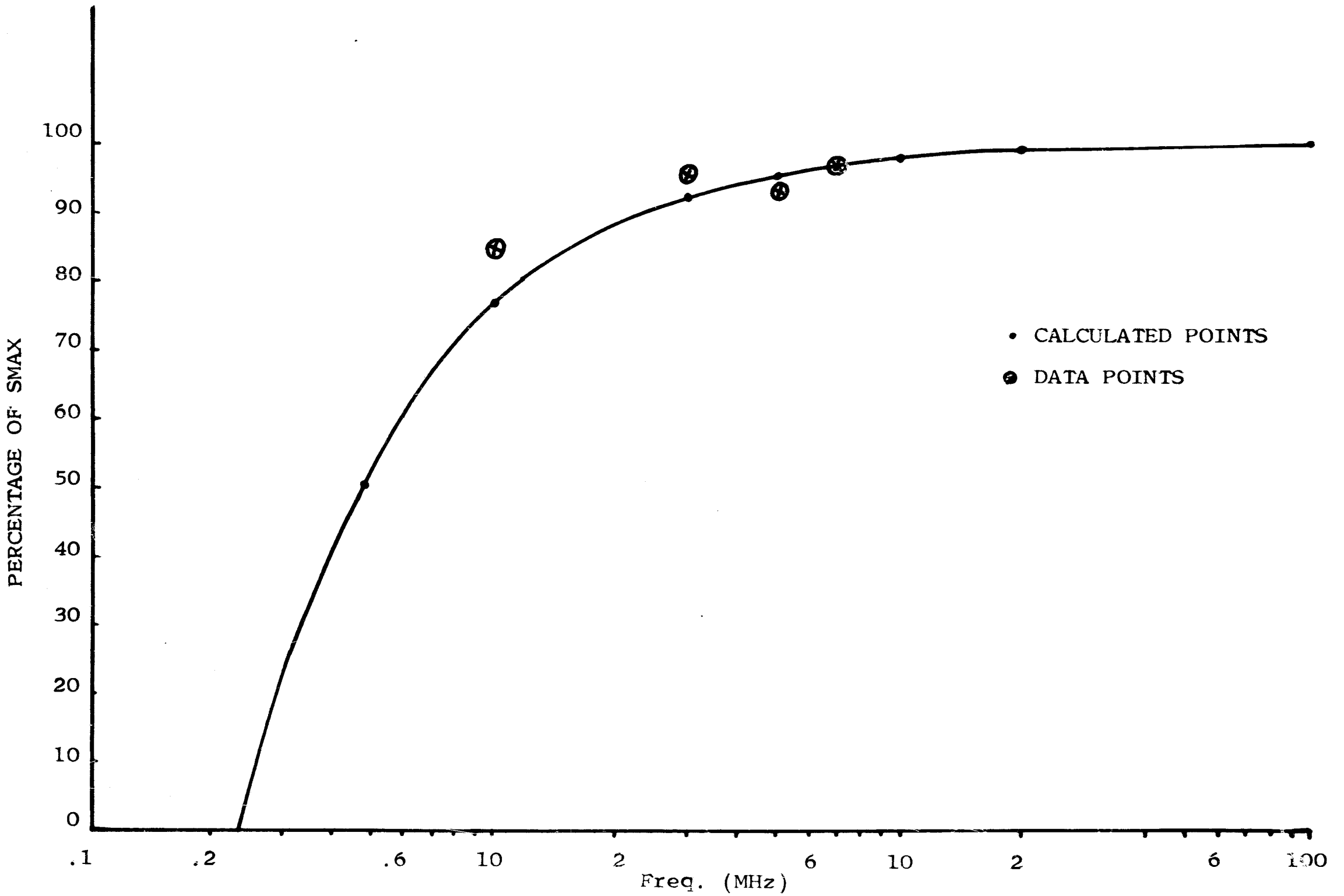

Figure 22. Stress Gradient Measurements Showing Measured Stress and Calculated Stress as a Function of Frequency.

V. GRAIN ORIENTATION EFFECTS

A. Factor Effecting Ultrasonic Velocity

It was anticipated at the beginning of this program that there would be effects observable with the ultrasonic stress measuring techniques due to other causes. A primary concern was that of the differential velocity due to the preferred orientation of grains. Almost all polycrystalline metals have a portion of the crystallites oriented with one of the major axes along the direction of rolling of a bar or plate. Measurements of the preferred grain orientation can be made using X-ray techniques. It was therefore anticipated that the difference in elasticity along the various axes of the crystallites would result in an inherent birefringence in samples which have been formed by rolling. Other possible effects might be observed due to a change in composition of the material throughout its thickness. Since grain orientation is the most likely cause of extraneous effects, emphasis was placed on studies which might reveal its effect.

The initial studies conducted on this program were concerned with the measurement of stresses in metallic samples subjected to externally applied known loads. With known stresses it was possible to develop the techniques of measuring stresses throughout the thickness of metallic materials as well as near the surface of the materials. A major objective, however, was the measurement of residual stress, that is inherent stresses within the material which are a result of forming processes rather than those due to external loads. These residual stresses are the greatest unknown factor in an actual structure. If there were no extraneous effects such as might be due to grain orientation, then the ultrasonic methods of stress analysis would provide a direct useful tool for the measurement of residual stress as well as those stresses due to external loading.

The most difficult part of developing methods of separating those effects which are due directly to residual stress and other effects which appear as residual stress, is the fact that additional methods of measurement are not available. It would be possible to measure the amount of preferred grain orientation by X-ray techniques and to compute the average effect on the velocity of ultrasonic wave propagation once the grain orientation has been determined. This approach would be extremely difficult.

B. Destructive Test

The second method of study of the problem is to perform a complete stress analysis of various types of specimens and make a comparison to destructive tests of the specimens. An important factor in such a study is the possible effects of the destructive procedures upon the sample. Before proceeding with such studies, a number of exploratory measurements were performed. It had been established that stress due to external loads could be measured accurately. Samples were therefore selected which could be permanently deformed by application of stresses exceeding the elastic limit of the material. In order to introduce stresses which could be studied in detail, long bars were subjected to bending for which a permanent bend was caused by the loading of the bar.

The bars were instrumented with strain gages so that the amount of permanent deformation could be determined. These measurements were supplemented by measurements of the change in shape of the bar. Measurements of the stress along the bent surface of the bar were made during the loading of the bars and again during the unloading. Immediately after unloading the bars, large stresses were observed near the surface and at the location of maximum curvature of the bar. Within twenty four hours after bending the bar, the apparent stress appeared to be relieved. These experiments were designed to show that actual residual stresses could be measured. The results appeared somewhat inconclusive since the amount of residual stress created was relatively small after the sample had been allowed to exhibit recovery. The experiments furthermore, did not appear to eliminate other effects as was necessary.

A further approach was to obtain measurements on samples for which the residual stress could be confirmed by destructive measurements. Since the net force on a sample subject to no external loads must be zero, it would be possible to account for the stress and any excess effects must be due to other effects such as grain orientation. First, a series of one half inch thick plates were examined with the ultrasonic measuring techniques. Measurements of the apparent stress through the thickness of the material and near the surface were obtained. The plates were 9 inches in length and 5 inches in width. Successive 1/4 inch wide strips were cut from each

side of the width of the plate. Micrometer measurements of the length were made at the location of each strip before and after cutting the strip from the sample. In this manner it was possible to compute the change in length of the strip and the resultant change in dimensions of the remainder of the plate. The average stress along the strip could then be computed with a knowledge of Young's modulus for the material.

Each plate was cut from a larger plate of the selected alloy of aluminum. Samples were cut which were along the direction of rolling and others were cut which were perpendicular to the direction of rolling. The maximum stress averaged along the length of any strip was less than 1000 pounds per square inch. The apparent bulk stress as measured by the ultrasonic methods was relatively uniform throughout the plates and showed a magnitude of as much as 15,000 psi. In other words, these particular plates appeared as if there was a uniform loading of the plate, which is impossible since there were no external forces. Furthermore, the destructive tests indicated that there was no corresponding change in dimensions of the plate which would account for the apparent stress. The effect which was measured in these plates is therefore due to other causes, primarily preferred grain orientation.

The next question was concerned with the measurement of actual residual stresses superimposed upon the effective stress as measured ultrasonically and caused by grain orientation. A series of measurements were performed in similarly shaped samples containing weldments. An extensive discussion of the results of stress measurements on welded plates is contained within a latter section of this report. The present discussion is concerned with the effects of other causes on the ultrasonic measurement of stress. The plates containing weldments are ideally suited to answer the present question concerning the separation of grain orientation from actual residual stress, since it has previously been determined that the presence of a weldment introduces considerable residual stress.

The plates selected were of the same alloys of aluminum as had been previously studied. The plates contained a butt weldment down the center of the plate. The first samples

had the weldment along the 9 inch length dimension with 3 3/4 inches of material each side of the weldment. For these studies eight locations were chosen for the ultrasonic measurement of bulk stress as illustrated in Figure 23. The sample was marked in 1/4 inch segments across its width and a micrometer was used to measure the approximate 9 inch length of each 1/4 inch segment. A pair of 1/4 inch strips were cut from the two sides of the plate, with measurements being made of each cut segment and an additional measurement of each 1/4 inch segment remaining in the plate. The ultrasonic stress measurements were also made after each pair of strips were cut. A complete history of the change in dimensions of the plate was therefore obtained along with the measurements of the apparent stress.

The stress distribution was then computed for each segment of the plate as it existed within the plate at the beginning of the experiment. The change in stress, as measured ultrasonically, was computed after each pair of segments was removed and compared to the change in stress indicated by the dimensional changes of the sample. Good agreement was obtained ultrasonically. The ultrasonic measurements are shown on the graph in Figure 24 indicating the close agreement to the destructive data. The destructive data shows the average stress along a 1/4 inch wide segment of the material as it existed in the sample before the first segment was removed.

It should be noted that the stress distribution in the welded plate indicates that there is a tensile stress averaged along the length of the weld and extending approximately 1/2 inch to each side of the weld. The remainder of the plate is in compression opposing the stress created by the weld. The magnitude of the average tensile stress is approximately 11,000 psi along the weld and the average compressive stress counteracting the weld stress is approximately 4000 psi. The ultrasonic measurements indicated that the stress along the weld varied considerably from the average being 12,700, 17,500, 10,700, 10,700, and 6,400 at the five locations which average to be equal to a stress of 11,600 psi as indicated in the Figure. It has therefore been shown that the ultrasonic method of measuring stress correlates with destructive tests, but is capable of showing the stress distribution in detail. The presence of grain orientation effects indicates that it is necessary to make measurements

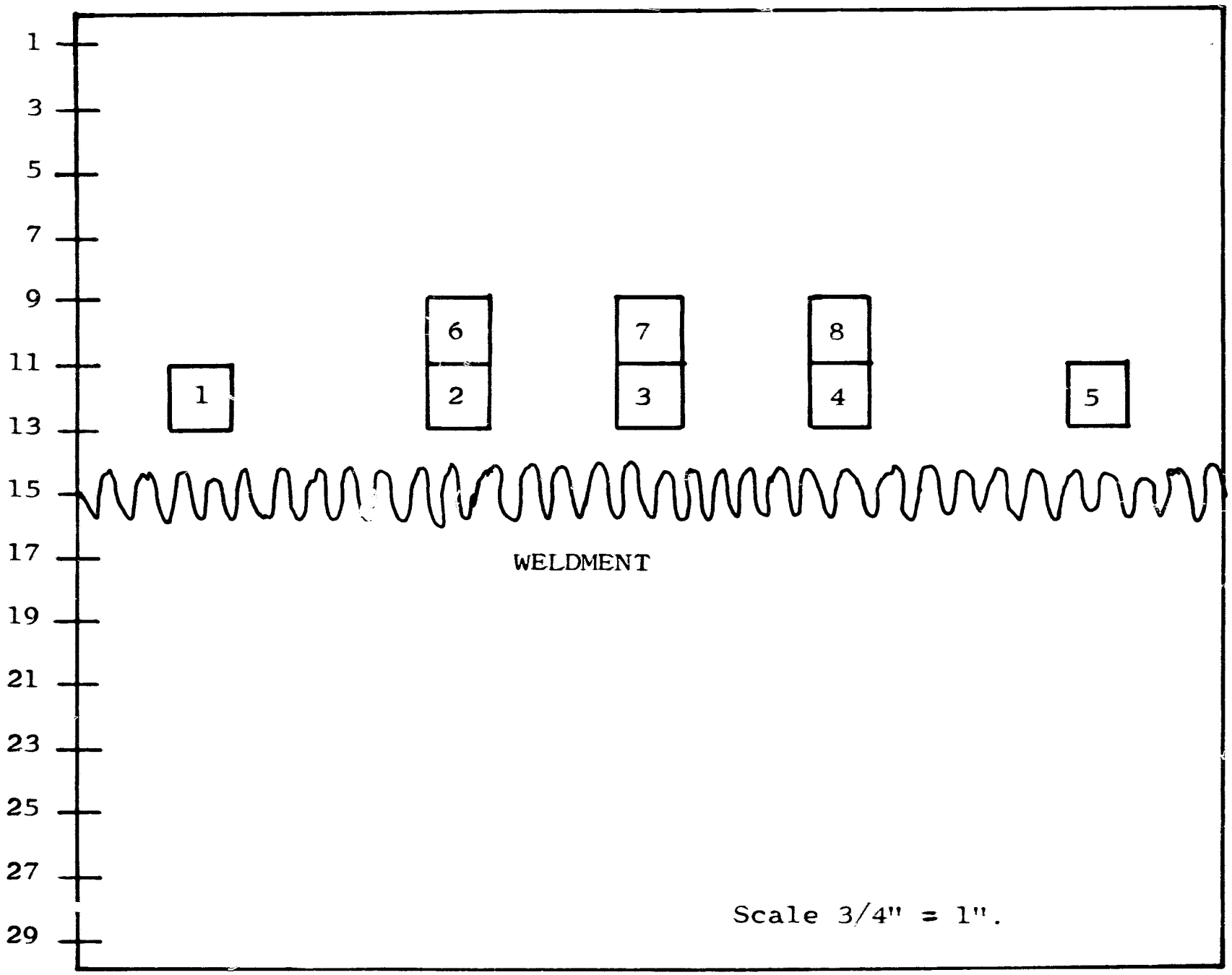

Figure 23. Illustration Showing Locations of Ultrasonic Measurements and $\frac{1}{4}$" Segments.

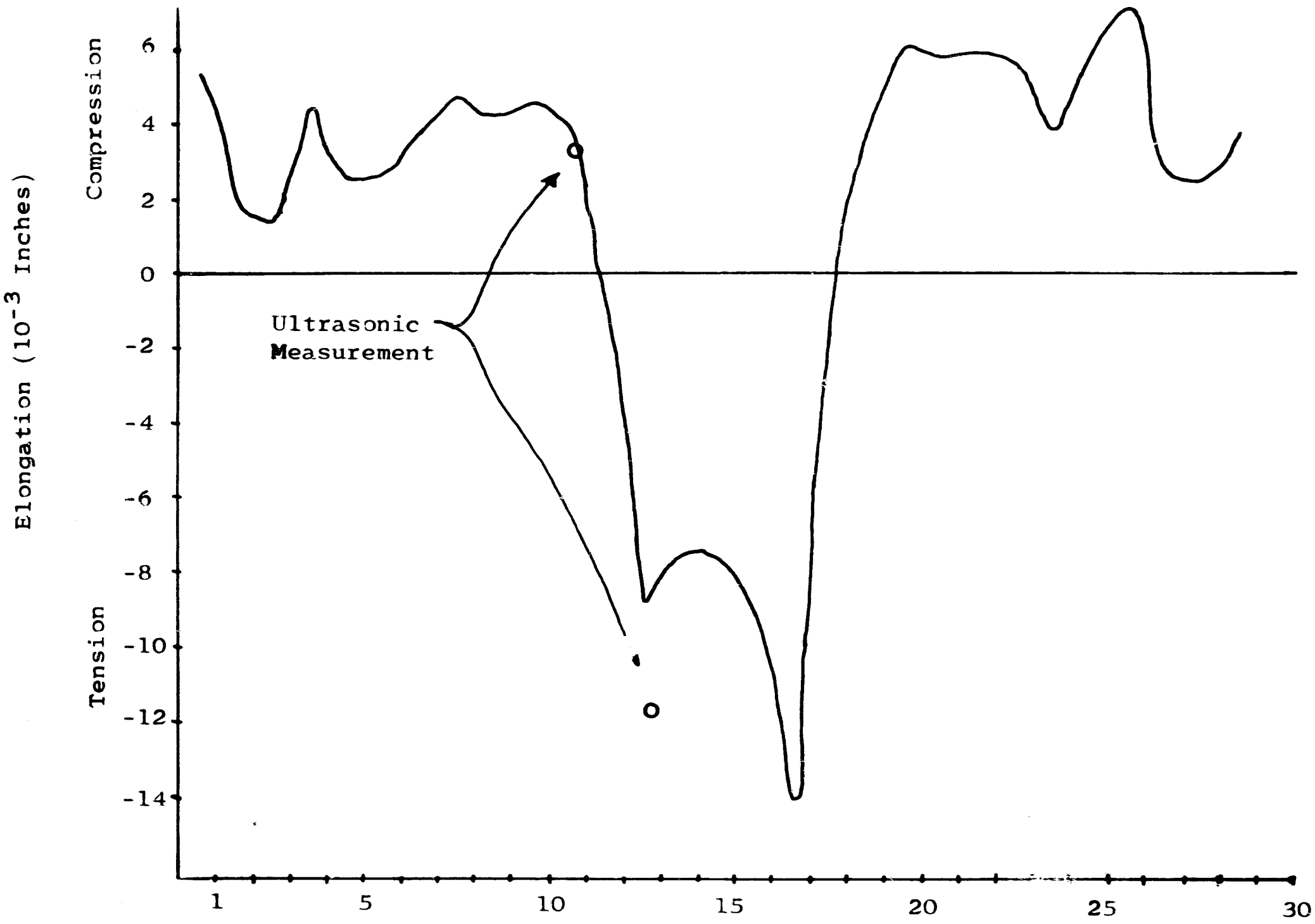

Figure 24. Elongation Change of $\frac{1}{4}$" Segments versus Segments Location.

on the plate before and after welding or it is possible to determine the effect of grain orientation on an average for typical plates of a particular geometry and alloy, and to then measure residual stress with some sacrifice in accuracy.

Due to the marked effect of the grain orientation on the absolute measurement of stress, it would appear that some effect might be observed on the elastic properties of the material. The ultrasonic measurements indicated that the Alloy 2014-T651 had an apparent stress due to grain orientation of 7,000 psi which appeared if the plate was in tension along one axis of the material. In order to examine this property of the material, a series of samples were cut from this particular alloy with half of the samples being oriented along the direction of the apparent tension and half being oriented transverse to the direction of apparent tension. The samples were then subjected to a destructive stress-strain determination performed in the Testing Laboratories of NASA at Huntsville, The actual stress strain curve for 2014-T651 is shown on the right of Figure 25. The solid curve is typical of those samples having the major axis of apparent stress transverse to the length of the sample and the dotted curve is typical of those samples having the major axis parallel to the length of the sample. It is noted that the proportional portion of the stress strain curve is lower for those samples which appear to be in tension due to grain orientation as compared to those samples which appear to have the transverse elements in tension. Furthermore, the difference in proportional limits is approximately 20,000 psi which is the amount of apparent tension 15,000 psi plus one third of the apparent tension. The tension in the transverse samples would be acting on a portion of the sample where the strain is due to Poisson's Ratio, so that the effect should be approximately one third in the opposite direction. It is most interesting, therefore, that the stress-strain curve for this particular alloy indicates an effect which is also revealed by the ultrasonic measurement. Even though the grain orientation must be accounted for in determining the actual residual stress in a sample, there is some effect on the elastic properties which may be determined by the ultrasonic measurements.

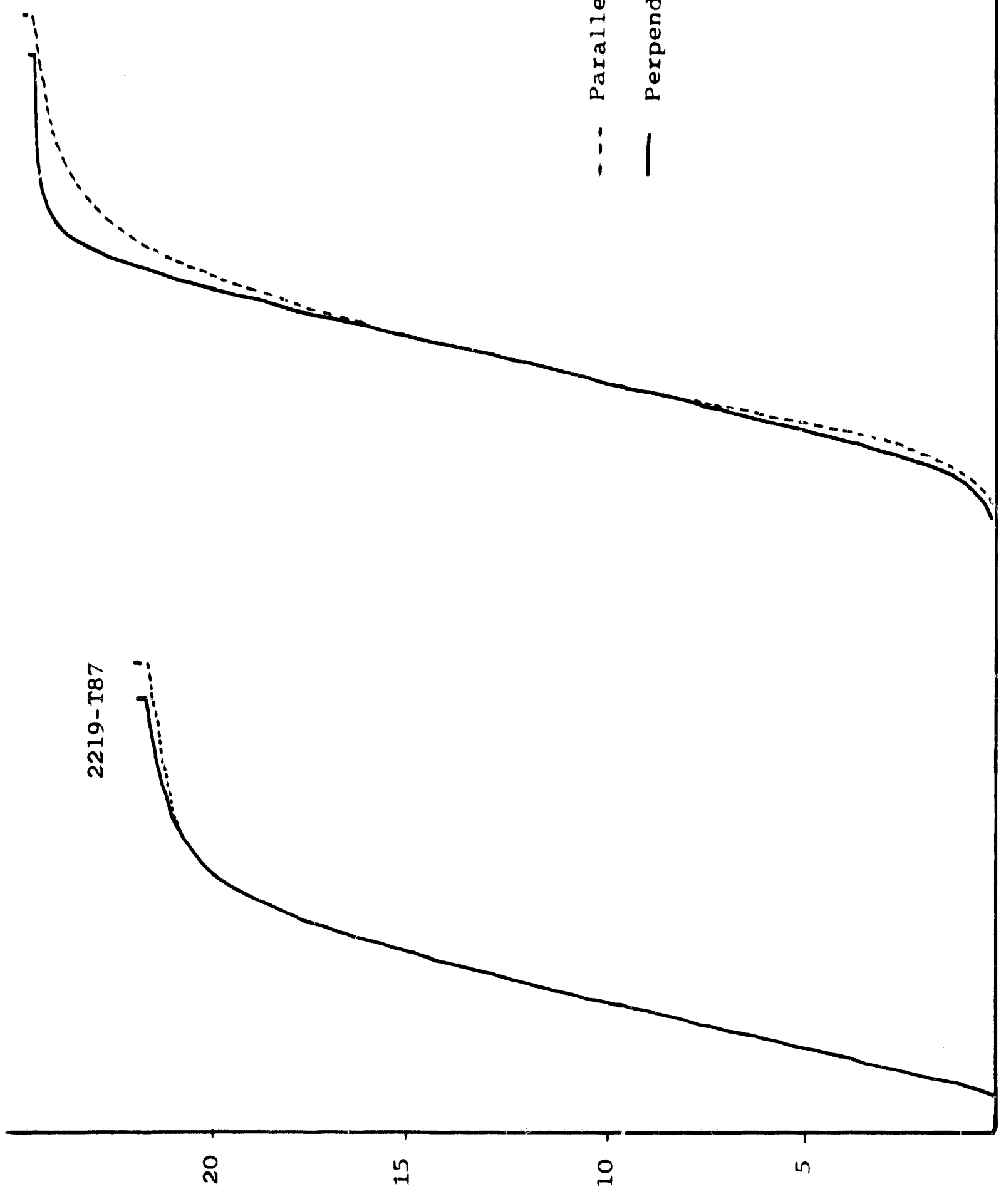

Figure 25. Stress - Strain Curves for Alloy 2014-T6 and Alloy 2219-T87.

The curve on the left of the Figure is plotted for similar samples of Alloy 2219 for which the apparent stress as determined ultrasonically was 7,000 psi. It is noted that the proportional limits for samples along and transverse to the axis of apparent tension are identical for this particular alloy. The actual curves appeared to contain differences, but the instrumentation was not sufficiently sensitive to allow for a confirmation of any effect.

These particular experiments must be considered exploratory and no absolute conclusions can be reached. It is an area of study that should be pursued since a method of measurement is now available which may lead to a better understanding of the behavior of metallic materials. At the present time, it is necessary to determine the effective stress as caused by grain orientation as measured by the ultrasonic methods. The effective stress may be measured precisely on a particular sample or an average determined for a particular plate or bar of a given alloy. The effective stress as indicated by grain orientation must then be subtracted from any subsequent measurements such as those caused by the welding process. Further study of the elastic properties of materials having marked grain orientation may reveal a new approach to the behavior of materials. The present data is insufficient to effectively assess the importance of grain orientation on the elastic properties of metals.

VI. INSTRUMENTATION

A. Circuit Description of the Frequency Null System

An instrument designed to measure surface stress was constructed based on the frequency null technique. The principle of operation of this instrument was discussed earlier in this report, and the block diagram is shown in Figure 4. A circuit diagram is shown in Figure 26. The RF oscillator is a continuous wave, variable frequency oscillator covering the range from 6 to 8 MHz and has a frequency stability of 1 part in 10^5. Its output is fed into an emitter follower isolating stage of Q_2. From this point, the continuous RF signal is fed to three separate sections of the system, the driving gated amplifier, the reference pulse gated amplifier and the frequency counter.

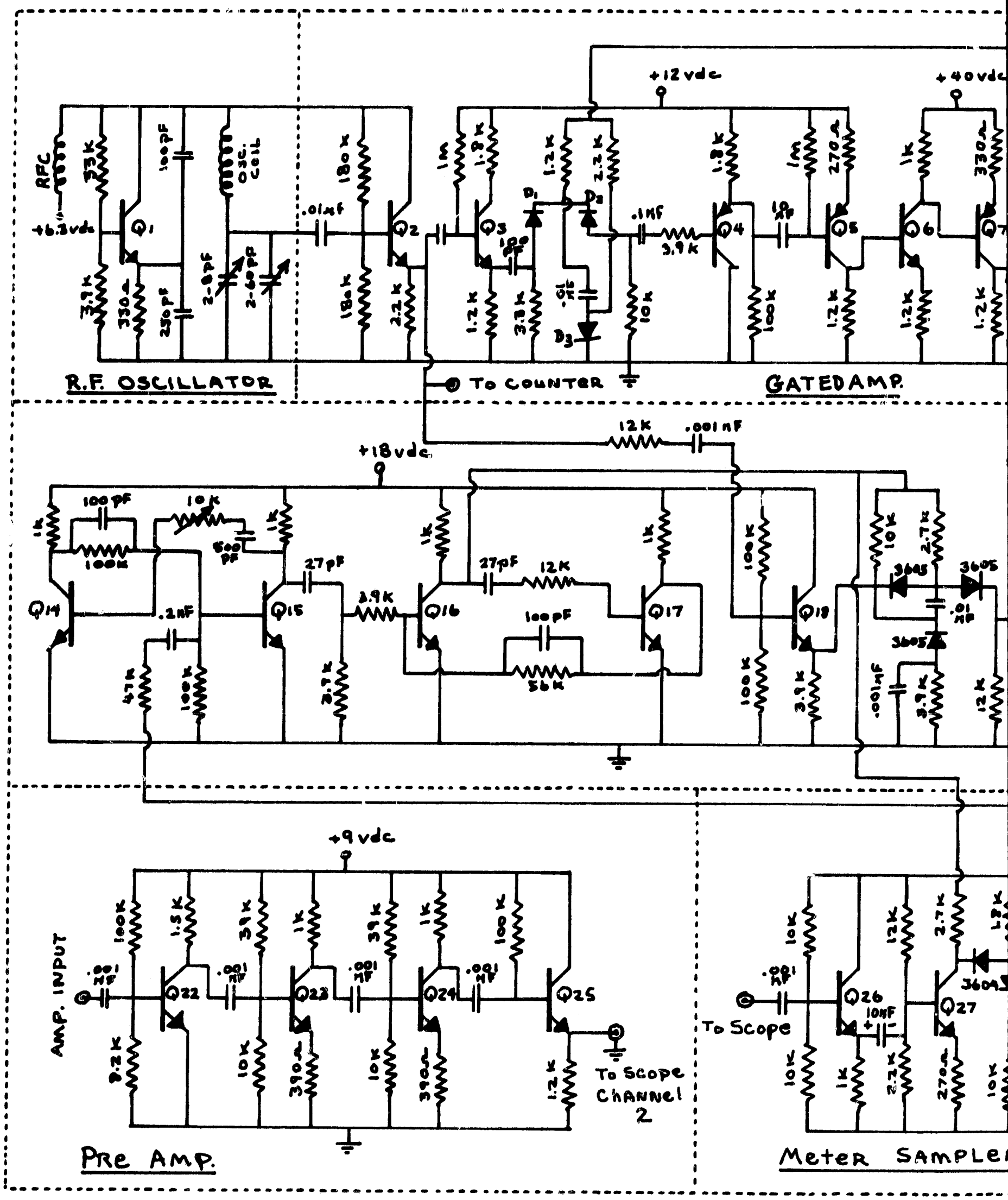

Figure 26. Circuit Diagram of the Frequency Null Instrument.

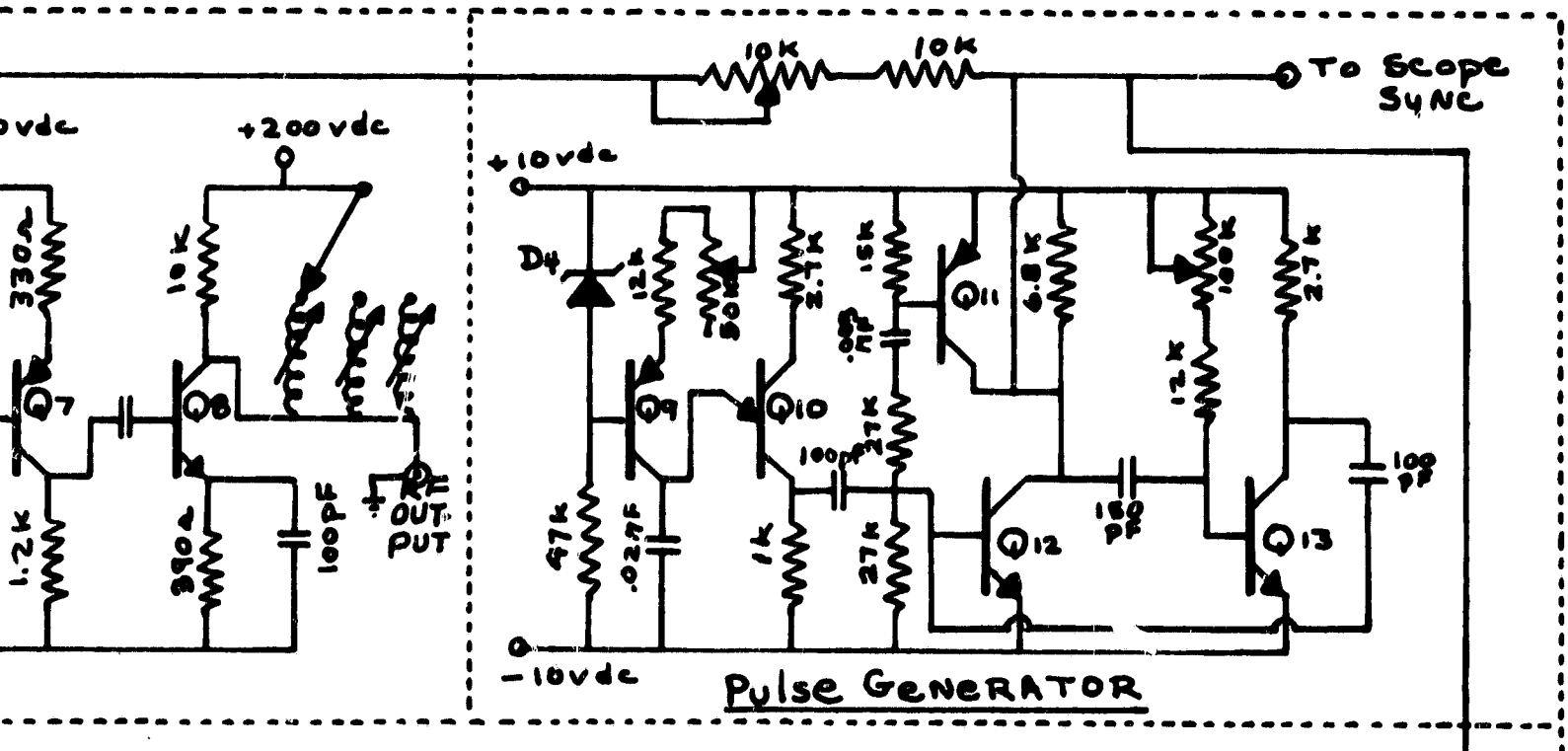
+200 vdc
330
10K
Q7
Q8
1.2K
390
100pF
RF OUTPUT
10K
10K
To Scope Sync
+10 vdc
D4
Q9
Q10
Q11
Q12
Q13
47K
.027
1K
27K
150 pF
100 pF
-10 vdc
Pulse Generator

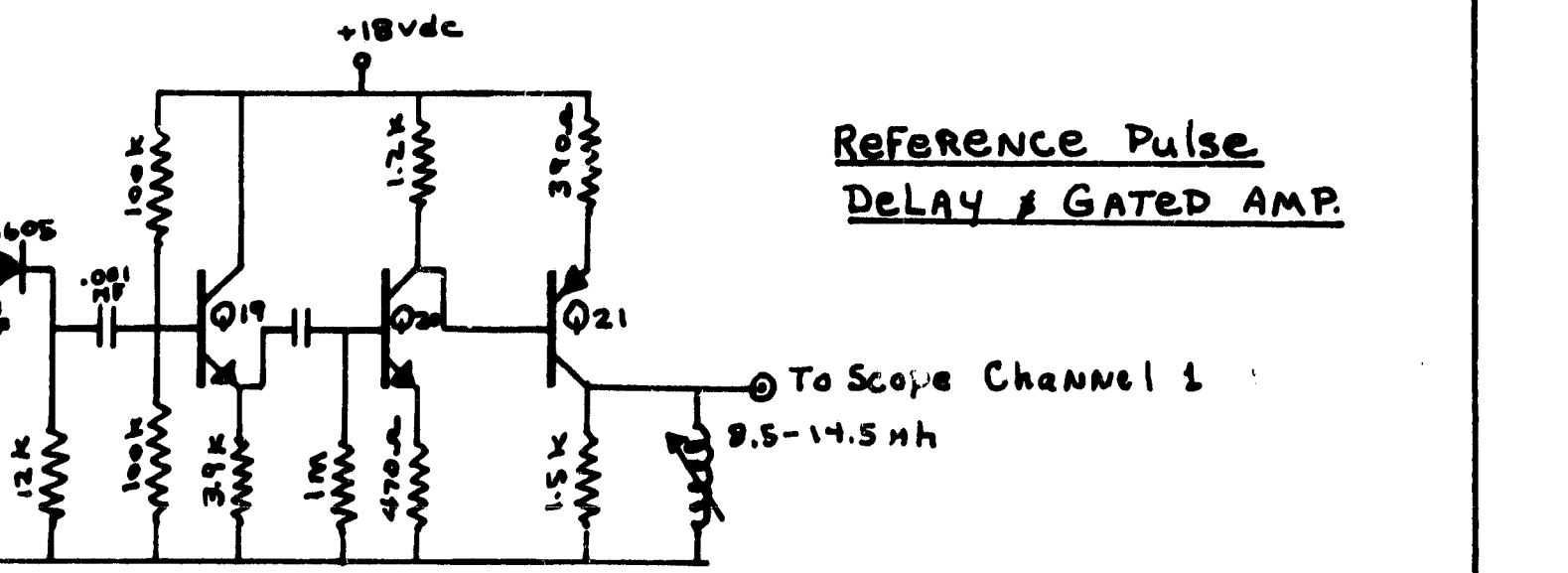
+18 vdc
100K
.001 MF
Q19
Q20
Q21
39K
470
1.5K
To Scope Channel 1
9.5-14.5 mh
Reference Pulse
Delay & Gated Amp.

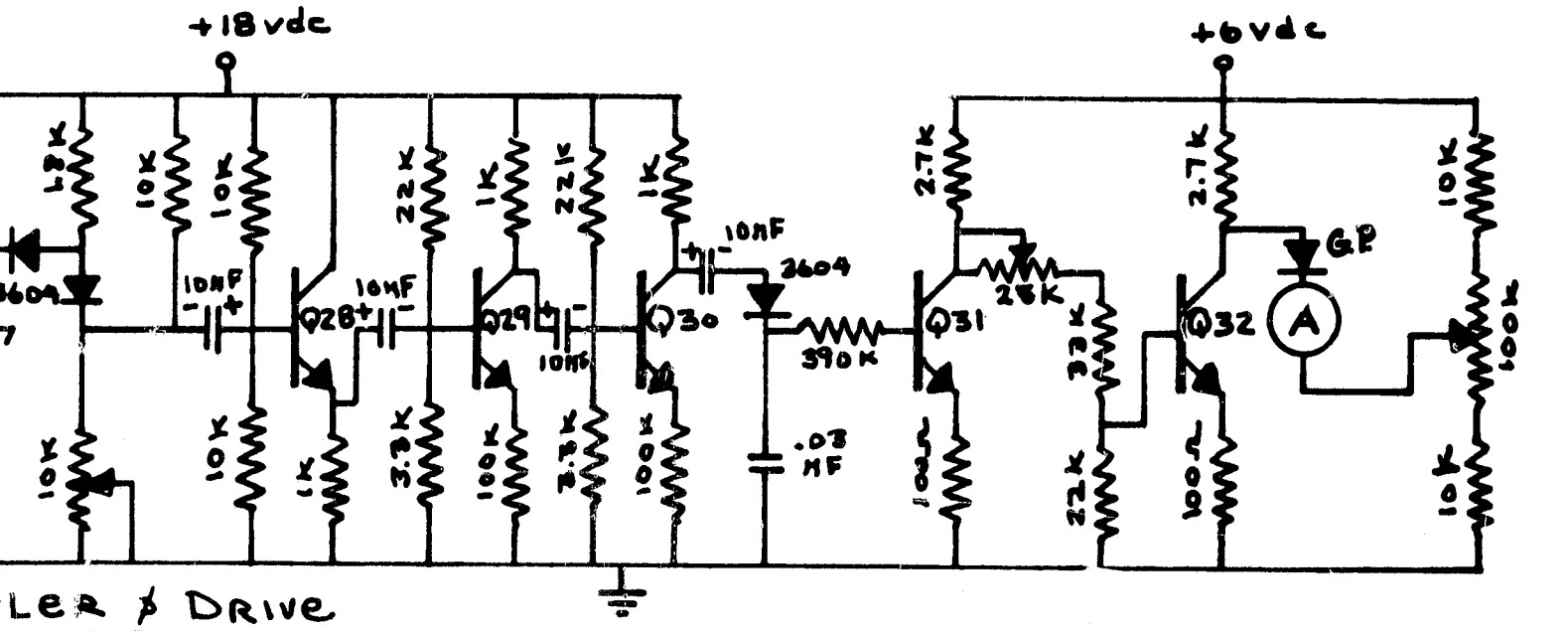
+18 vdc
+6 vdc
10MF
2604
Q28
Q29
Q30
Q31
Q32
390K
.03 MF
25K
GP
A
2.7K
22K
100
10K
ler & Drive

Fig. 26-A

The driving gated amplifier consists of an input stage Q_5, which drives a diode gate arranged in a "Tee" configuration. The gating of the continuous RF signal occurs when the output of the pulse generator goes negative with respect to ground thereby forward biasing D_1 and D_2, and reverse biasing D_3. When the gating pulse goes positive, D_1 and D_2 are then biased in the reversed mode while D_3 is biased in the forward direction. Therefore, the RF signal is allowed to pass through the gate during the time the output of the pulse generator is negative, but is greatly attenuated when the pulse generator output is positive. The "on to off" ratio at the gate output is better than 40 db.

It is noted that during the time the gate is in the "on" mode its output has a negative DC offset which serves to properly bias Q_4 from cutoff into Class A operation. This then allows the signal to pass into the amplifying stages of Q_5, through Q_8. In each of the amplifying stages, advantage of the DC offset is taken so that each of these stages also go from cutoff during the "off" period to Class A operation during the "on" period. Note that the amplifying stages are alternately NPN and PNP transistors to correct for the change in polarity of the DC offset voltage after each stage of amplification. By this technique, a further increase of 40 db in the "on-to-off" ration is obtained.

The collector circuit of Q_8 is the output for the RF driving pulse feeding the transducer assembly. This particular stage, referred to as the high voltage amplifier, has an RF output of 150 volts peak to peak. The switchable, variable inductors in the collector circuit serve to eliminate the DC offset and form a low "Q" parallel resonant circuit with the output cable capacity connecting to the transducer assembly.

The continuous wave RF output of the oscillator is also fed to a second gated amplifier, the reference pulse gated amplifier. This gated amplifier operates in a similar manner to the main or RF driving pulse gated amplifier discussed above. The oscillator signal reaches Q_{18} and is then gated into the amplifying stages of Q_{19}, Q_{20}, and Q_{21}. The RF pulse output of the latter stage is fed to channel 1 of the oscilloscope used in the system.

A very basic part of the total system is the pulse generator. Transistors Q_9 and Q_{10} form a relaxation oscillator which serves to trigger the single shot multivibrator formed by Q_{11}, Q_{12}, and Q_{13}. From the circuit diagram it is seen that when the 0.02 microfarad capacitor in the collector circuit of Q_9 charges to a certain value, the unijunction transistor Q_{10} breaks down. When this occurs a triggering pulse is derived which turns transistor Q_{12} to the "on" mode. Transistor Q_{13} then goes into the "off" mode for a time depending on the variable time constant in the base circuit of Q_{13}. At the time Q_{13} resumes conduction, Q_{12} is again returned to the off mode by the differentiating circuit from the collector of Q_{13} to the base of Q_{12}. It is also noted that Q_{11} goes into a short period of conduction at the same time, shunting the collector load resistor of Q_{12}. By this means a fast rise time of the output pulse of the pulse generator is obtained.

Transistor Q_{12} then remains cut off until another trigger-pulse is received from the relaxation oscillator. Note that the repetition time of the relaxation oscillator can be controlled by changing the charging rate of the 0.02 capacitor with the variable resistor in the emitter circuit of Q_9. Therefore, the output pulse of the generator has a variable repetition rate which varies from 300 to 1200 pulses per second. Also the time duration or width of the output pulse is controllable from 1 to 10 microseconds by the variable resistor in the base circuit of Q_{12}.

The output of the pulse generator which goes from +10 to -10 volts during the time Q_{12} is conducting, is fed to three points in the system. It is connected through a variable resistor to the diode gate of the main gated amplifier which drives the transducer assembly. The variable resistor controls the amplitude of the DC offset in the amplifying stages to give the maximum RF output at Q_8. In addition, the pulse generator output is AC coupled to the pulse delay circuitry comprised of Q_{14} through Q_{17}. Transistors Q_{14} and Q_{15} form a single shot multivibrator which has a controllable period with the 10,000 ohm potentiometer in the base circuit of Q_{14}. When the output of the pulse generator goes negative Q_{15} is cut off. At the time Q_{15} resumes conduction, depending on the time constant in

the base circuit of Q_{14}, a positive going voltage spike occurs at the base of Q_{16}. Both Q_{16} and Q_{17} form second single shot multivibrator. Normally Q_{16} is cut off while Q_{17} is conducting. When the positive spike is received at Q_{16} the conducting state of these two transistors is changed for a period of time determined by the RC time constant in the base of Q_{17}. This time constant is such that the positive output pulse at the collector of Q_{16} has a duration of 1.5 microseconds. Therefore, a positive pulse occurs at the output of the pulse delay circuit for a duration of 1.5 microseconds at some time after the negative pulse occurs at the pulse generator output. The exact time at which the delayed pulse occurs is controlled by the variable time constant of the single shot multivibrator of Q_{14} and Q_{15}. With the component values shown in Figure 26 a delay of 3 to 30 microseconds is obtained.

Before the sampling circuit is discussed, it is convenient to consider another portion of the system. The transducer assembly used with the frequency null system is the double lucite wedge previously discussed. Briefly, this assembly has a sending crystal and a receiving crystal. The sending crystal is supplied with the RF driving voltage from the gated amplifier. The received ultrasonic signal is amplified by the preamplifier. Referring to Figure 26, it is seen that the preamplifier is a standard broad band RC coupled amplifier. The amplifier consists of three amplifying stages, Q_{22}, Q_{23}, and Q_{24}, followed by the emitter follower stage of Q_{25}. Typically, the gain of the preamplifier is 60 db at 7 MHz. Its output is fed into channel 2 of the oscilloscope.

The oscilloscope used in the system is a Tektronix Type 422. It is dual channel with a vertical deflection system covering a frequency range from DC to 15 MHz. As has been mentioned above, the oscilloscope receives inputs from three sections of the frequency null system. A synchronizing pulse is supplied by the pulse generator in order to initiate a trace at the beginning of every RF driving pulse. Channel 1 of the oscilloscope receives the RF pulse from the reference pulse gated amplifier while channel 2 is connected to the preamplifier output which is the received ultrasonic signal. Provision is made in the oscilloscope circuitry so that the

signals in channel 1 and 2 can be added (or subtracted), presented on alternate sweeps, or viewed separately. By properly delaying the gating pulse from the pulse delay section of the frequency null system, it is possible to make the RF reference pulse occur during the time of the received ultrasonic signal. A typical illustration of the time relationships between the RF driving pulse, the received signal, and the reference pulse are shown in Figure 5.

B. Operation of the Frequency Null Instrument

During the normal mode of operation of the frequency null system, the oscilloscope adds the received signal with the reference signal. Therefore, when these two RF signals are 180° out of phase a null is achieved. To make the actual reading of the null easier, a sampling circuit was added to the system. This circuit is comprised of transistors Q_{26} through Q_{30}. From the block diagram of the system, it is seen that the sampling circuit receives inputs from the oscilloscope and from the pulse delay circuit. The input signal at Q_{26} is derived internally from the vertical amplifier section of the oscilloscope. The control pulse which gates the reference pulse gated amplifier is also fed to the collector circuit of Q_{27}. When this pulse is present, Q_{27} amplifies the signal present at the emitter of Q_{26} and allows further amplification by stages Q_{28}, Q_{29}, and Q_{30}. In other words, the sampling circuit behaves like a gated amplifier which only amplifies during the time when the RF reference pulse is generated.

As a result when the oscilloscope is in the add mode, the sampling circuit amplifies the resulting addition of the reference pulse and received pulse only during the time that the reference pulse is generated. Note than an amplitude detecting circuit is employed in the collector circuit of Q_{30}. The voltage appearing on the 0.03 microfarad capacitor in this collector circuit is a DC voltage proportional to the amplitude of the added reference and received pulse. The DC voltage is further amplified by stages employing Q_{31} and Q_{32}. An ammeter is driven by the output of Q_{32}. Therefore, when the resultant voltage of the added signals is a minimum, the null meter reads

a minimum value. Sensitivity of the meter drive is varied by the 25,000 ohm potentiometer in the collector of Q_{31} while the position of the meter pointer is controllable by the 100,000 ohm potentiometer in the collector of Q_{32}. Now that the functional description of the circuitry of the frequency null system has been discussed, the following section gives a discussion on how the system is used to make an ultrasonic surface stress analysis measurement.

First, a location on a sample is chosen and the double lucite wedge transducer assembly is applied. In Figure 27, it is seen that the transducer assembly is centrally loaded by a loading frame apparatus. The force applied to the assembly is of the order of 100 pounds. This enables the generation and reception of ultrasonic surface waves without the use of any couplant. The RF output pulse from the gated amplifier is connected to either one of the BNC connectors of the transducer assembly by means of a coaxial cable. The other connector of the assembly is likewise connected to the preamplifier of the instrument. The front panel of the instrument is shown in Figure 28.

When the instrument is first turned on, a five minute warm up period should be allowed. Initially, the frequency of the oscillator is adjusted for approximately 7 MHz, which is indicated by the readout of the frequency counter. The trigger function switches on the oscilloscope are set in the external, AC, and negative slope positions. This allows the oscilloscope to trigger on the negative pulse from the pulse generator when the trigger level control is adjusted properly. The horizontal sweep is then set to the 5 microsecond per centimeter range.

If the mode switch of the oscilloscope is placed in the alternate position with AC coupling, it is possible to observe the reference RF pulse on the channel 1 trace while the trace of channel 2 displays the received ultrasonic surface wave. It may be necessary to adjust the tuning coils at the output of the RF pulse gated amplifier to compensate for the cable capacity. Also the pulse amplitude control (PAC) is adjusted

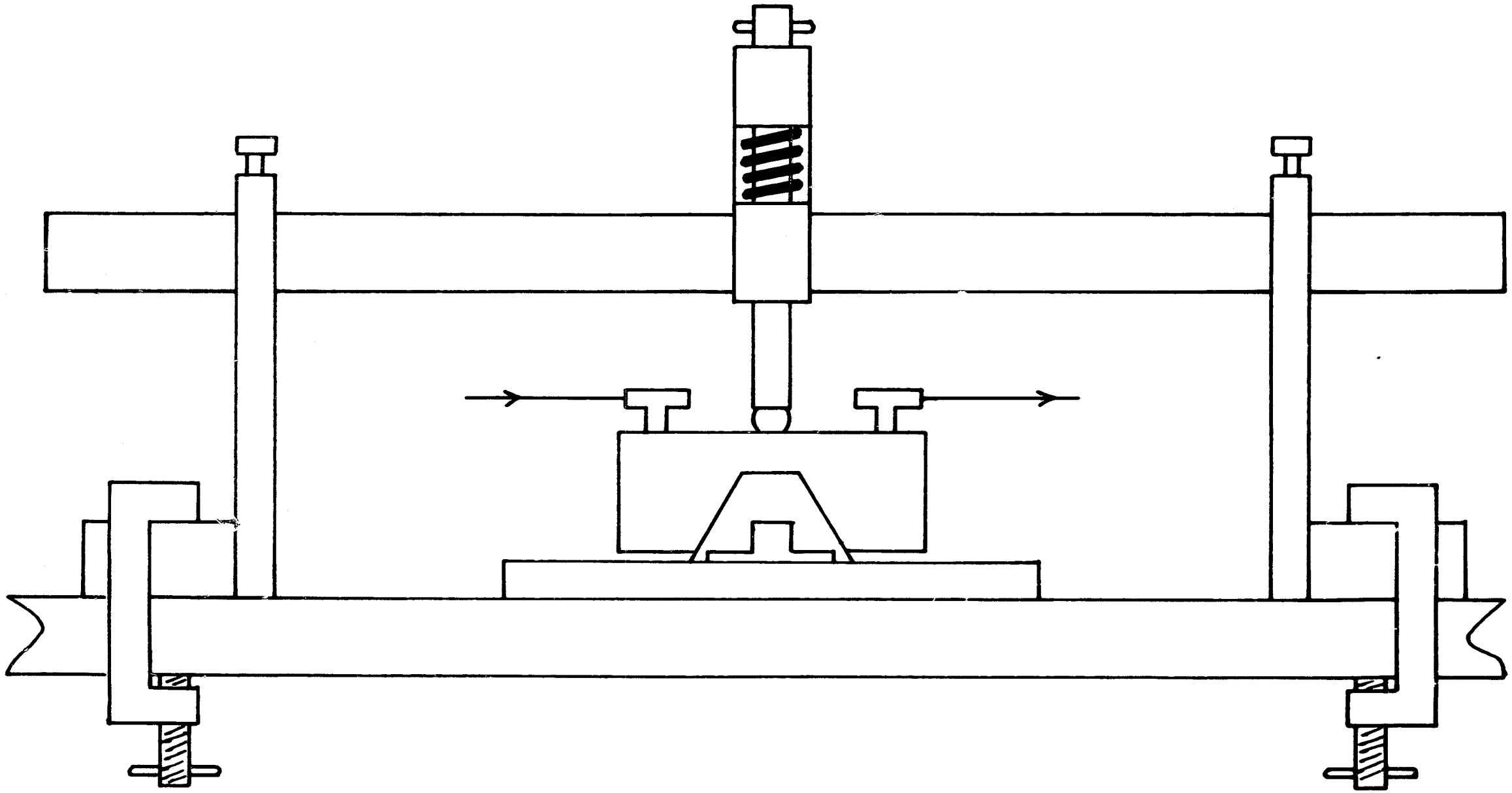

Figure 27. Loading Frame Apparatus Used to Load the Surface Wave Transducer Assembly.

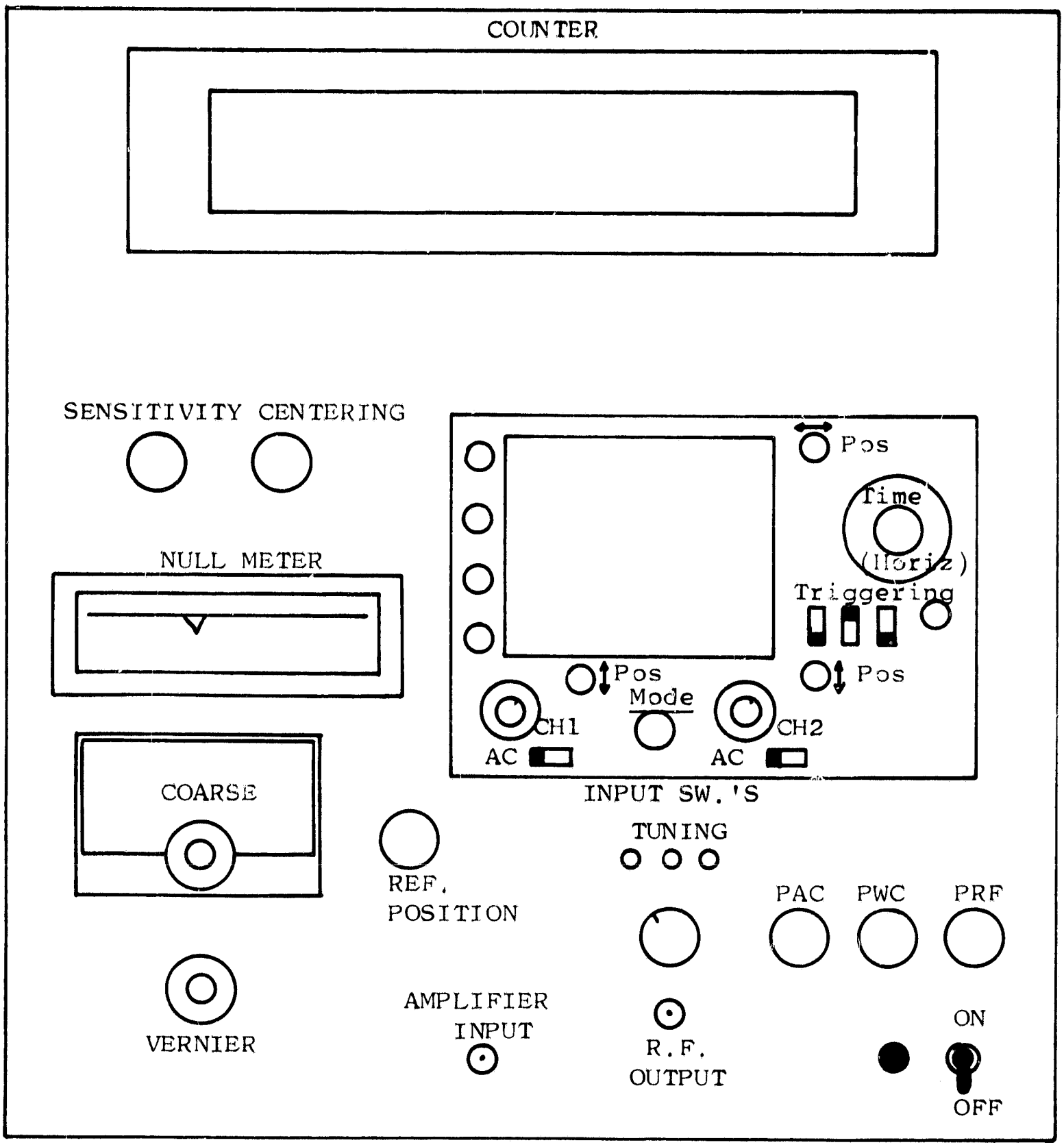

Figure 28. Front Panel of Frequency Null Instrument Showing Controls Position.

for a maximum undistorted signal on trace of channel 2. Once the received signal is optimized, the pulse width control (PWC) is adjusted so that the received pulse has a width of approximately 8 microseconds. Also the pulse repetition frequency (PRF) is adjusted to give an output pulse once every millisecond. This is accomplished by switching the sweep time to 1 millisecond per centimeter and observing one pulse every millisecond.

The sweep time is then returned to the 5 microsecond per centimeter position, and by the use of attenuator controls on the two channels of the oscilloscope, the reference pulse and received pulse are adjusted so that they are approximately the same amplitude. The reference pulse position control is now adjusted so that the reference pulse occurs during the midportion of the received signal.

The oscilloscope is now placed in the add mode, which adds the incoming signals on channel 1 and 2. The coarse frequency adjustment of the oscillator is turned until a minimum signal is obtained during the time of the reference pulse as viewed on the oscilloscope trace. By using the vernier oscillator adjustment and the variable attenuators of the scope inputs, a better null is obtained. An illustration of the oscilloscope presentation of a proper null is shown in Figure 29. Further adjustment of the vernier frequency control and observation of a minimum indication on the null meter gives the proper frequency for the null occurance. This frequency is then read from the frequency counter.

The transducer is then rotated on the sample at the same location, usually in 10^{o} increments. For each new position the amplitude and frequency controls are adjusted until a minimum is read on the null meter. Once again the frequency at which the null occurs is observed and recorded. Therefore, the variation of surface wave velocity at the chosen location versus orientation can be observed.

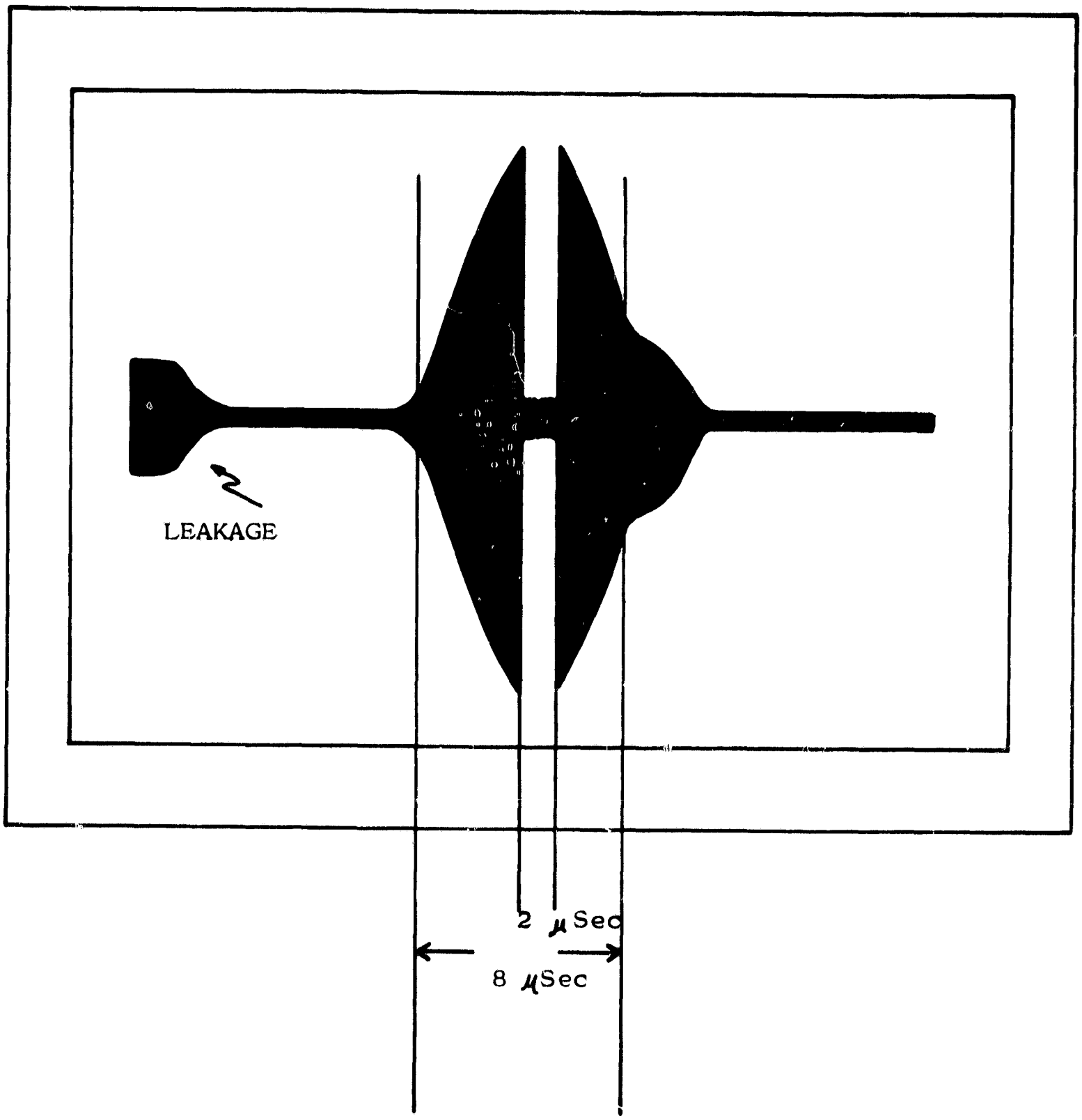

Figure 29. Oscilloscope Presentation Illustrating Proper Signal Null.

VII. ULTRASONIC STRESS ANALYSIS APPLICATION

A. Introduction

The measurement of residual stress in plates containing weldments was incorporated within the general scope of this program as a practical application of ultrasonic stress analysis. The objective of this portion of the program was to investigate the stress distribution in plates of two thicknesses and two alloys of aluminum which contained butt weldments. This objective was incorporated within the program, before all of the stress measuring techniques described thus far had been developed. This particular application allowed for the further development of techniques since actual problems, typical of those that might be encountered in the field, were introduced. This section of the report deals primarily with the results of the stress measurements, but necessarily includes a discussion of the techniques which had to be developed to allow for the desired measurements.

B. Destructive Tests of Welded Plates

The stress distribution in plates containing weldments has been the subject of previous investigation using both destructive type tests[1] and tests involving the use of strain gages.[2] As in other investigations, it is of value to understand as much as is available concerning the problem under investigation. For this reason, a number of measurements were made as

---

[1]Private Document from Earl Hasemeyer entitled "A Method of Estimating Residual Stresses in 0.25 inch Thick 2219-T87 Aluminum Alloy Plate Weldments," September 11, 1967.

[2]Report SM-49077, "Residual Stresses in Mig Welds," Missile and Space Systems Division, Douglas Aircraft Company, Inc., Santa Monica, California. October 1965.

an extension of previous investigations, to supplement the measurements which were made by the ultrasonic methods of stress analysis. First, a duplication of the destructive tests of a sample containing a weldment was performed.

The techniques employed by Hasemeyer, et al, were followed on a test specimen one half inch thick and of aluminum Alloy 2014-T6. The weldment was in the center of the 9 inch length dimension with two and one half inches of material each side of the weldment. The procedure was to measure the change in length of the weld as succeeding 1/4 inch wide segments were removed symmetrically about the weld. From these measurements it was possible to compute the average stress existing along the weld. The results of the initial measurements were in close agreement with Hasemeyer.

The procedure was then varied to allow for a determination of the actual stress that existed throughout the plate so that a check of ultrasonic measurements could be performed. The new procedure involved the measurement of the deformation of plates containing weldments which were either along the length of the plate or transverse to the plate. Measurements were made of the length of each 1/4 inch wide segment of the plate before and after each pair of 1/4 inch wide segments were removed from the plate. In this manner a complete history of the stress change in the plate was obtained. The results of these measurements are given in Figures 30 and 31. In Figure 30 the plate contained a weldment along the length of the plate and in Figure 31 the weldment was along the width of the plate.

It is seen that there is a tensile stress along the weldment extending approximately 1/2 inch to each side of the weldment. The remainder of the plate is in a state of compression along the length dimension. There is also a state of tension in the central portion of the plate transverse to the weld. Again the outer portions of the plate are in compression. It is further noted that the tensile stress is more concentrated along the length of the weld than it is transverse to the weld. The true stress distribution in the plate must

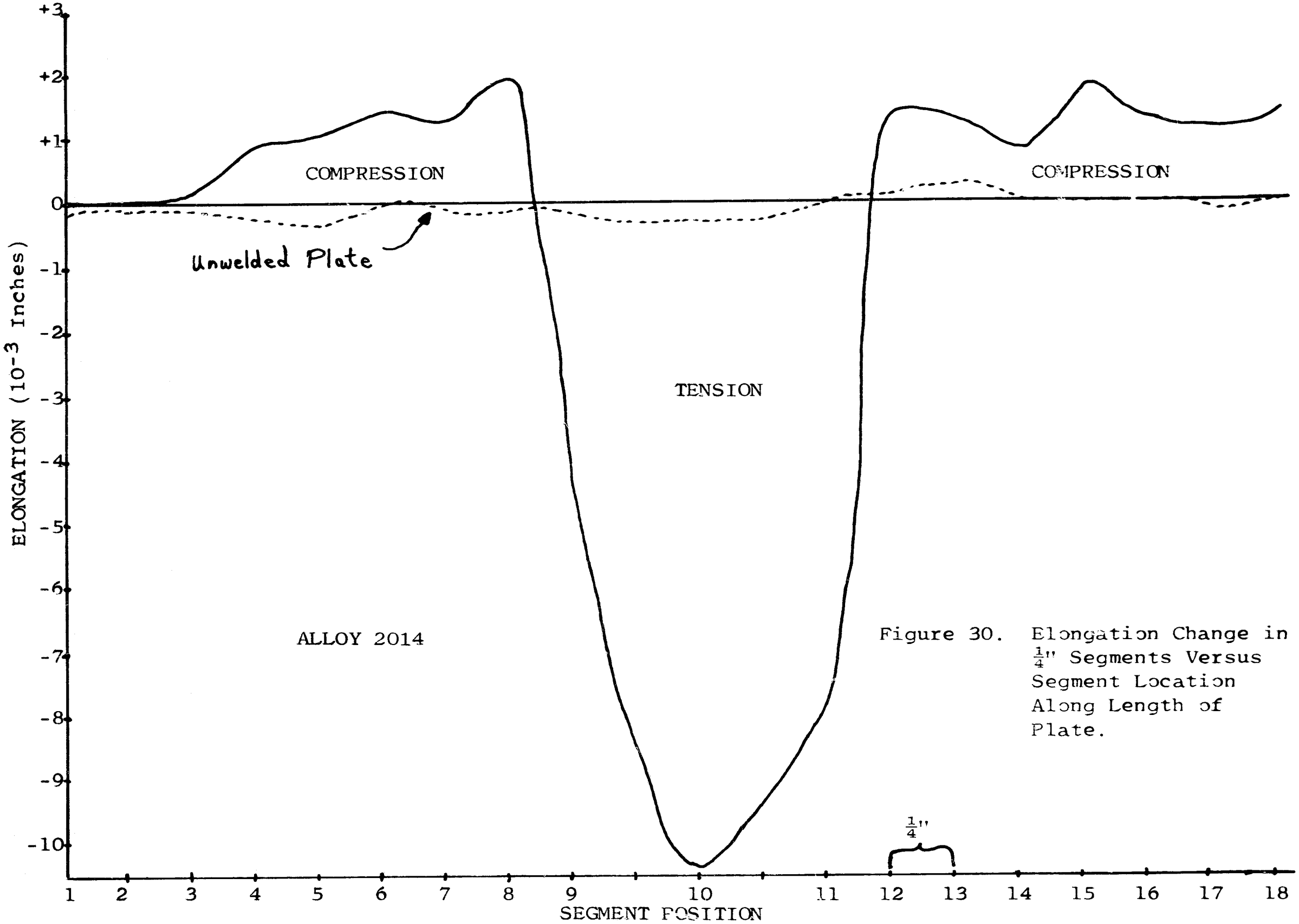

Figure 30. Elongation Change in $\frac{1}{4}$" Segments Versus Segment Location Along Length of Plate.

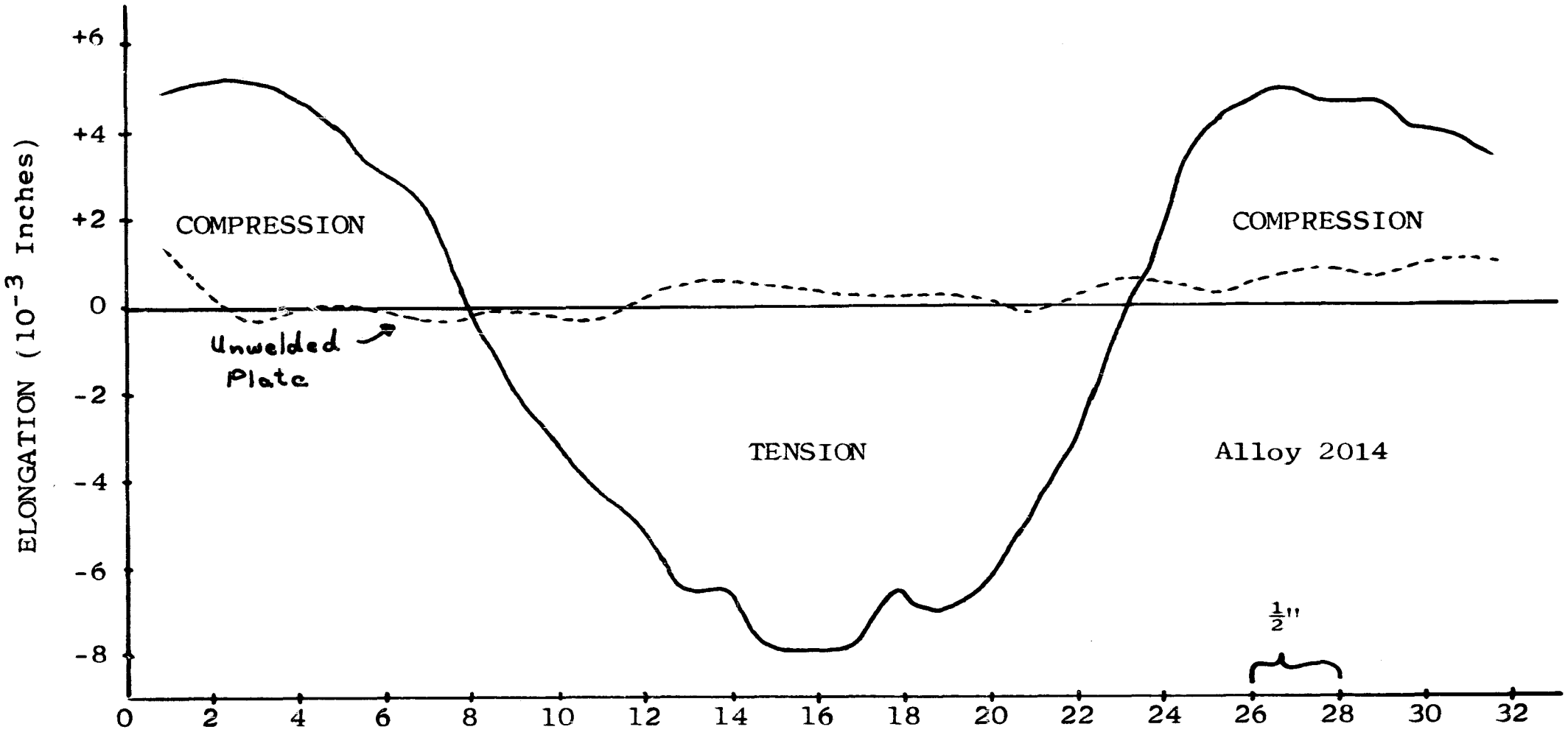

Figure 31. Elongation Change in $\frac{1}{4}$" Segments Versus Segment Location Along Width of the Plate.

therefore consist of contours of constant stress being somewhat elliptical and oriented about the weld as illustrated in Figure 32.

The results of these destructive tests appear reasonable since the welding process involves the melting of the material along the weld, which subsequently cools to room temperature. During the cooling process the material in and near the weldment should shrink in both dimensions resulting in a state of tension, while the surrounding material will oppose the shrinking by exerting a compressive force. It would further be expected that variation in the temperature of the weldment would cause local variations in the stress. Such a condition would be emphasized at the beginning and end of the weld. If we re-examine the data in Figure 31, it is seen that the tensile stress along the weld is a maximum at the beginning of the weld and only the average of the measured stress corresponds to that of the destructive data which inherently measures the average stress along the portion of material removed.

VIII. SURFACE WAVE STUDIES OF WELDED PLATES

A. Locations Selected for Measurements on Welded Plates

In order to study the effect of welding on plates, the surface wave technique involving the modified time of flight system was used. To determine the change in stress due to welding, it was necessary to take a series of readings at specific locations on the two plates to be welded and then to take another series of readings at the same locations after welding. This procedure is similar to that used with strain gages. In this case, however, the transducer assembly is removed, whereas the strain gage is left in place. Figure 33 shows the locations selected. Eleven locations were selected along the edges to be welded with nine located near the center of the plate and an additional measurement at each end where the weld is started or stopped. In addition, twelve more locations were selected perpendicular to the edge which was to be welded at locations 1, 5, and 9. Also shown in Figure 33 are the locations on the opposite side, since both surfaces

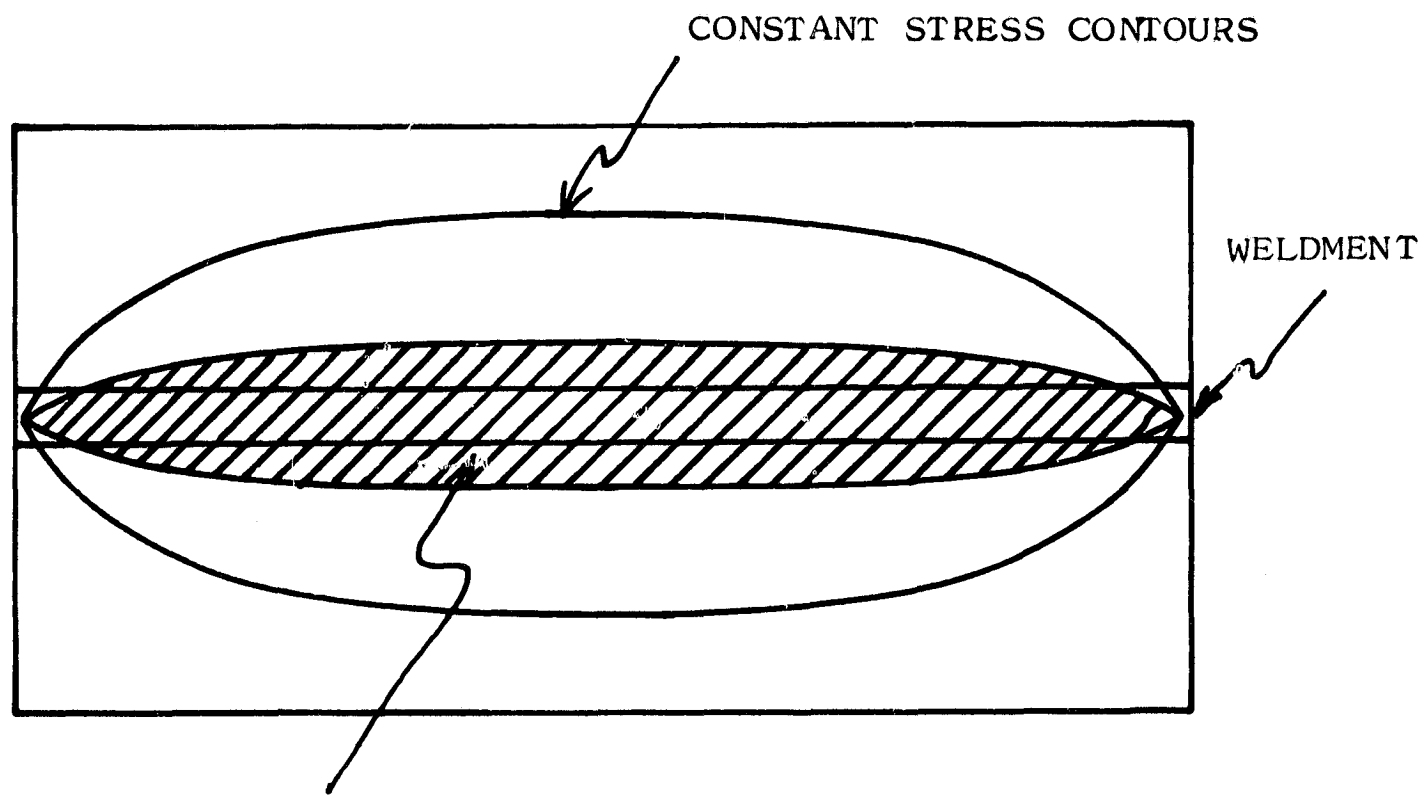

Figure 32. Contours of Constant Stress

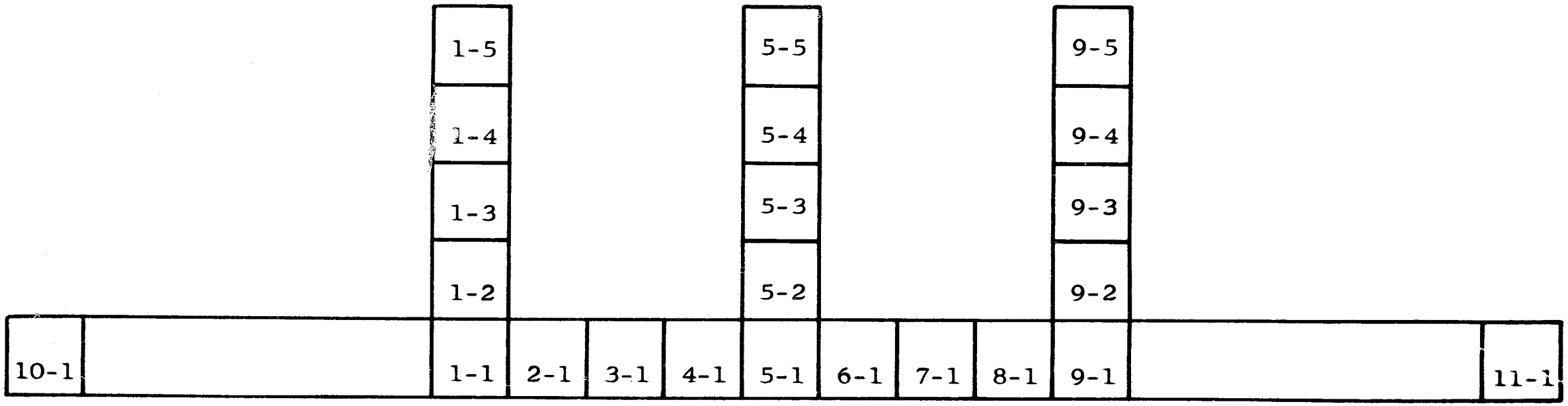

P1 S2

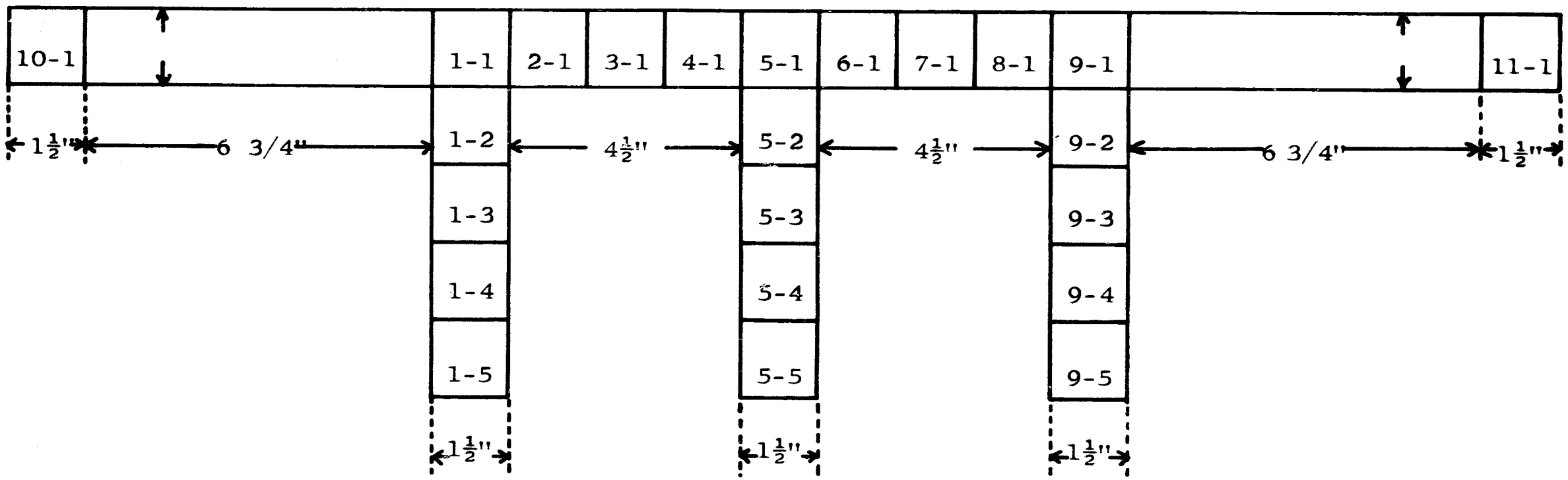

P1 S1

Figure 33. Locations for Surface Stress Measurements on Plates To be Welded. Measurements Made on the Top Side and Bottom Side of the Plate.

of the plate were examined. In Figure 34, it is shown how the selected locations would be when the two plates were welded together.

B. Modified Time of Flight Tests and Results

The plates of Alloy 2014-T6 and Alloy 2219-T87 used in this series of tests were 30 inches by 9 inches by approximately 1/2 inch thick. At each of the 23 locations shown above a group of four readings were taken; two parallel to the edge to be welded and two perpendicular to the edge. The orientation of the apparent stress in the plates had previously been determined to be rectangularly oriented with the plate by the frequency null technique using the lucite wedge transducer. Both the parallel and perpendicular transit times are determined relative to an arbitrary reference using the ultrasonic delay line. The actual reading recorded is the time in nanoseconds as read on the oscilloscope to bring the signal and the delay line signal into phase. The period for a 7 MHz signal is approximately 143 nanoseconds, and the maximum amount of delay necessary was less than half of this value. It was therefore necessary to adjust the variable delay to restore the signals to be in phase for the closest cycle of the sine wave. The actual procedure involves adjusting the signal to be in phase with the delay line for an orientation of the transducer parallel to the weld. The transducer is then rotated 90^{o} to perpendicular to the weld and the delay vernier of the oscilloscope is readjusted to bring the signals into phase. The difference is then recorded. This procedure is repeated to obtain two sets of readings.

In all of these tests the parallel readings were taken parallel to the edges of the plate to be welded or to the weld in the welded plates. In order to be consistent, the parallel readings were always taken as a reference and the perpendicular readings were subtracted from the parallel readings. This allows for a determination of the relative velocity in the two directions, indicating either tension or compression. It has already been determined that a compressive stress causes an increase in velocity and a tensile stress causes a decrease in velocity. Referring to Table II, and location 1-11 for plate P3, side 2, this would indicate that before welding the

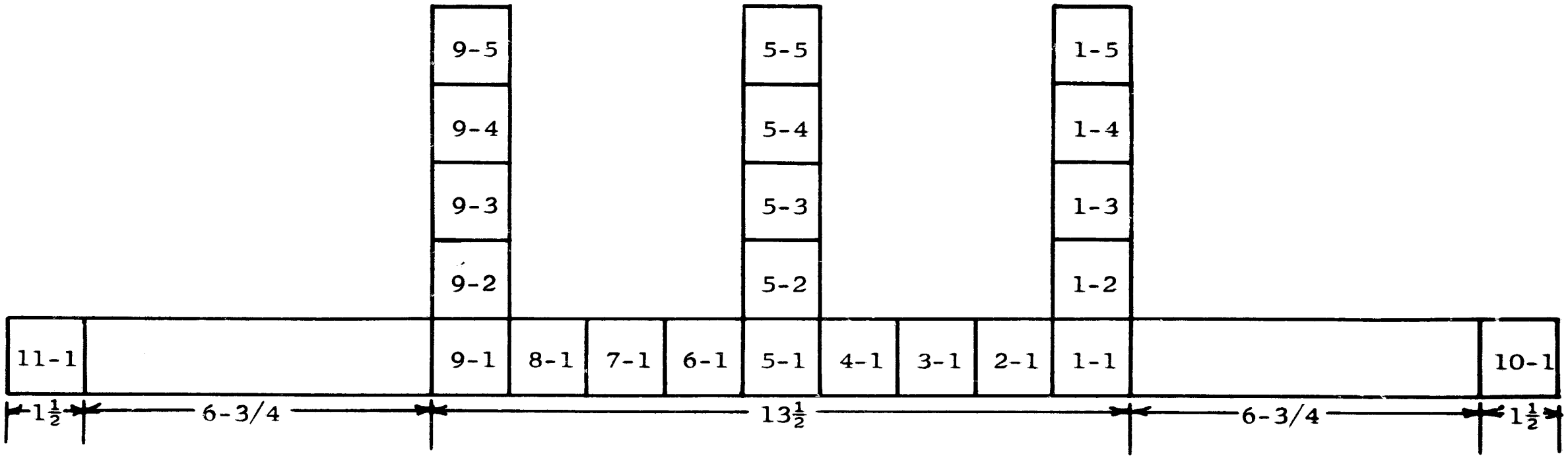

Figure 34. Locations for Surface Stress Measurements After Welding.

TABLE II

KNIFE EDGE - SURFACE WAVE

P Series (Alloy 2014 T-6; Thickness 0.5 Inches)

(Readings in Nano-seconds)

	$P_3 S_2$	First Pass Side			$P_6 S_2$		
Position	Before	After	Diff.	Position	Before	After	Diff.
1-11	39	19	-20	1-10	31	29	-2
1-9	22	37	+15	1-1	19	20	+1
1-8	19	56	+37	1-2	17	21	+4
1-7	35	22	-13	1-3	27	33	+6
1-6	23	-29	-52	1-4	20	36	+16
1-5	15	0	-15	1-5	25	10	-15
1-4	30	37	+7	1-6	27	30	+3
1-3	28	30	+2	1-7	31	3	-28
1-2	39	35	-4	1-8	30	34	+4
1-1	20	20	0	1-9	31	27	-4
1-10	45	24	-21	1-11	13	23	+10

	$P_3 S_1$	Second Pass Side			$P_6 S_1$		
Position	Before	After	Diff.	Position	Before	After	Diff.
1-11	11	2	-9	1-10	28	28	0
1-9	18	---		1-1	10	---	
1-8	17	25	+8	1-2	17	15	-2
1-7	15	7	-8	1-3	12	14	+2
1-6	10	18	+8	1-4	20	-2	+22
1-5	22	---		1-5	18	---	
1-4	11	39	+28	1-6	10	15	+5
1-3	15	13	-2	1-7	35	12	-23
1-2	21	40	+19	1-8	15	16	+1
1-1	25	---		1-9	7	---	
1-10	30	35	+5	1-11	17	18	+1

parallel "time of flight" was 39 nanoseconds greater than the perpendicular. The parallel direction of propagation is therefore slower than the perpendicular direction. After welding the parallel reading was 19 nanoseconds greater than the perpendicular reading. The parallel direction therefore increased its velocity relative to the perpendicular by a change of 20 nanoseconds in propagation time due to welding. The parallel direction of the plate either increased in compression or the perpendicular direction increased in tension. This interpretation will be discussed later in this report.

The above procedure was followed to obtain readings at each location for the six 1/2 inch thick plates of Alloy 2014-T6 which was designated as the "P" series. The six plates of Alloy 2219-T87 was designated as the "S" series. Table II gives the data obtained for plates P3 and P6, showing the before as well as the after welding data and the differences which resulted from welding the two plates together. These data are for the eleven locations along the weld. Table III gives the difference resulting from the weldment for all six plates of the "P" series for locations along the weldment for the two sides of the plates classified by the first and second passes of the welding.

In Figure 35, the average for the six plates of each location along the weld are shown. In this Figure the average differences due to the welding have been converted to stress in pounds per square inch. It should again be noted that these stresses are introduced near the surface of the material and are not necessarily indicative of the stress throughout the thickness of the material. Table IV shows the differences for those locations extending perpendicular to the weldment at locations 1, 5, and 9. In Figures 36A and 36B the average for the six plates at each location perpendicular to the weld are shown for both the first and second passes. Here again, the average differences due to welding have been converted to stress.

Similar tests were made on Alloy 2219-T87. This group of six plates, the "S" series, were also studied before welding. In Table V, typical results obtained on two plates are given. It should be noted that there are wide variations in readings between two adjacent locations. Also, the readings

TABLE III

KNIFE EDGE - SURFACE WAVE

F Series (Alloy 2014 T-6; Thickness 0.5 Inches)

(Differences between Before and After Welding)

First Pass Side

Position	P_1 S_2	P_2 S_2	P_3 S_2	P_4 S_2	P_5 S_2	P_6 S_2
1-11	---	---	-20	-6	---	
1-9	+9	-8	+15	+14	+3	-4
1-8	+10	-16	+37	-7	+4	+4
1-7	-42	+3	-13	+39	+15	-28
1-6	-1	-1	-52	-25	-8	+3
1-5	-16	+1	-15	-20	+27	-15
1-4	+2	+1	+7	---	-11	+16
1-3	-19	-21	+2	+27	-28	+6
1-2	-14	-16	-4	-11	-17	+4
1-1	-9	-21	0	+6	-14	+1
1-10	-26	-8	-21	---	---	-2

Second Pass Side

Position	P_1 S_1	P_2 S_1	P_3 S_1	P_4 S_1	P_5 S_1	P_6 S_1
1-11	+44	---	-9	---	---	0
1-9	---	---	---	---	---	---
1-8	+28	+5	+8	+13	-6	-2
1-7	-35	+2	-8	+7	-28	+2
1-6	-13	+3	+8	+17	0	+22
1-5	---	---	---	---	---	---
1-4	+15	+22	+28	+33	-11	+5
1-3	-8	+15	-2	+2	+20	-23
1-2	+31	-10	+19	+2	-15	+1
1-1	---	---	---	---	---	---
1-10	---	+6	+5	-25	-6	+1

AVERAGE SURFACE STRESS CHANGE DUE TO WELDING FOR 6 PLATES

ALLOY 2014-T6 "P" SERIES

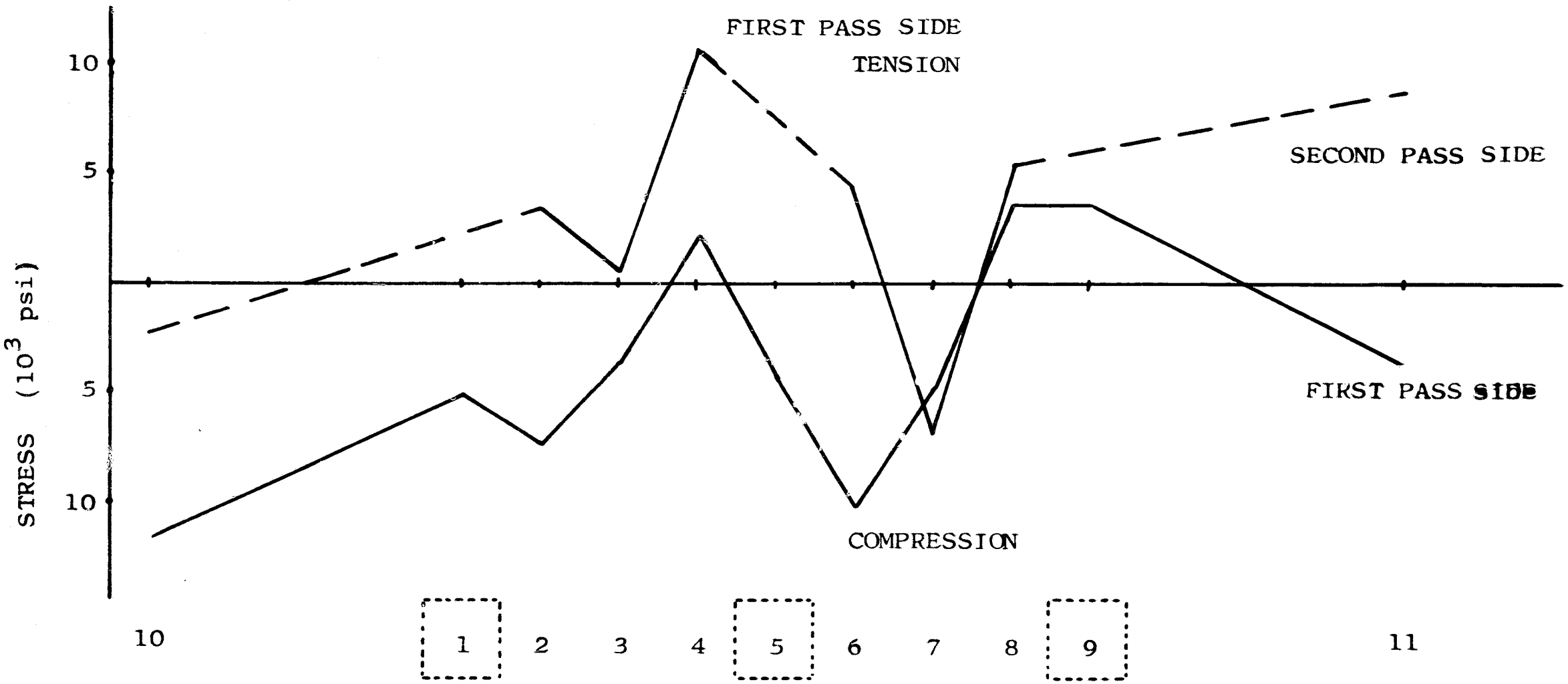

Figure 35. Average of six plates. Surface Stress Change Versus Locations Along the Weld. Alloy 2014-T6.

TABLE IV

KNIFE EDGE - SURFACE WAVE

P Series (Alloy 2014 T-6; Thickness 0.5 Inches)

(Differences between Before and After Welding)

First Pass Side

Position	$P_1 S_2$	$P_2 S_2$	$P_3 S_2$	$P_4 S_2$	$P_5 S_2$	$P_6 S_2$
1-1	-9	-21	0	+6	-14	+1
1-2	+21	-23	-22	-2	-31	-3
1-3	-4	+6	-2	-4	-13	-22
1-4	-13	+16	-7	+25	-6	-37
1-5	-26	+23	-11	+6	-25	-8
5-1	-16	+1	-15	-20	+27	-15
5-2	+10	+6	-11	-20	+4	+3
5-3	+5	+7	+3	-13	-14	-20
5-4	+2	+20	0	-22	+8	-5
5-5	-16	-30	-26	-23	-11	-16
9-1	+9	-7	+15	+14	+3	-4
9-2	+2	-26	-4	-10	-6	-11
9-3	+38	-12	+2	+4	-2	-15
9-4	+13	-31	+3	-7	+34	+16
9-5	-14	+9	-2	+40	+12	+8

Second Pass Side

Position	$P_1 S_1$	$P_2 S_1$	$P_3 S_1$	$P_4 S_1$	$P_5 S_1$	$P_6 S_1$
1-1	---	---	---	---	---	---
1-2	+21	-23	-22	-2	-31	-2
1-3	-15	+12	-11	+10	+5	-2
1-4	-17	+6	-19	-18	+22	-19
1-5	-32	-32	+24	-6	+9	-9
5-1	---	---	---	---	---	---
5-2	---	---	---	---	---	---
5-3	---	---	---	---	---	---
5-4	---	---	---	---	---	---
5-5	---	---	---	---	---	---
9-1	---	---	---	---	---	---
9-2	+2	-26	-4	-10	-6	-11
9-3	+38	-12	+2	+4	-2	-15
9-4	+13	-31	+3	-7	+34	+16
9-5	-14	+9	-2	-40	+12	+8

AVERAGE CHANGE DUE TO WELDING - PERPENDICULAR TO WELD

ALLOY 2014-T6 "P" SERIES

FIRST PASS SIDE

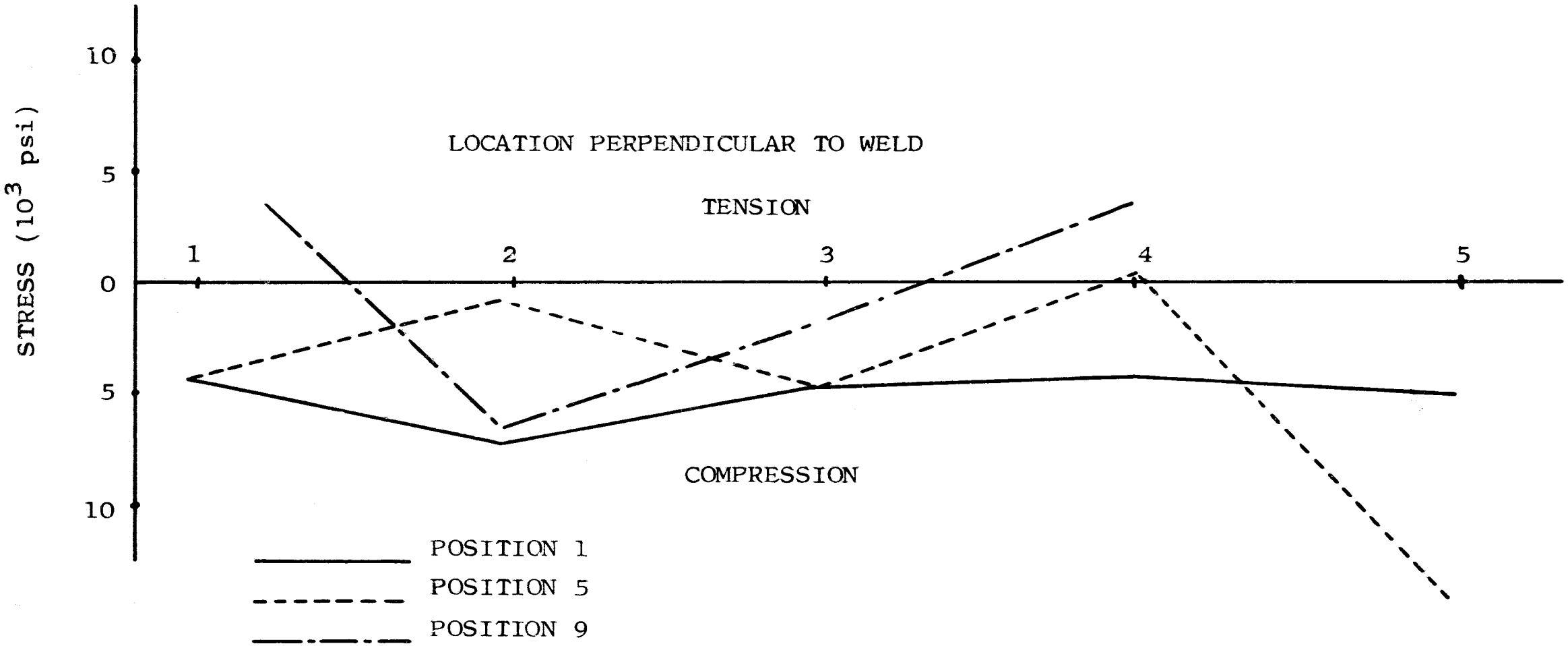

Figure 36A. Average of Six Plates. Surface Stress Versus Locations Perpendicular to Weld. Alloy 2014-T6. First Pass.

AVERAGE CHANGE DUE TO WELDING - PERPENDICULAR TO WELD

ALLOY 2014-T6 "P" SERIES

SECOND PASS SIDE

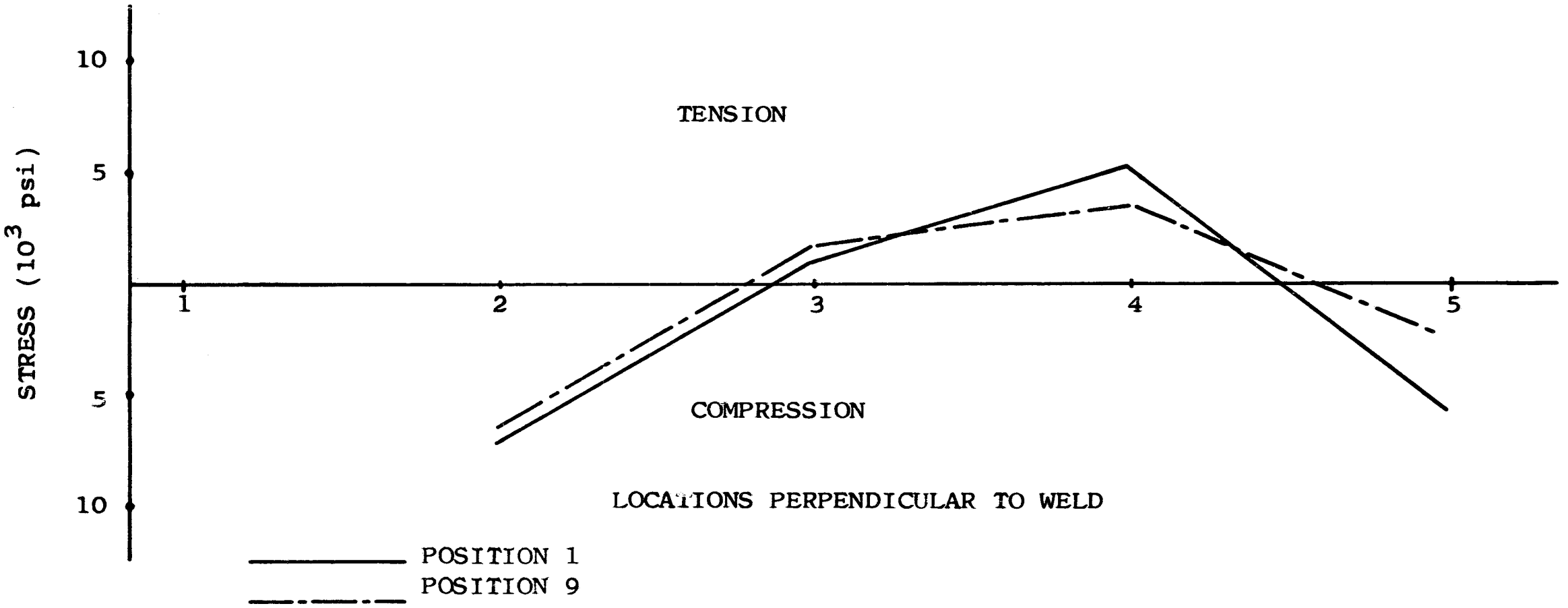

Figure 36B. Average of Six Plates. Surface Stress versus Locations Perpendicular to Weld. Alloy 2014-T6. Second Pass.

TABLE V

KNIFE EDGE - SURFACE WAVE

S Series (Alloy 2219-T87; Thickness 0.5 Inches)

(Readings in Nano-seconds)

	S_1 S_2	First Pass Side			S_2 S_2		
Position	Before	After	Diff.	Position	Before	After	Diff.
1-11	-1	-24	-23	1-10	-18	-26	-8
1-9	-39	-40	-1	1-1	-24	-28	-4
1-8	---	-36	---	1-2	-28	-12	+16
1-7	-26	0	+26	1-3	-18	-5	+13
1-6	-21	-18	+3	1-4	-21	-11	+10
1-5	-23	-37	-14	1-5	-24	-20	+4
1-4	-25	-1	+24	1-6	-20	-10	+10
1-3	-23	-14	+9	1-7	-14	-18	-4
1-2	-46	-47	-1	1-8	-16	-20	-4
1-1	-5	-5	0	1-9	-12	-29	-17
1-10	-2	-28	-26	1-11	-2	-26	-24

	S_1 S_1	Second Pass Side			S_2 S_1		
Position	Before	After	Diff.	Position	Before	After	Diff.
1-11	-36	-18	-18	1-10	-9	-29	-20
1-9	-8	-28	-20	1-1	+5	-30	-35
1-8	-25	-26	-1	1-2	-7	-7	0
1-7	-21	-26	-5	1-3	-1	-36	-35
1-6	-8	-32	-24	1-4	-23	-24	-1
1-5	-24	-11	+9	1-5	-29	-45	-16
1-4	-18	-30	-12	1-6	-4	-23	-19
1-3	-14	-20	-6	1-7	-32	-11	+21
1-2	-21	-28	-7	1-8	-7	-21	-14
1-1	-16	-32	-16	1-9	-9	-29	-20
1-10	-21	-28	-7	1-11	-9	-29	-20

before welding are negative indicating that the velocity perpendicular to the weld is slower than that parallel to the weld. This is in contrast to the situation observed for the Alloy 2014-T6.

The surface of the plates of Alloy 2219-T87 contained Leuder Lines caused by the successive stretching of the plates in two directions. The resultant of this process was that the surface contained ridges which were as much as 0.005 inches deep. The knife edge transducer must set flat within its area of contact to produce repeatable results. If the ridges had been oriented rectangularly with the plate, readings could have been obtained. The ridges, however, were oriented at about 60^{o} with the axes of the plate and repeatable readings were impossible. The surfaces of these plates were therefore refinished by polishing with an abrasive paper. Even so, the measurements obtained on this particular alloy were subject to considerably more variation than was observed on the 2014-T6 plates.

The readings on the "S" series plates were taken before and after welding. The differences between before and after welding for all of the plates of the "S" series along and perpendicular to the weld are shown in Table VI. Figure 37, and Figure 38 show plots of the average change due to welding for the six plates, again classified according to the first and second passes of the weldment. Here again, the average stress parallel to the weld shows an increase in compressive stress for both passes. Figures 39 and 40 show the change in stress due to welding, for the locations perpendicular to the weld.

An overall average for the six plates of both alloys was calculated for each of the passes. In order to compare the destructive tests that were performed, it is necessary to average over the length of the plate. For the Alloy 2014-T6, the stress parallel to the weld increased approximately 3,400 pounds per square inch as averaged over the length of the weld and for the locations centered 1 1/4 inches from the weldment. For the second pass side the stress decreased in compression on the average, by approximately 3,100 pounds per square inch. It should be noted that at this distance from the weld, the destructive tests showed a transition from tension to compression. Furthermore, some of the plates were subjected to considerable warping. Figure 41 shows a plot of the change in

TABLE VI

KNIFE EDGE - SURFACE WAVE

S Series (Alloy 2219-T87; Thickness 0.5 Inches)

(Differences between Before and After Welding)

First Pass Side

Position	S_1 S_2	S_2 S_2	S_3 S_2	S_4 S_2	S_5 S_2	S_6 S_2
1-11	-23	-24	-32	---	-38	-5
1-9	-1	-17	-18	---	-56	-21
1-8	---	+4	-21	-2	-32	-21
1-7	+26	-4	-10	+20	-43	+10
1-6	+3	+10	-13	-9	-12	0
1-5	-14	+4	-8	-5	-11	-7
1-4	+24	+10	-6	-12	-22	0
1-3	+9	+13	-7	+2	-66	+18
1-2	-1	+16	-7	---	-45	-14
1-1	0	-4	-8	+8	-26	-3
1-10	-26	-8	-1	---	---	+21

Second Pass Side

Position	S_1 S_1	S_2 S_1	S_3 S_1	S_4 S_1	S_5 S_1	S_6 S_1
1-11	-18	-20	+21	-33	-30	+16
1-9	-20	-37	---	+26	---	---
1-8	-1	-14	-13	+28	-18	+21
1-7	-5	+21	+10	-7	+4	+11
1-6	-24	-19	+14	+25	-4	+12
1-5	+9	-16	---	+10	---	---
1-4	-12	-1	+7	+26	+7	+15
1-3	-6	-35	+20	+18	+20	+18
1-2	-7	0	+16	+39	+16	+7
1-1	-16	-35	---	+33	---	---
1-10	-7	-20	-19	+47	-19	+23

TABLE VI Continued

KNIFE EDGE - SURFACE WAVE

S Series (Alloy 2219-T87; Thickness 0.5 Inches)

(Differences between Before and After Welding)

First Pass Side

Position	S_1 S_2	S_2 S_2	S_3 S_2	S_4 S_2	S_5 S_2	S_6 S_2
1-1	0	-4	-8	+8	-26	-3
1-2	-14	-13	-14	-16	+9	-12
1-3	-12	-12	-10	+6	+7	-26
1-4	-34	-19	+4	-7	-1	-12
1-5	+4	-15	-2	+7	-39	-14
5-1	-14	+4	-8	-5	-11	-1
5-2	---	-7	+8	-4	+10	-20
5-3	---	-15	-16	-17	-6	-11
5-4	---	-4	-25	+25	-1	0
5-5	-28	-23	+1	-5	+2	-1
9-1	-1	-17	-18	---	---	-35
9-2	-34	-3	-6	-45	-15	+9
9-3	-32	-10	-39	-24	-12	-19
9-4	-18	-17	+4	+7	+8	-27
9-5	-4	+4	-39	+7	+18	-9

Second Pass Side

Position	S_1 S_1	S_2 S_1	S_3 S_1	S_4 S_1	S_5 S_1	S_6 S_1
1-1	-16	-38	---	+33	---	---
1-2	+8	+4	-15	+14	+19	+10
1-3	+18	-8	-4	+21	+2	-6
1-4	+15	+9	+13	+32	-12	-11
1-5	+4	-9	-16	+35	-7	+9
5-1	+9	---	---	+10	---	---
5-2	---	---	---	---	---	---
5-3	---	---	---	---	---	---
5-4	---	---	---	---	---	---
5-5	---	---	---	---	---	---
9-1	-20	-34	---	+26	---	---
9-2	-34	-3	+6	-45	-15	+9
9-3	-32	-10	-39	-24	-12	-19
9-4	-18	-17	+4	+7	+8	-27
9-5	-4	+4	-39	+7	+18	-9

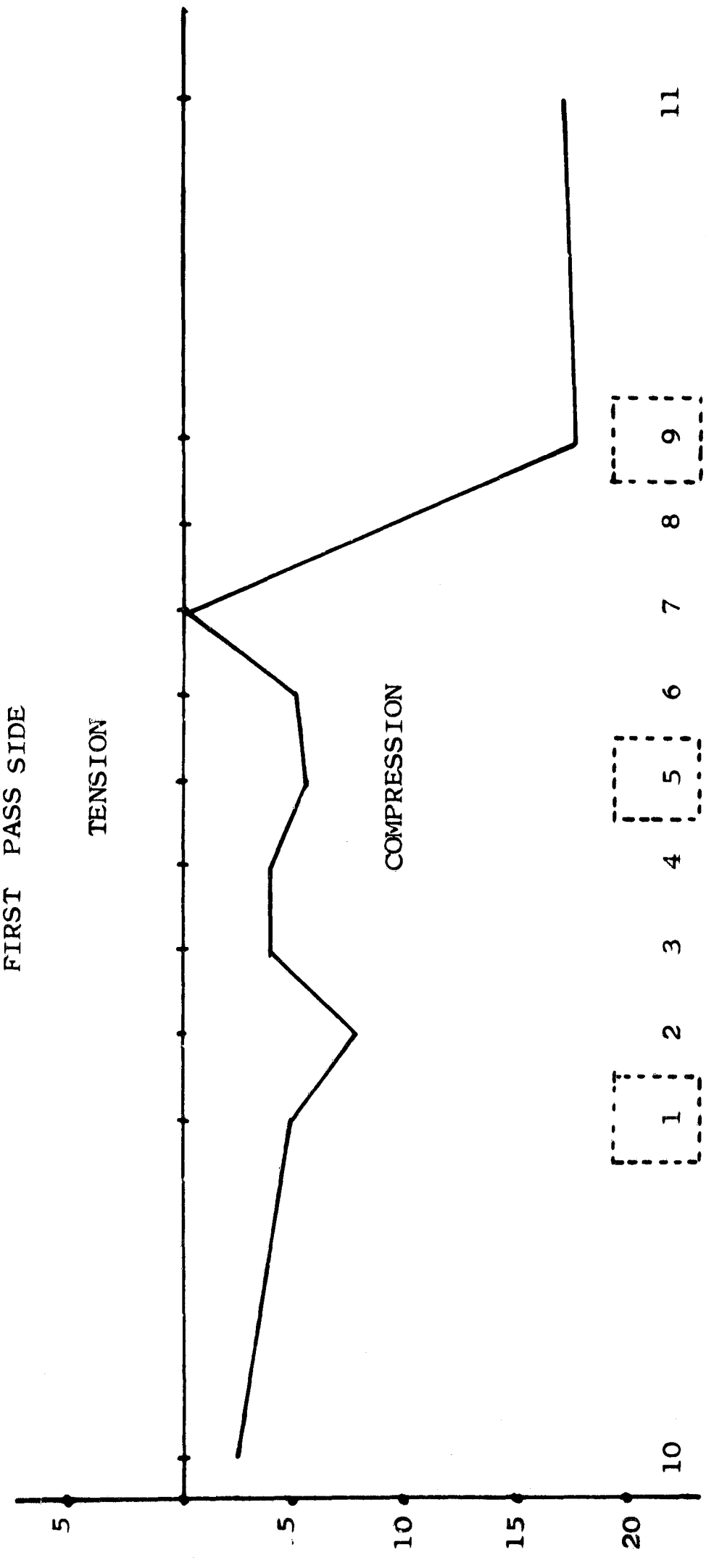

Figure 37. Average of Six Plates. Surface Stress Change Versus Location along Weld. Alloy 2219-T87. First Pass.

AVERAGE CHANGE DUE TO WELDING FOR 6 PLATES

ALLOY 2219-T87 "S" SERIES

SECOND PASS SIDE

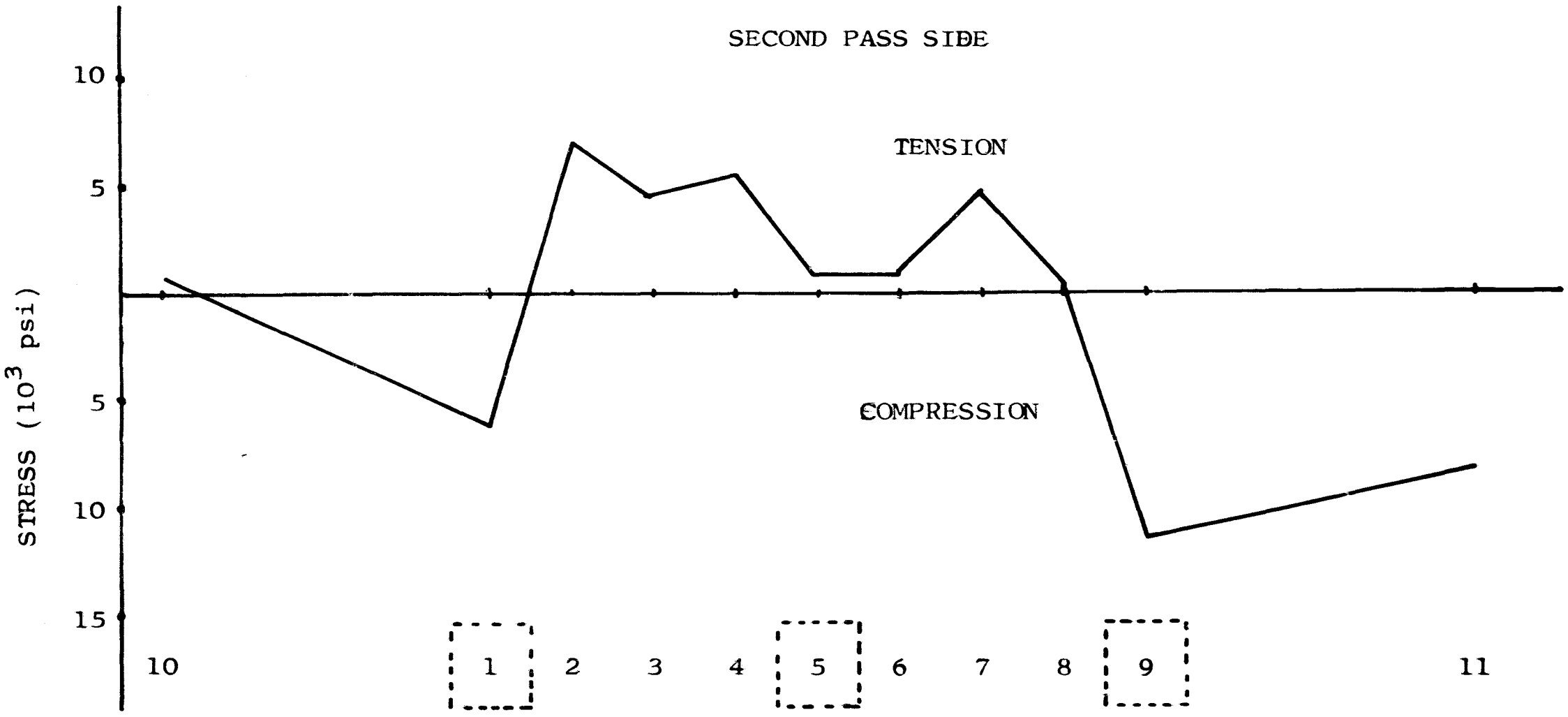

Figure 38. Average of Six Plates. Surface Stress Change Versus Locations Along Weld. Alloy 2219-T87. Second Pass.

AVERAGE CHANGE DUE TO WELDING - PERPENDICULAR TO WELD

ALLOY 2219-T87 "S" SERIES

FIRST PASS SIDE

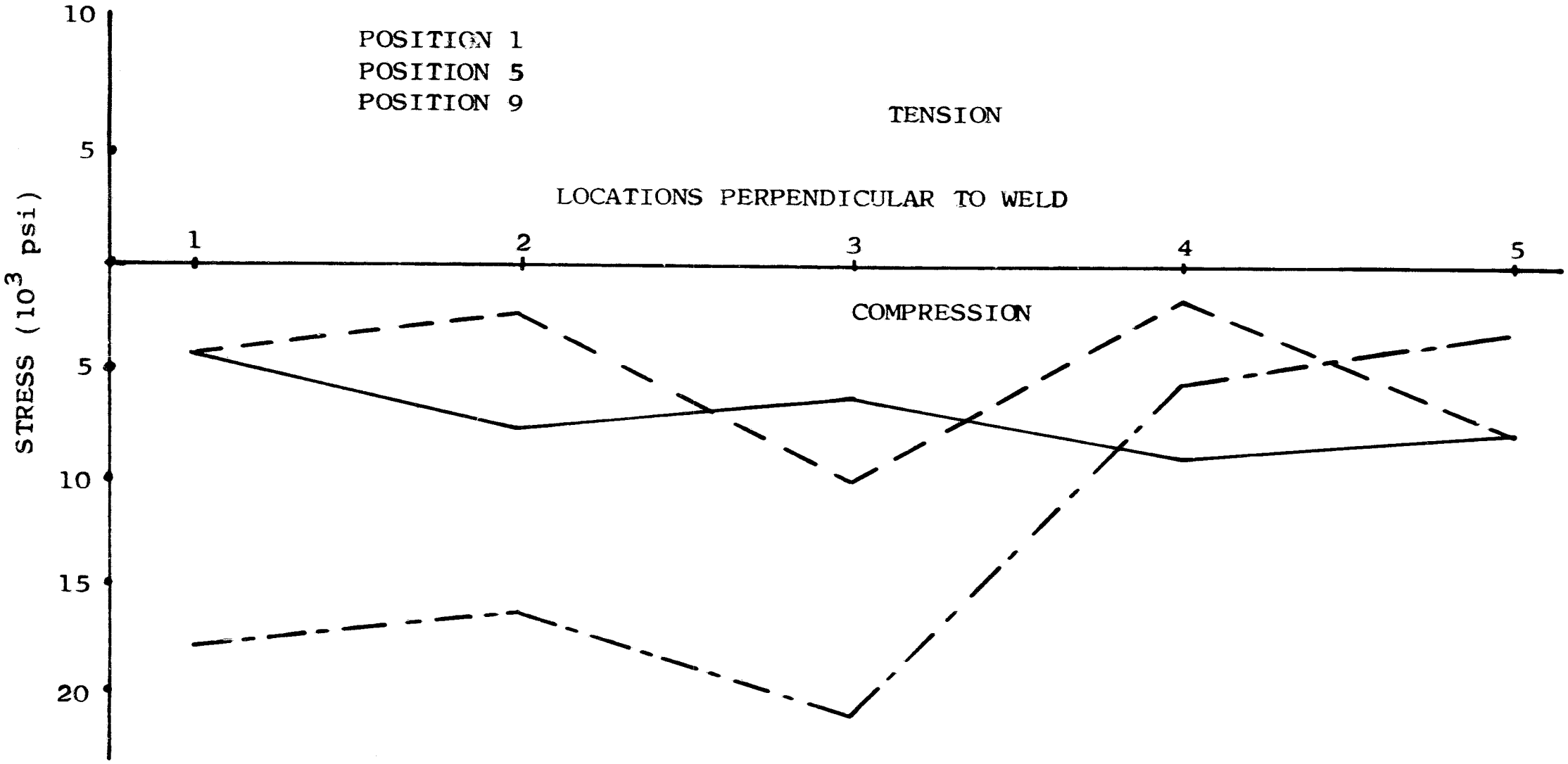

Figure 39. Average of Six Plates. Surface Stress Change Versus Location Perpendicular to the Weld. Alloy 2219-T87. First Pass.

AVERAGE CHANGE DUE TO WELDING - PERPENDICULAR TO WELD

ALLOY 2219-T87 "S" SERIES

SECOND PASS SIDE

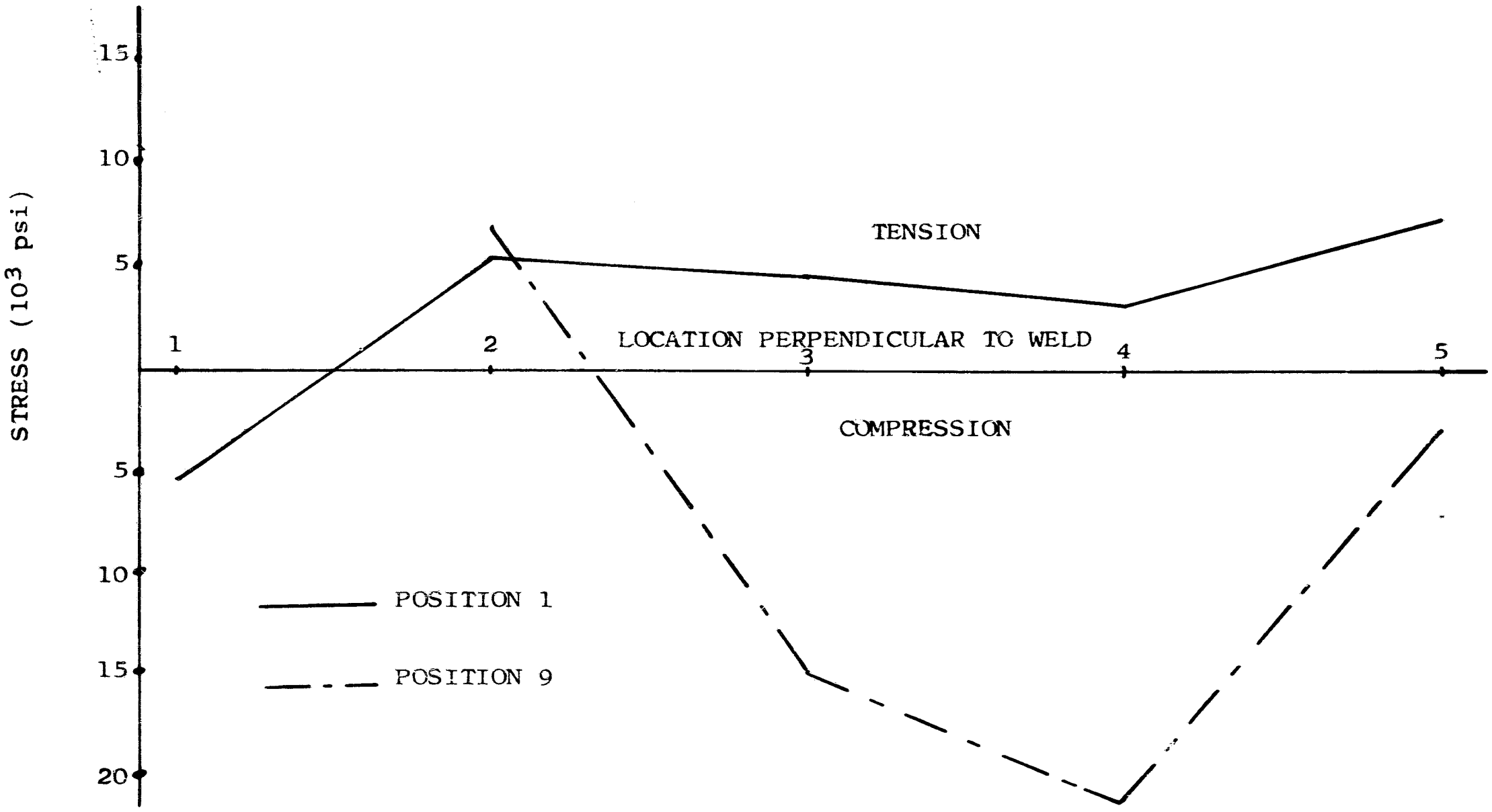

Figure 40. Average of Six Plates. Surface Stress Change Versus Locations Perpendicular to the Weld. Alloy 2219-T87. Second Pass.

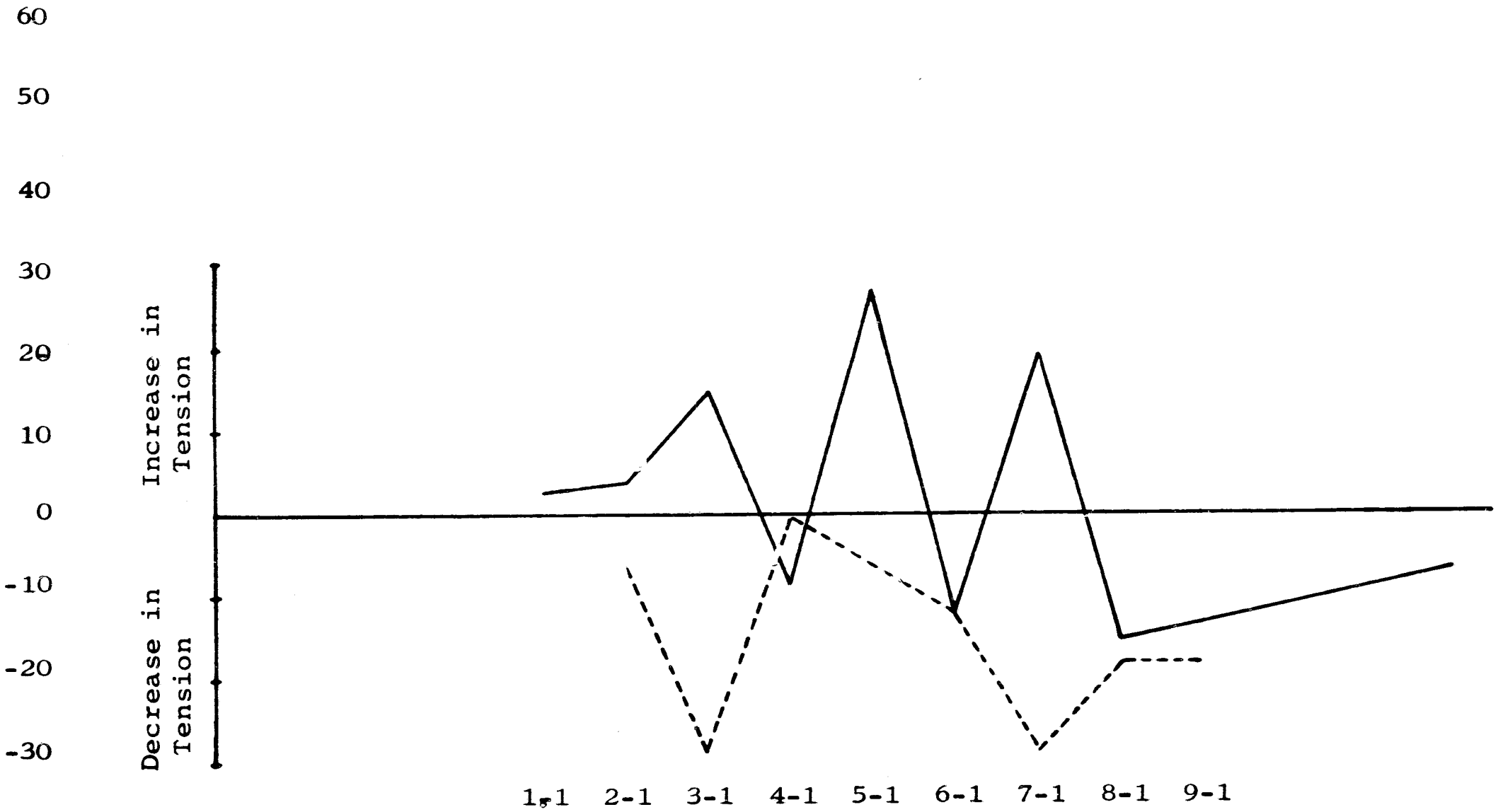

Figure 41. The Change in Surface Stress on Top and Bottom of a Plate Adjacent to the Weld Which Showed Marked Warping.

stress along the weld for a particular plate that exhibited marked warping. It is noted that the stress on the two sides of the plate varied in magnitude and direction. For this particular plate, little correlation with stress measured through the thickness would be obtained. Figure 42 illustrates a plate that exhibited little warping and the stress change on both sides of the plate correspond in magnitude and direction. For this plate, the stress through the thickness would correspond to the surface stress observed. The fact that compression was observed on one side, on the average, and tension on the opposite side, was therefore influenced by the warping of the plates, as well as the fact that this particular location of measurements was in the transition region between tension and compression which exists near the weld.

The locations extending perpendicular to the weld are located at least 2 1/2 inches from the weld and extend further outward. The destructive tests indicated that this portion of the plate should be in compression in a direction along the weld with an average magnitude of approximately 3000 pounds per square inch. The average of the measurements of surface stress on the first side pass was 2,200 psi and on the second pass side 3,000 psi. It is again noted that the curvature of the plates influence the average stress in this region.

For the Alloy 2219-T87, the first pass side increased by 7,000 psi and the second pass side increased compressively by 200 psi as observed for locations 1 1/4 inches from the weld. Again, considerable curvature of the plates was noted. At the locations more remote from the weld, the average stress was 3,900 and 4,200 for the first and second passes respectively. Again, the stress is in compression in the direction along the weld consistent with the destructive tests.

C. Frequency Null Tests and Results

In addition to the modified time of flight measurements obtained on the welded plates, measurements employing the frequency null system were made on the "P" and "S" series of plates as well as the "B" series of plates. The "B" series is 2014-T6, 0.125 inch thick plates. The locations chosen for these measurements were 1-2, 9-2, and 5-3 on each side of a given plate. For each of these locations, the transducer

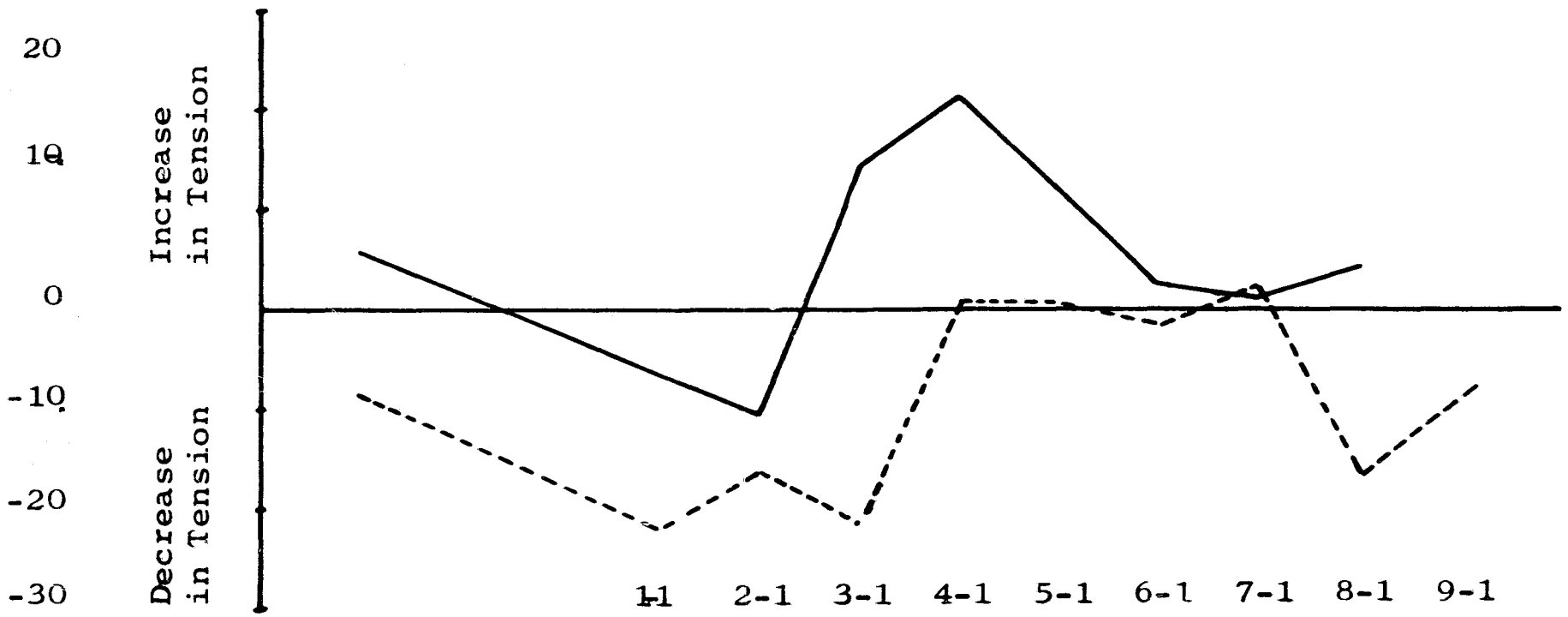

Figure 42. The Change in Surface Stress on Top and Bottom of a Plate Adjacent to the Weld Which Showed Little Warping.

assembly was rotated in 10° increments and the frequency change noted for the 19 positions. To be consistent in all measurements, position 1 was always chosen so that the sending crystal of the transducer assembly propagated the surface wave parallel to the side of the plate prepared for welding. The transducer assembly was then rotated in a clockwise fashion to the next position.

After frequency readings for the 19 positions were obtained, the minimum frequency recorded was then subtracted from all of the other readings. For a given series of plates, the data at locations 1-2 and 9-2 was averaged. Data taken at location 5-3 was also averaged. In other words, readings obtained at positions 1 for locations 1-2 and 9-2 for a given series of plates were added and divided by 24 since there were 4 locations for each of the 6 plates in a series. The same averages were also calculated for the other 18 positions at these locations. Note that there were only 12 numbers to average at each position for the 5-3 locations. This averaging calculation was conducted before and after welding in order to determine any gross effect due to the welding that would support the destructive test.

Averages for the three series of plates are presented in Table VII. The actual before and after data for locations 1-2 and 9-2 for the "B" series of plates is given in Tables VIII and IX. A plot of the averages is given in Figure 43. In a similar manner the before and after data for location 5-3 is given for the "B" series followed by a graph showing the averages plotted. This same order of data is followed for the "P" and "S" series. Note that in all the curves that present a plot of averaged data, the dashed curve represents the change after welding. The curves of Figures 43 and 44 show that there is very little change in frequency versus orientation for the "B" series of plates before welding. Once the plates have been welded, however, the shape of the curve changes such that there appears to be a compressive loading parallel to the weldment. The frequency being higher at position 1 than at position 10 indicates this conclusion which was substantiated by the destructive tests described earlier. Also it is observed that there is a larger increase in frequency noted after

TABLE VII

B Series (Alloy 2014-T6)

Thickness 0.125 Inches

(Frequency in KHz

Location 5-3				Locations 1-2 and 9-2		
Position	Before	After	Difference	Before	After	Difference
1	1.92	3.66	-1.74	2.49	5.45	-2.96
2	1.74	3.34	-1.60	1.80	4.33	-2.53
3	1.66	3.02	-1.36	1.45	4.40	-2.95
4	1.63	2.59	- .96	1.26	3.20	-1.94
5	1.49	2.14	- .65	1.08	2.41	-1.33
6	1.61	2.05	- .44	1.39	1.81	- .42
7	1.95	1.42	+ .53	1.85	1.94	- .09
8	2.68	1.86	+ .82	2.60	2.49	+ .11
9	2.84	2.17	+ .67	3.43	2.78	+ .65
10	3.02	2.36	+ .66	3.62	2.36	+1.26
11	2.84	1.87	+ .97	3.27	1.94	+1.33
12	2.50	1.40	+1.10	2.47	1.52	+ .95
13	1.57	1.53	+ .04	1.73	1.94	- .21
14	.91	1.36	- .45	.97	1.77	- .80
15	.96	1.98	-1.02	1.10	2.11	-1.01
16	1.06	2.20	-1.14	1.10	2.72	-1.62
17	1.65	3.25	-1.60	1.35	3.90	-2.55
18	1.62	3.18	-1.56	1.77	4.63	-2.86
19	1.87	3.63	-1.76	2.15	5.02	-2.87

Change in Stress at 5-3

.66 -(-1.74) = 2.40 KHz

$$\frac{2.40\ \text{KHz}}{\frac{1.00\ \text{KHz}}{10^3\ \text{psi}}} \quad 2.40 \times 10^3 \text{ psi}$$

(Compression parallel to Weldment)

Change in Stress at 1-2 and 9-2

1.26 -(-2.96) = 4.22 KHz

$$\frac{4.22\ \text{KHz}}{\frac{1.00\ \text{KHz}}{10^3\ \text{psi}}} \quad 4.22 \times 10^3 \text{ psi}$$

(Compression parallel to Weldment)

TABLE VII Continued

P Series (Alloy 2014-T6)

Thickness 0.5 Inches

(Frequency in KHz

Location 5-3				Locations 1-2 and 9-2		
Position	Before	After	Difference	Before	After	Difference
1	2.28	1.65	+ .63	1.87	2.00	- .13
2	1.30	1.56	- .26	1.55	1.62	- .07
3	1.03	1.60	- .57	1.55	1.67	- .12
4	1.74	1.98	- .24	2.60	2.42	+ .18
5	3.39	3.96	- .57	4.84	3.91	+ .93
6	5.81	6.39	- .58	7.50	6.30	+1.20
7	8.71	8.20	+ .51	10.33	8.70	+1.63
8	11.63	11.18	+ .45	13.22	11.35	+1.87
9	13.45	13.17	+ .28	15.09	13.00	+2.09
10	14.13	13.17	+ .96	15.68	13.43	+2.25
11	13.20	12.82	+ .38	15.01	12.91	+2.10
12	11.24	11.22	+ .02	12.65	11.14	+1.51
13	8.55	8.47	+ .08	9.66	8.61	+1.05
14	5.19	5.86	- .67	6.93	5.51	+1.43
15	2.64	3.85	-1.21	4.03	3.07	+ .96
16	1.49	2.49	-1.00	2.19	1.48	+ .71
17	.60	1.43	- .83	1.58	.90	+ .68
18	.59	1.05	- .46	1.38	1.26	+ .12
19	1.02	1.25	- .23	1.36	1.59	- .23

Change in Stress at 5-3

.96 -(.66) = 0.33 KHz

$$\frac{.33 \text{ KHz}}{\frac{1.00 \text{ KHz}}{10^3 \text{ psi}}} = 0.33 \times 10^3 \text{ psi}$$

(Compression parallel to Weldment)

Change in Stress at 1-2 and 9-2

2.25 -(-.13) = 2.38 KHz

$$\frac{2.38 \text{ KHz}}{\frac{1.00 \text{ KHz}}{10^3 \text{ psi}}} = 2.38 \times 10^3 \text{ psi}$$

(Compression parallel to Weldment)

TABLE VII Continued

S Series (Alloy 2219-T87)

Thickness 0.5 Inches

(Frequency in KHz

Location 5-3				Locations 1-2 and 9-2		
Position	Before	After	Difference	Before	After	Difference
1	12.36	11.62	+ .74	11.48	13.08	-1.60
2	10.70	10.75	- .05	9.85	11.78	-1.93
3	8.41	7.58	+ .83	7.42	9.57	-2.15
4	5.74	4.96	+ .78	4.91	6.82	-1.91
5	3.50	2.70	+ .80	2.71	3.56	+ .85
6	1.88	1.71	+ .17	1.73	1.93	- .20
7	2.08	1.41	+ .67	1.83	1.29	+ .54
8	2.95	2.00	+ .95	2.79	1.61	+1.18
9	3.47	3.10	+ .37	3.90	2.37	+1.53
10	4.44	3.89	+ .55	4.08	2.98	+1.10
11	4.21	3.32	+ .89	3.33	2.84	+ .49
12	2.92	2.74	+ .18	2.06	1.66	+ .40
13	1.95	1.70	+ .25	.91	.98	- .07
14	1.72	1.90	- .18	.97	1.73	- .76
15	3.05	3.22	- .17	2.76	3.32	- .56
16	5.49	5.23	+ .26	5.31	6.53	-1.22
17	8.24	7.93	+ .31	8.05	9.67	-1.62
18	10.37	10.29	+ .08	10.10	12.20	-2.10
19	11.53	11.55	- .02	10.63	13.09	-2.46

Change in Stress at 5-3

$.55 - (.74) = -0.19$ KHz

$$\frac{-0.19 \text{ KHz}}{\frac{0.950 \text{ KHz}}{10^3 \text{ psi}}} = -0.2 \times 10^3 \text{ psi}$$

(Tension parallel to Weldment)

Change in Stress at 1-2 and 9-2

$1.10 - (-1.60) = 2.70$ KHz

$$\frac{2.70 \text{ KHz}}{\frac{0.950 \text{ KHz}}{10^3 \text{ psi}}} = 2.84 \times 10^3 \text{ psi}$$

(Compression parallel to Weldment)

TABLE VIII

FREQUENCY - NULL SURFACE WAVE DATA

B Series (Alloy 2014-T6; Thickness 0.125 Inches)

(Frequency in KHz

Before Welding

Plate No.	B-1				B-2				B-3			
Side No.	S_1		S_2		S_1		S_2		S_1		S_2	
Location	1-2	9-2	1-2	9-2	1-2	9-2	1-2	9-2	1-2	9-2	1-2	9-2
Position												
1	3.63	4.28	1.87	2.48	3.52	.21	.97	1.93	4.16	1.50	1.27	2.92
2	3.87	2.04	1.52	1.51	2.26	1.18	0.00	.80	3.80	1.25	.54	2.26
3	2.72	.97	1.78	1.19	1.91	0.00	.13	.52	3.44	.81	0.00	1.80
4	1.36	1.57	1.42	1.19	1.85	.36	.71	.62	3.35	.61	1.44	.46
5	2.14	0.00	1.46	1.41	2.22	.20	1.17	.62	3.21	0.00	.86	.51
6	1.85	.54	2.15	.88	2.86	1.10	2.33	1.31	2.67	.35	1.90	1.39
7	2.56	1.04	2.85	1.17	3.25	1.79	3.16	2.24	3.17	1.78	1.93	2.62
8	3.43	1.73	3.04	1.87	5.06	3.13	3.88	3.18	3.87	3.37	2.23	4.14
9	5.23	1.35	2.79	5.22	6.06	3.66	4.64	3.43	4.78	4.36	3.30	5.41
10	4.96	1.76	2.65	4.20	5.45	3.49	5.14	2.58	5.41	3.68	4.97	5.49
11	3.92	.62	2.69	3.46	4.51	2.89	4.37	3.26	3.64	3.85	5.43	3.32
12	1.70	1.85	3.36	2.00	5.12	1.80	4.77	3.25	2.13	2.01	3.88	2.95
13	1.50	.79	3.70	1.40	2.03	1.07	3.80	2.62	1.04	1.27	3.05	.67
14	1.11	1.02	2.82	.63	.58	.25	3.52	1.15	0.00	.86	2.80	0.00
15	.11	1.01	1.66	0.00	.25	.47	.97	0.00	1.13	1.11	1.90	1.31
16	0.00	.71	.13	1.08	0.00	.25	.31	.03	1.79	.66	1.56	2.52
17	1.34	1.81	0.00	.09	1.10	1.09	.05	0.00	2.46	.86	2.20	2.57
18	2.65	2.04	.54	.80	2.06	.40	.33	.20	2.40	1.83	2.75	2.92
19	3.16	2.15	.62	1.35	2.24	1.10	.41	.60	3.16	2.61	2.83	3.04

TABLE VIII Continued

Plate No.	B-4				B-5				B-6			
Side No.	S_1		S_2		S_1		S_2		S_1		S_2	
Location	1-2	9-2	1-2	9-2	1-2	9-2	1-2	9-2	1-2	9-2	1-2	9-2
Position												
1	3.19	3.09	0.00	3.76	1.57	1.63	0.00	4.62	1.96	2.84	3.66	4.74
2	1.94	1.41	.32	2.00	2.09	.82	.21	3.66	1.56	1.74	3.29	3.04
3	.94	1.00	1.19	0.00	1.67	1.92	1.49	2.74	.79	1.25	2.06	4.44
4	.14	1.06	1.02	.71	1.46	3.39	1.58	1.10	.51	.52	1.56	2.14
5	.09	1.01	1.80	.48	.09	2.05	2.35	.75	.41	1.05	1.24	.89
6	0.00	.95	1.99	1.45	0.00	1.52	3.08	.21	.46	.57	1.19	2.69
7	.12	1.55	3.11	1.42	.92	.84	4.48	0.00	.80	.75	.93	2.C1
8	1.01	1.85	3.70	.79	1.99	1.29	4.78	1.08	2.01	.83	2.18	1.89
9	1.10	1.81	4.18	2.26	3.40	5.12	6.10	1.16	1.36	1.80	3.88	0.00
10	1.04	2.49	3.71	3.61	1.75	5.50	7.14	1.44	3.61	1.78	3.84	1.29
11	1.14	2.57	4.11	3.41	2.47	4.80	4.14	3.15	2.16	1.50	3.77	3.35
12	1.16	.99	2.39	3.69	1.15	3.80	4.09	.81	1.76	.94	2.38	3.29
13	1.31	.84	1.79	2.02	1.55	2.71	2.08	.68	.62	0.00	1.69	3.29
14	1.57	.85	2.37	1.42	1.45	1.89	2.00	1.72	.32	.41	1.24	1.74
15	1.44	.12	.44	1.51	2.57	.69	2.06	1.53	.03	1.01	0.00	2.04
16	1.98	0.00	.41	1.95	3.69	.57	1.18	3.00	.10	1.41	1.94	1.24
17	1.58	1.94	.90	1.81	1.77	0.00	.07	3.47	0.00	2.01	3.51	1.90
18	2.36	1.85	.78	2.86	1.56	.74	1.18	3.57	1.09	2.37	3.69	1.59
19	1.78	2.60	.73	3.78	2.11	1.48	1.69	4.50	1.43	2.48	4.41	1.40

TABLE IX

FREQUENCY - NULL SURFACE WAVE DATA

B Series (Alloy 2014-T6; Thickness 0.125 Inches)

(Frequency in KHz

After Welding

Plate No.	B-1				B-2				B-3			
Side No.	S_1		S_2		S_1		S_2		S_1		S_2	
Location	1-2	9-2	1-2	9-2	1-2	9-2	1-2	9-2	1-2	9-2	1-2	9-2
Position												
1	3.93	5.82	1.79	3.74	5.96	---	9.77	2.46	7.33	14.96	---	---
2	4.49	5.24	2.06	3.33	4.87	---	0.00	2.66	6.42	12.00	---	---
3	4.12	3.73	.82	2.34	3.73	---	9.58	3.57	5.20	10.74	---	---
4	2.28	1.65	.87	1.91	2.65	---	8.55	3.26	4.49	---	---	---
5	1.58	.64	.38	1.41	2.91	---	7.66	2.88	3.02	---	---	---
6	.14	.16	.41	1.50	2.94	---	7.61	2.06	3.24	0.00	---	---
7	.25	.42	.05	1.60	2.97	---	8.08	2.35	.75	2.98	---	---
8	.24	3.00	0.00	1.30	0.00	---	10.06	3.33	1.85	2.68	---	---
9	1.35	2.04	.87	3.37	4.28	---	10.43	0.00	.07	7.02	---	---
10	2.44	.94	1.42	2.30	4.26	---	9.27	1.11	0.00	4.54	---	---
11	.78	0.00	1.26	1.39	5.19	---	8.24	.37	1.77	2.93	---	---
12	0.00	.20	1.91	.36	3.82	---	8.96	.05	.99	1.57	---	---
13	1.29	.12	2.99	0.00	4.25	---	8.81	0.00	3.90	---	---	---
14	1.52	1.39	2.09	1.47	5.43	---	7.41	1.31	2.06	---	---	---
15	.95	2.05	2.46	1.00	2.27	---	7.53	1.57	3.01	---	---	---
16	2.06	.52	1.66	1.59	1.14	---	9.35	1.99	4.35	6.46	---	---
17	1.90	1.14	1.66	2.49	4.71	---	10.08	1.80	4.24	12.37	---	---
18	3.66	3.78	2.56	3.04	5.02	---	9.13	4.45	5.04	13.02	---	---
19	4.31	3.47	2.49	3.54	5.80	---	9.48	4.31	5.50	12.58	---	---

TABLE IX Continued

Plate No.	B-4				B-5				B-6			
Side No.	S_1		S_2		S_1		S_2		S_1		S_2	
Location	1-2	9-2	1-2	9-2	1-2	9-2	1-2	9-2	1-2	9-2	1-2	9-2
Position												
1	3.34	3.43	3.78	4.46	4.02	---	5.49	6.30	3.20	5.18	8.30	2.27
2	4.41	2.46	2.97	3.54	3.27	---	4.60	5.85	2.92	5.86	7.38	1.83
3	4.40	2.79	2.05	3.60	---	---	5.95	5.41	2.58	4.13	5.83	1.21
4	3.75	2.56	.97	3.20	---	---	4.14	4.66	2.00	2.42	3.55	.86
5	3.12	1.71	.42	2.41	---	---	2.18	3.79	1.81	1.56	1.55	.14
6	2.24	1.03	0.00	2.14	4.17	---	2.28	2.51	1.14	.57	0.00	0.00
7	3.47	.86	.70	1.92	5.30	---	1.47	1.91	.54	0.00	.12	.24
8	4.10	1.23	.41	2.69	8.81	---	.47	1.60	1.93	.11	1.96	.54
9	2.70	.93	1.43	1.83	7.38	---	.45	1.14	1.80	1.93	2.59	1.24
10	.67	0.00	1.48	1.66	5.85	---	.47	.90	1.12	1.43	3.60	1.60
11	2.32	.85	.83	2.27	---	---	1.08	1.48	.02	1.34	1.56	1.40
12	.05	.98	1.87	1.34	---	---	0.00	1.62	.35	1.55	.97	.80
13	.96	1.39	.59	.88	---	---	.09	1.32	0.00	1.20	1.86	.66
14	0.00	1.34	.28	0.00	---	---	.55	0.00	1.49	.86	1.27	.18
15	.46	2.15	1.19	.51	.46	---	2.28	.12	2.19	1.92	2.94	.74
16	.58	3.90	1.70	1.13	0.00	---	2.57	2.16	2.02	3.02	3.59	1.49
17	3.31	4.39	2.33	1.70	1.56	---	3.12	2.60	3.49	4.74	4.46	2.23
18	3.85	4.13	1.53	2.38	2.29	---	4.79	4.16	4.00	5.12	4.33	2.60
19	4.37	3.68	2.27	3.24	4.37	---	5.87	5.09	3.40	5.09	5.14	3.20

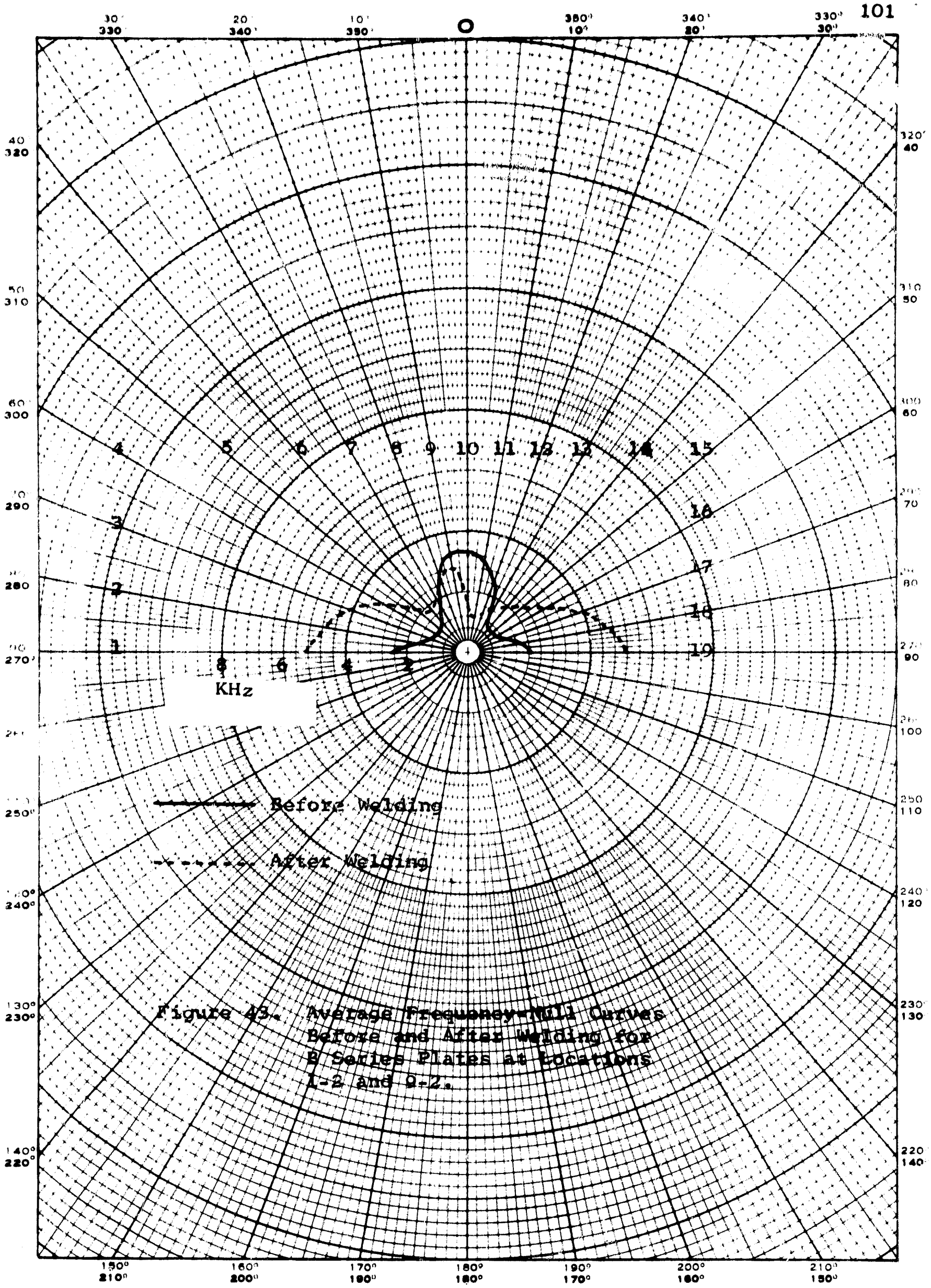

Figure 43. Average Frequency-Null Curves Before and After Welding for B Series Plates at Locations 1-2 and 9-2.

TABLE X

FREQUENCY - NULL SURFACE WAVE DATA

B Series (Alloy 2014-T6; Thickness 0.125 Inches)

(Frequency in KHz
Location 5-3
Before Welding

Plate No.	B-1		B-2		B-3		B-4		B-5		B-6	
Side No.	S_1	S_2	S_1	S_2	S_1	S_2	S_1	S_2	S_1	S_2	S_1	S_2
Position												
1	.25	1.10	1.64	1.57	2.33	3.70	3.40	1.22	1.11	1.36	3.37	2.00
2	1.05	1.35	1.29	.51	3.34	3.32	2.40	1.20	.57	1.44	2.77	1.64
3	1.70	1.30	.42	.90	3.04	3.03	2.75	1.20	.91	1.73	2.44	.45
4	1.89	1.49	.78	1.46	2.99	2.92	1.91	1.85	1.41	1.54	1.29	0.00
5	.52	1.68	0.00	1.59	2.97	2.43	1.34	1.90	1.97	1.79	1.22	.51
6	0.00	1.76	1.87	1.76	2.76	2.17	1.71	2.24	2.61	1.04	.06	.49
7	1.33	2.97	1.93	1.56	2.28	2.27	2.69	2.66	3.97	0.00	1.06	.72
8	1.97	3.41	2.95	2.76	1.76	2.64	2.69	4.07	4.37	1.56	1.38	2.39
9	2.22	3.59	3.36	3.89	.76	3.59	2.84	3.74	4.52	3.36	1.47	3.72
10	2.75	3.59	3.67	3.42	0.00	3.50	2.86	3.74	4.20	2.91	1.50	4.05
11	3.00	3.08	4.70	3.28	.33	2.47	2.24	2.66	4.55	3.05	.74	3.93
12	1.59	2.95	4.40	2.34	.60	3.82	1.66	3.36	3.84	2.60	0.00	2.82
13	1.59	1.62	2.42	2.12	.39	2.92	1.07	1.48	1.66	1.37	.66	1.60
14	1.50	0.00	1.51	.93	.76	3.10	.45	0.00	0.00	1.43	.45	.74
15	1.11	0.00	1.10	1.06	1.35	1.58	0.00	.17	1.55	1.09	1.24	1.23
16	.65	.79	1.40	.99	2.09	0.00	.61	.17	1.00	1.09	2.04	1.90
17	1.88	.77	1.12	.06	1.86	.20	1.39	.17	2.12	2.98	5.70	1.54
18	2.25	.48	1.47	0.00	2.31	1.20	1.39	.12	1.86	2.54	4.03	1.83
19	2.50	.82	1.59	.45	2.61	1.70	1.90	.31	2.14	1.80	3.82	2.84

TABLE XI

FREQUENCY - NULL SURFACE WAVE DATA

B Series (Alloy 2014-T6; Thickness 0.125 Inches)

(Frequency in KHz
Location 5-3
After Welding

Plate No.	B-1		B-2		B-3		B-4		B-5		B-6	
Side No.	S_1	S_2	S_1	S_2	S_1	S_2	S_1	S_2	S_1	S_2	S_1	S_2
Position												
1	4.22	1.60	2.26	1.47	7.43	1.47	4.19	2.56	2.44	4.35	5.96	5.94
2	4.23	.70	2.11	1.35	6.90	1.35	4.32	1.14	3.33	3.40	5.37	5.87
3	3.36	.52	1.40	1.75	7.33	1.75	3.00	1.46	3.22	2.53	6.09	3.84
4	3.31	0.00	2.07	1.48	5.36	1.48	2.81	1.17	3.10	1.43	5.93	2.96
5	4.04	1.29	2.56	2.32	3.18	2.32	0.00	.28	2.68	.52	4.64	1.85
6	5.03	.76	2.75	3.47	0.00	3.47	1.56	1.17	1.32	.86	3.27	.96
7	.01	.97	2.50	3.21	.98	3.21	.53	.46	1.73	.58	2.89	0.00
8	0.00	.56	1.92	3.94	2.29	3.94	.45	1.47	2.25	1.79	1.74	1.99
9	.03	.99	2.73	4.79	2.10	4.73	.70	1.85	3.12	1.14	1.62	2.21
10	2.16	1.33	2.48	4.04	4.25	4.04	1.22	1.59	2.48	1.29	1.46	1.97
11	4.95	.93	1.86	1.57	.61	1.57	1.70	1.01	3.88	1.05	.83	2.53
12	2.76	1.19	1.71	2.47	.43	2.47	2.11	.27	1.22	.43	0.00	1.81
13	3.87	1.67	.70	1.66	3.44	1.66	2.81	.09	0.00	.57	1.19	.66
14	5.61	2.70	0.00	0.00	2.95	0.00	2.39	0.00	.54	0.00	1.47	.64
15	2.87	3.49	1.21	1.09	3.96	1.09	2.12	1.19	2.02	1.24	1.64	1.78
16	3.78	4.34	2.99	.23	3.57	.23	2.65	.59	1.39	1.67	2.52	2.39
17	6.05	4.41	2.62	1.70	6.44	1.70	4.16	.99	.46	2.82	4.20	3.44
18	4.56	3.24	3.07	2.37	5.03	2.37	2.88	.75	1.36	3.88	4.76	3.84
19	4.94	4.94	3.22	1.27	5.84	1.27	4.19	1.46	1.79	4.40	5.70	4.55

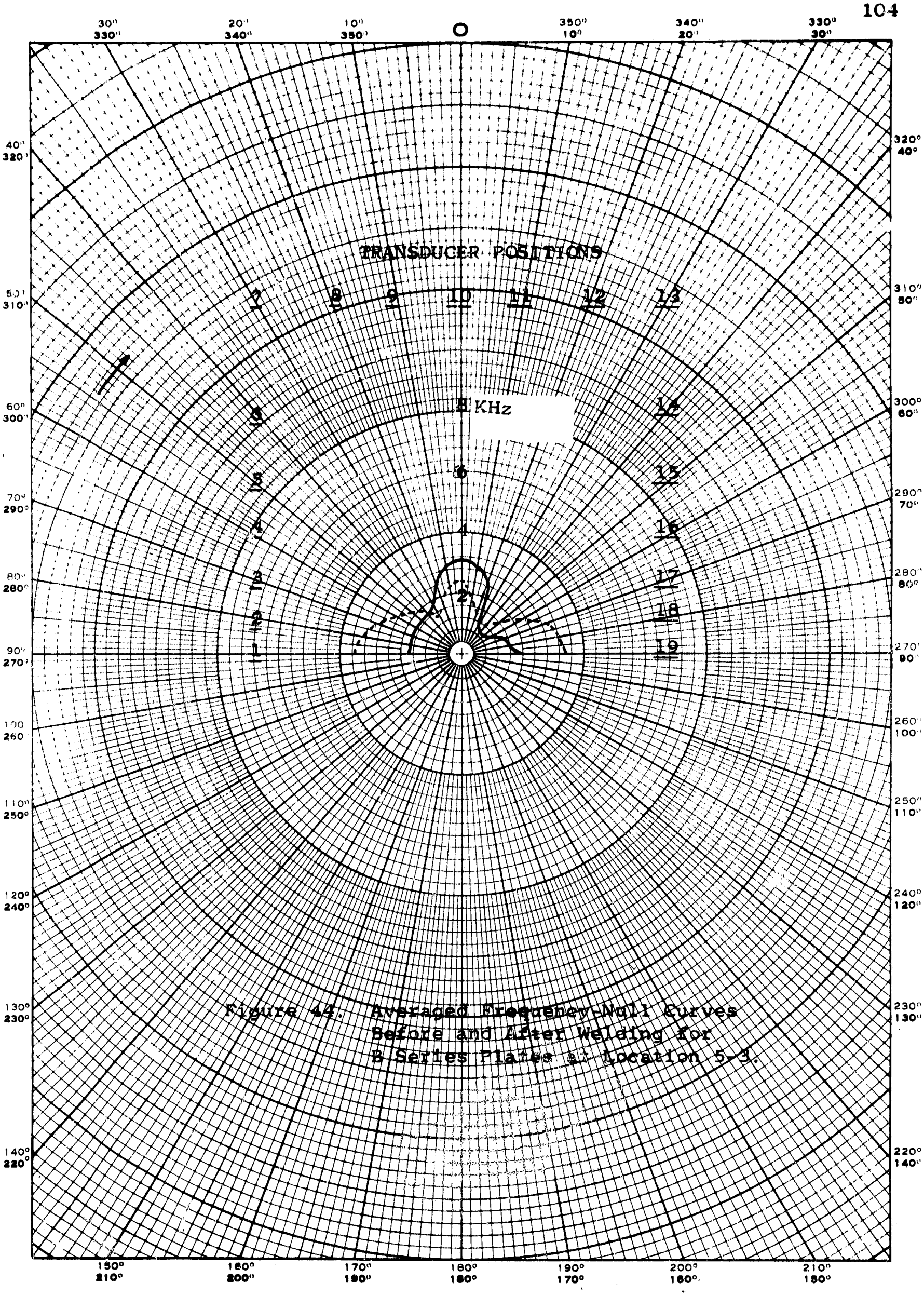

Figure 44. Averaged Frequency-Null Curves Before and After Welding for B Series Plates at Location 5-3.

TABLE XII

FREQUENCY - NULL SURFACE WAVE DATA

P Series (Alloy 2014-T6; Thickness 0.5 Inches)

(Frequency in KHz

Before Welding

Plate No.	P-1				P-2				P-3			
Side No.	S_1		S_2		S_1		S_2		S_1		S_2	
Location	1-2	9-2	1-2	9-2	1-2	9-2	1-2	9-2	1-2	9-2	1-2	9-2
Position												
1	1.18	1.19	3.19	5.75	2.27	1.41	5.56	1.29	1.71	.30	.14	3.05
2	2.53	.31	4.20	2.23	1.83	.70	6.56	.99	.66	.02	0.00	0.00
3	2.36	0.00	4.28	0.00	2.82	0.00	7.99	0.00	0.00	0.00	.64	.41
4	4.50	1.23	5.40	1.75	5.15	.87	9.35	.97	.99	1.56	1.33	1.66
5	5.96	2.13	5.60	4.35	6.72	2.87	11.86	2.99	2.90	2.35	4.26	3.75
6	8.69	3.42	8.60	6.12	10.03	5.28	14.32	5.78	5.30	5.47	7.35	8.67
7	12.20	5.58	12.32	9.09	11.80	8.71	16.69	9.89	9.72	9.24	10.72	12.45
8	14.23	9.82	15.95	12.15	14.55	12.37	19.33	12.95	11.21	10.39	14.62	16.74
9	15.78	10.73	18.16	15.55	15.99	14.93	19.88	14.61	12.27	12.03	17.65	16.20
10	16.45	11.11	18.15	16.94	15.65	16.13	20.89	15.18	13.01	11.46	18.86	16.85
11	15.48	10.20	17.92	18.50	15.20	14.52	21.65	15.30	12.93	10.19	17.92	16.37
12	14.18	9.58	14.62	20.25	12.15	12.83	17.07	11.91	12.94	9.71	14.41	14.97
13	11.26	6.42	10.14	18.17	9.13	9.46	12.29	8.29	8.73	7.09	9.88	11.63
14	7.54	3.01	6.80	16.10	6.51	5.78	7.66	3.87	6.19	3.19	8.25	7.68
15	3.93	1.61	3.26	14.69	4.55	4.60	4.60	1.56	3.61	1.62	4.54	3.10
16	2.28	.03	0.00	11.91	2.01	1.27	1.12	.14	1.93	1.24	3.32	1.80
17	0.00	.18	.15	9.45	1.00	1.98	.42	.51	2.25	1.10	1.82	1.35
18	.84	.33	1.16	7.40	0.00	.67	.33	.31	2.07	.99	.36	2.54
19	.23	.63	3.10	4.55	.25	1.03	0.00	.51	2.01	2.14	.46	2.63

TABLE XII Continued

Plate No.	P-4				P-5				P-6			
Side No.	S_1		S_2		S_1		S_2		S_1		S_2	
Location	1-2	9-2	1-2	9-2	1-2	9-2	1-2	9-2	1-2	9-2	1-2	9-2
Position												
1	2.85	1.90	0.00	4.80	1.29	2.54	1.22	.75	2.09	0.00	.27	.10
2	4.06	0.00	.90	2.14	2.23	.75	2.29	1.09	1.48	1.11	.70	.39
3	2.44	1.78	1.31	0.00	2.82	0.00	2.01	3.36	2.42	2.20	0.00	.28
4	3.92	2.37	4.88	1.10	3.98	1.30	2.05	4.60	3.46	2.43	.10	1.44
5	6.65	6.76	6.24	3.36	8.30	3.90	3.16	6.75	4.97	4.11	2.00	4.27
6	8.05	9.01	7.84	6.40	10.33	7.10	5.46	9.56	6.79	7.51	5.26	7.70
7	11.15	9.22	10.38	9.60	10.50	9.92	8.21	11.96	8.15	9.89	8.60	12.03
8	13.40	11.57	12.16	12.07	14.04	13.57	11.20	14.89	9.10	13.36	12.75	15.80
9	15.80	14.23	15.71	13.58	17.37	15.88	13.55	15.57	9.95	15.09	16.50	15.38
10	15.40	16.18	15.21	12.78	18.74	16.93	15.69	17.86	10.30	15.64	16.20	14.68
11	13.39	12.58	14.28	10.90	15.93	16.70	14.71	17.53	10.53	14.36	19.10	14.12
12	10.70	10.23	11.22	8.10	10.53	14.58	11.67	12.91	5.97	12.70	18.45	12.00
13	8.25	8.93	8.42	7.03	7.46	11.10	9.09	8.16	5.62	10.11	16.00	9.11
14	6.65	5.23	4.18	3.27	4.98	6.80	6.36	5.54	2.90	7.68	13.56	6.50
15	2.25	3.83	2.45	.62	4.25	3.47	3.37	4.64	1.38	4.92	9.66	4.26
16	1.40	2.73	2.02	.34	.98	.64	1.77	3.36	.83	2.94	6.99	1.60
17	0.00	1.73	2.06	2.49	0.00	.68	.27	1.16	.73	1.86	5.90	.81
18	.40	1.27	2.06	4.37	.48	1.10	0.00	0.00	1.27	1.25	3.10	.95
19	2.20	1.12	1.86	2.84	.36	1.00	.86	2.76	0.00	.84	1.26	0.00

TABLE XIII

FREQUENCY - NULL SURFACE WAVE DATA

P Series (Alloy 2014-T6; Thickness 0.5 Inches)

(Frequency in KHz

After Welding

Plate No.	P-1				P-4				P-2			
Side No.	S_1		S_2		S_1		S_2		S_1		S_2	
Location	1-2	9-2	1-2	9-2	1-2	9-2	1-2	9-2	1-2	9-2	1-2	9-2
Position												
1	2.32	1.15	1.86	1.96	1.20	2.14	2.68	7.59	1.12	.64	2.12	1.97
2	1.90	2.68	3.19	0.00	1.00	1.07	2.00	3.87	1.21	1.98	4.62	.22
3	3.31	2.29	3.68	.67	1.44	.88	2.45	2.11	2.20	1.88	6.54	0.00
4	3.72	3.51	4.35	2.04	1.85	1.34	2.96	.88	4.09	1.77	8.65	.78
5	5.35	4.99	4.25	2.97	3.00	3.58	6.23	3.11	4.51	3.40	10.27	1.57
6	9.39	6.26	5.97	5.35	6.36	5.66	6.92	4.01	7.91	4.59	14.96	4.79
7	10.47	8.55	8.14	7.24	6.86	8.26	8.82	6.63	9.99	6.13	17.76	7.37
8	14.37	11.28	10.87	9.37	9.04	10.71	11.13	7.79	11.85	7.83	20.42	10.23
9	15.74	12.62	13.75	10.19	11.46	13.73	12.17	9.30	14.20	11.74	19.51	11.67
10	15.84	13.17	13.96	10.96	12.84	13.68	13.23	10.18	13.59	13.20	17.35	11.73
11	14.39	12.60	12.31	10.79	11.84	12.84	11.12	9.36	13.24	11.81	15.71	12.30
12	12.38	10.62	10.17	9.13	10.11	10.13	8.25	7.36	10.99	10.09	17.24	11.73
13	9.33	8.46	8.16	7.07	7.80	9.05	4.76	5.05	7.02	7.87	14.79	9.30
14	5.79	4.60	4.48	6.01	6.27	6.21	3.77	3.32	4.55	5.39	9.42	5.33
15	3.72	2.64	2.10	1.90	2.91	4.49	2.39	.52	1.64	3.39	6.98	4.06
16	2.68	1.05	.06	.52	0.00	1.34	1.14	0.00	.94	2.48	4.92	4.99
17	0.00	.44	0.00	.79	0.00	.81	0.00	4.03	0.00	1.28	1.98	1.26
18	2.49	0.00	1.54	.98	.13	.64	1.29	6.81	.87	.76	0.00	2.19
19	2.40	.19	2.58	2.05	.24	0.00	2.97	7.72	.61	0.00	.99	2.84

TABLE XIII Continued

Plate No.	P-5				P-3				P-6			
Side No.	S_1		S_2		S_1		S_2		S_1		S_2	
Location	1-2	9-2	1-2	9-2	1-2	9-2	1-2	9-2	1-2	9-2	1-2	9-2
Position												
1	3.45	.80	3.18	2.51	2.19	.12	1.85	2.38	.80	1.17	1.74	1.05
2	4.10	0.00	2.38	.23	1.88	0.00	1.53	.07	1.15	1.34	.39	2.14
3	6.46	.08	2.60	0.00	0.00	.09	.73	.09	.64	.85	.50	.61
4	8.70	1.25	2.51	1.46	1.02	.82	1.48	0.00	.61	1.28	.37	2.55
5	10.59	1.95	3.05	2.51	2.48	2.62	3.57	3.00	2.23	3.13	1.34	4.05
6	12.24	4.66	5.18	5.23	3.67	3.44	7.29	8.43	3.60	4.63	3.41	7.23
7	9.74	8.68	7.86	6.39	5.28	7.70	9.92	14.00	4.32	8.68	8.86	11.07
8	11.74	11.87	9.84	9.68	9.35	9.09	14.67	15.10	6.58	12.09	14.31	13.29
9	13.44	14.39	13.57	10.44	9.52	9.53	18.16	16.34	7.02	14.04	16.33	13.22
10	14.92	15.85	13.94	11.18	9.83	9.97	17.12	16.65	8.21	13.92	16.15	14.79
11	15.90	14.52	13.54	10.88	9.98	9.55	17.81	15.80	7.04	13.04	20.45	13.64
12	9.82	12.73	10.51	9.89	8.76	7.42	16.03	15.51	6.63	11.52	18.83	11.51
13	10.49	9.43	8.54	6.78	6.82	5.22	11.30	11.49	6.63	7.74	14.67	8.80
14	6.12	6.26	5.54	4.47	4.19	2.30	7.70	8.42	1.81	5.09	9.34	5.97
15	5.33	3.69	2.77	1.74	2.61	1.32	5.46	4.42	.40	2.15	3.79	3.26
16	1.09	2.08	.71	1.80	.74	.39	1.52	2.81	.35	.11	2.20	1.59
17	0.00	1.22	0.00	.94	.15	.21	.07	3.60	.55	0.00	3.78	.65
18	2.18	1.15	1.01	1.35	.06	.99	.69	2.54	0.00	.67	1.97	0.00
19	4.17	.61	1.41	.48	1.08	2.92	0.00	1.69	.95	1.75	0.00	.45

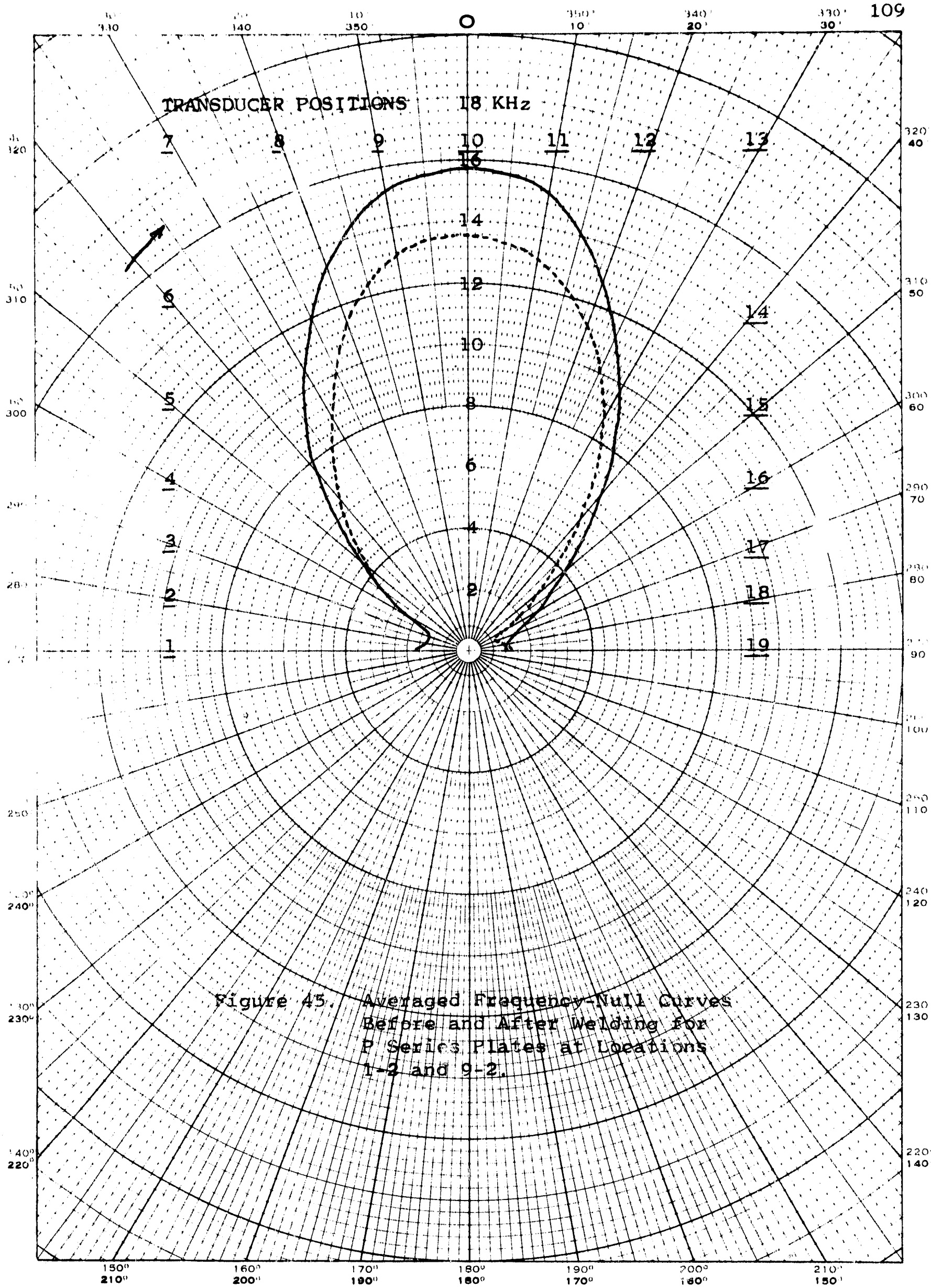

Figure 45. Averaged Frequency-Null Curves Before and After Welding for P Series Plates at Locations 1-2 and 9-2.

TABLE XIV

FREQUENCY - NULL SURFACE WAVE DATA

P Series (Alloy 2014-T6; Thickness 0.5 Inches)

(Frequency in KHz

Location 5-3

Before Welding

Plate No.	P-1		P-2		P-3		P-4		P-5		P-6	
Side No.	S_1	S_2	S_1	S_2	S_1	S_2	S_1	S_2	S_1	S_2	S_1	S_2
1	1.46	1.18	.93	2.83	2.61	2.54	2.02	.87	6.20	3.02	2.61	1.04
2	.93	.45	1.30	2.10	1.48	1.41	1.13	.63	2.80	1.23	2.20	0.00
3	1.40	.47	.53	1.90	2.06	0.00	1.90	.04	.72	1.74	1.60	.03
4	2.57	1.48	.93	2.60	4.10	.14	1.87	1.54	0.00	2.54	2.30	.78
5	4.36	2.28	3.74	5.24	5.58	1.54	3.97	3.86	.87	3.63	3.69	1.88
6	5.76	5.02	5.00	8.04	7.38	5.40	7.38	6.92	2.70	5.99	6.00	4.17
7	9.79	7.32	8.52	12.60	9.95	8.22	10.20	10.36	4.12	8.12	7.70	7.60
8	11.76	10.58	10.98	15.78	12.90	9.74	13.02	13.00	8.74	11.63	10.74	10.68
9	13.02	11.91	13.94	16.60	14.84	10.45	14.44	16.79	10.70	14.34	11.92	12.42
10	13.39	12.98	14.51	16.78	15.22	11.77	14.46	17.73	12.57	15.00	11.92	13.18
11	12.43	12.89	13.94	14.80	14.80	12.54	12.73	16.72	10.70	14.10	10.85	11.88
12	10.83	11.50	11.84	10.80	13.37	11.49	11.43	13.41	8.42	12.10	9.28	10.42
13	7.87	8.85	8.57	7.62	10.67	8.37	8.14	13.41	6.50	8.73	6.56	7.28
14	5.07	5.80	4.90	4.60	7.22	4.99	5.53	6.33	4.78	5.70	3.50	3.84
15	2.77	3.27	2.37	3.03	3.60	4.00	2.65	4.52	1.04	2.99	.70	.68
16	1.26	3.06	.40	1.87	1.88	2.58	.45	2.72	.53	1.75	1.22	.19
17	.46	.94	.29	.58	.80	2.00	0.00	0.00	1.72	0.00	.33	.13
18	0.00	0.00	0.00	0.00	0.00	1.68	.17	.24	3.70	1.09	.15	.10
19	.64	.91	.53	.72	.69	2.22	.81	.74	4.24	.52	0.00	.16

TABLE XV

FREQUENCY - NULL SURFACE WAVE DATA

P Series (Alloy 2014-T6; Thickness 0.5 Inches)

(Frequency in KHz

Location 5-3

After Welding

Plate No.	P-1		P-2		P-3		P-4		P-5		P-6	
Side No.	S_1	S_2	S_1	S_2	S_1	S_2	S_1	S_2	S_1	S_2	S_1	S_2
Position												
1	2.86	1.96	.35	1.22	0.00	2.86	1.20	.98	2.56	1.98	.84	2.99
2	2.07	0.00	0.00	1.06	1.62	3.14	1.00	.70	5.84	0.00	.84	2.44
3	0.00	.67	2.40	.81	1.57	2.57	1.44	.94	4.38	.40	1.63	2.35
4	1.69	2.04	3.47	1.75	.63	5.06	1.85	.98	3.25	.39	2.61	0.00
5	6.92	2.97	6.27	3.81	3.38	6.82	3.00	2.95	3.38	2.47	3.57	2.03
6	8.34	5.35	6.84	6.12	6.42	8.84	6.36	5.65	8.09	4.82	6.32	3.52
7	8.75	7.24	8.75	10.58	8.30	8.70	6.86	7.89	8.84	7.30	8.16	7.02
8	12.31	9.37	10.84	12.93	13.29	10.62	9.04	11.03	13.55	10.60	10.22	10.42
9	15.25	10.19	13.49	14.97	14.35	10.46	11.46	12.93	17.94	12.56	12.38	12.11
10	14.20	10.96	12.04	15.52	13.26	11.64	12.84	13.03	16.58	13.65	12.11	12.21
11	14.30	10.79	13.24	14.80	12.99	11.84	11.84	12.18	15.33	13.58	12.71	10.21
12	13.01	9.13	11.37	12.25	10.84	12.98	10.11	10.30	14.33	11.00	10.09	9.22
13	10.45	7.07	9.58	8.08	10.61	7.91	7.80	8.15	10.75	6.79	6.63	7.82
14	8.96	6.01	5.60	5.07	6.78	5.60	6.27	4.26	6.66	5.32	3.96	5.89
15	6.49	1.90	3.40	3.06	5.44	4.40	2.91	3.49	5.19	2.25	2.88	4.83
16	4.12	.52	.83	2.45	4.25	3.35	0.00	1.14	5.42	2.76	1.58	3.51
17	4.31	.79	.19	.64	2.21	0.00	0.00	.80	2.69	1.19	.39	3.94
18	3.16	.98	.25	.52	1.14	1.56	.13	.56	0.00	1.51	0.00	2.79
19	4.52	2.05	.88	0.00	.47	2.29	.24	0.00	1.67	.40	.08	2.37

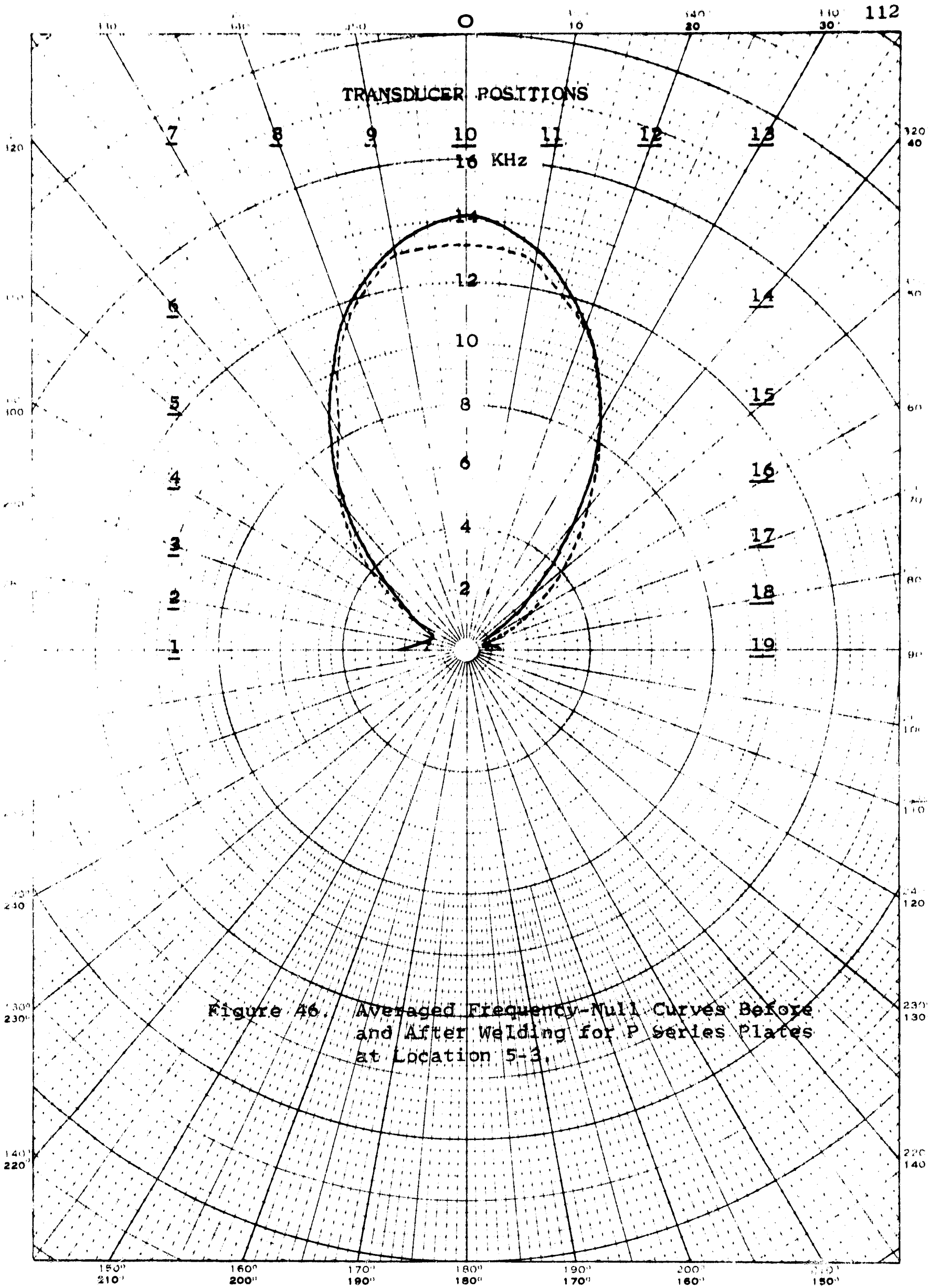

Figure 46. Averaged Frequency-Null Curves Before and After Welding for P Series Plates at Location 5-3.

TABLE XVI

FREQUENCY - NULL SURFACE WAVE DATA

S Series (Alloy 2219-T87; Thickness 0.5 Inches)

(Frequency in KHz

Before Welding

Plate No.	S-1				S-2				S-3			
Side No.	S_1		S_2		S_1		S_2		S_1		S_2	
Location	1-2	9-2	1-2	9-2	1-2	9-2	1-2	9-2	1-2	9-2	1-2	9-2
Position												
1	12.94	15.57	6.90	11.18	4.94	9.51	14.81	14.16	12.23	12.28	16.95	16.01
2	12.85	14.43	6.53	7.89	3.83	9.26	13.02	12.61	11.69	10.28	13.72	13.23
3	10.76	11.80	5.34	5.82	4.90	7.30	10.07	10.66	6.77	7.40	9.13	9.64
4	7.80	8.83	4.02	3.42	2.94	5.37	6.37	7.51	3.47	4.11	3.56	6.01
5	6.41	5.79	2.14	3.53	1.31	2.31	2.67	3.92	1.05	1.30	1.72	3.16
6	4.16	3.88	2.17	1.46	0.00	.89	1.17	1.81	0.00	0.00	1.30	2.92
7	2.82	3.03	1.88	1.09	.07	.66	.43	1.22	1.74	.20	2.87	4.18
8	2.23	1.96	1.90	1.15	1.72	4.05	2.33	1.20	4.84	.12	5.35	9.03
9	1.95	2.49	2.96	1.78	3.17	4.97	2.91	2.65	6.98	2.02	7.03	6.94
10	1.94	2.42	2.64	2.76	3.91	5.95	3.83	2.99	7.58	1.80	8.00	8.01
11	1.88	1.27	2.38	1.22	3.67	5.10	2.99	2.77	7.70	2.41	6.47	4.61
12	0.00	1.23	1.14	.54	2.54	2.36	.58	1.73	4.70	3.18	4.17	1.27
13	.97	0.00	0.00	0.00	1.15	.76	.01	0.00	3.75	1.74	0.00	0.00
14	1.00	.32	.09	1.71	.81	0.00	0.00	.63	2.85	1.08	.02	.84
15	2.67	5.29	1.64	4.02	.84	2.11	2.90	2.29	3.83	3.61	1.22	4.21
16	6.27	10.46	3.77	7.66	1.24	4.10	5.73	5.46	7.25	5.72	4.94	9.14
17	9.51	13.78	5.93	8.22	3.31	6.78	9.57	8.81	9.00	8.15	9.42	13.40
18	11.84	15.18	7.22	8.26	4.56	8.09	12.71	11.46	10.30	11.92	13.95	13.87
19	11.73	15.57	7.26	9.03	4.44	9.14	14.21	12.46	12.44	13.04	16.05	15.51

TABLE XVI Continued

Plate No.	S-4				S-5				S-6			
Side No.	S_1		S_2		S_1		S_2		S_1		S_2	
Location	1-2	9-2	1-2	9-2	1-2	9-2	1-2	9-2	1-2	9-2	1-2	9-2
Position												
1	15.03	12.42	12.21	6.30	9.18	15.59	13.99	---	9.76	8.33	5.82	9.92
2	11.69	12.51	8.93	4.89	7.80	13.90	11.22	---	8.51	8.14	4.34	7.17
3	9.29	9.78	7.39	3.03	5.63	10.52	7.76	---	6.34	7.04	2.56	3.77
4	4.37	6.57	4.89	2.22	4.82	7.59	7.60	---	4.07	4.90	1.63	1.77
5	.68	3.82	1.57	1.09	4.83	5.20	3.84	---	1.91	3.69	.67	0.00
6	2.83	3.57	.25	1.06	4.70	3.27	0.00	---	.51	2.57	.97	1.05
7	.64	3.69	0.00	1.71	5.08	3.80	1.40	---	0.00	1.93	2.41	1.67
8	2.10	2.05	1.86	3.54	5.83	3.80	1.09	---	.93	2.61	3.38	1.84
9	1.50	1.30	2.80	4.41	6.91	6.82	3.41	---	4.58	3.54	4.09	2.66
10	1.82	1.92	2.30	4.24	7.08	7.50	4.08	---	5.17	2.20	5.16	1.06
11	1.23	0.00	2.67	3.70	5.60	7.23	4.10	---	5.06	1.78	3.84	.26
12	.09	1.02	1.98	2.06	4.36	3.27	2.77	---	4.41	.56	1.86	1.43
13	0.00	1.58	1.91	.77	1.98	3.29	2.19	---	2.87	0.00	.36	.05
14	2.55	2.69	2.03	.26	0.00	0.00	1.15	---	2.50	.91	0.00	.86
15	5.67	4.64	3.40	0.00	1.71	4.92	1.98	---	2.44	1.44	1.18	2.33
16	9.60	6.40	6.27	1.72	1.39	10.70	7.20	---	1.04	1.64	1.90	4.64
17	11.46	9.67	9.60	3.47	3.46	12.25	9.72	---	5.27	4.22	3.71	8.27
18	11.57	8.92	11.22	6.10	5.38	14.45	17.92	---	6.28	5.86	5.78	10.31
19	10.53	10.47	11.53	5.40	8.78	16.19	---	---	8.91	8.16	7.02	10.19

TABLE XVII

FREQUENCY - NULL SURFACE WAVE DATA

S Series (Alloy 2219-T87; Thickness 0.5 Inches)

(Frequency in KH_z

After Welding

Plate No.	S-1				S-2				S-3			
Side No.	S_1		S_2		S_1		S_2		S_1		S_2	
Location	1-2	9-2	1-2	9-2	1-2	9-2	1-2	9-2	1-2	9-2	1-2	9-2
Position												
1	13.07	17.38	11.35	14.14	8.60	9.30	17.23	14.63	16.58	15.25	17.15	12.44
2	12.46	16.42	9.17	11.88	7.92	8.84	15.45	14.07	15.47	15.18	14.46	11.44
3	12.38	14.74	7.88	9.39	5.95	6.73	11.70	11.20	12.27	---	11.53	8.40
4	9.73	10.95	7.24	5.88	5.37	3.46	7.36	7.69	12.97	---	8.28	5.46
5	6.31	7.95	4.69	1.90	4.79	.71	4.23	3.79	---	---	4.97	2.50
6	4.25	4.90	3.01	.86	.86	.29	.96	.85	---	---	4.45	1.55
7	1.36	3.36	1.79	0.00	0.00	.65	.23	.20	0.00	0.00	4.21	.98
8	0.00	2.53	.21	.84	.98	1.85	.37	0.00	3.32	1.09	5.80	3.05
9	.74	1.69	.91	.05	2.19	3.09	1.94	2.33	3.66	1.14	8.01	3.84
10	.34	3.62	1.41	.60	2.01	3.50	2.55	2.80	6.16	1.65	8.73	5.87
11	.14	3.20	.74	2.52	3.08	3.06	1.89	2.96	7.58	---	6.64	5.11
12	.18	3.13	1.87	1.55	2.10	1.43	.52	1.26	3.90	---	4.26	2.74
13	.06	0.00	0.00	1.46	1.91	.51	0.00	.36	2.64	---	2.84	0.00
14	1.71	1.36	.87	2.96	2.08	0.00	.94	1.93	5.01	---	0.00	.04
15	3.68	4.27	3.41	6.06	2.45	1.84	4.75	3.74	4.86	---	1.28	.55
16	7.48	7.21	5.59	9.11	3.27	3.91	7.84	8.25	11.61	---	6.27	4.78
17	9.63	12.10	8.56	13.44	5.72	6.79	11.49	11.04	14.38	11.61	9.54	9.69
18	12.11	15.43	11.61	13.38	7.47	8.99	15.56	14.01	16.18	12.86	15.21	13.04
19	13.28	18.15	11.66	14.26	8.56	10.25	16.53	14.88	14.02	14.62	16.10	13.04

TABLE XVII Continued

Plate No.	S-4				S-5				S-6			
Side No.	S_1		S_2		S_1		S_2		S_1		S_2	
Location	1-2	9-2	1-2	9-2	1-2	9-2	1-2	9-2	1-2	9-2	1-2	9-2
Position												
1	9.45	15.26	13.10	10.93	6.02	9.24	17.27	23.55	8.78	6.96	12.44	13.73
2	8.55	14.37	12.67	9.77	5.42	7.83	13.91	19.97	8.30	6.18	10.29	12.59
3	7.24	12.10	10.27	8.40	4.53	5.79	11.58	16.97	5.50	4.67	9.55	9.88
4	4.81	11.23	5.22	6.61	4.04	2.74	8.37	11.10	2.99	3.68	5.17	5.05
5	3.12	3.08	2.44	4.16	2.59	.98	5.14	5.53	.97	3.03	3.44	1.34
6	1.32	1.92	.02	2.88	1.87	0.00	1.59	2.81	0.00	1.91	3.00	3.07
7	2.76	1.75	.03	1.57	2.27	.06	1.62	1.88	.31	1.28	2.27	2.33
8	.03	1.43	.20	2.82	3.67	.77	0.00	.04	.29	2.54	2.92	3.81
9	1.33	0.00	0.00	2.17	4.62	2.33	2.68	.26	2.77	3.50	3.69	3.98
10	1.70	1.02	.14	1.46	5.70	2.00	3.12	1.19	2.66	5.18	4.43	3.58
11	.81	.43	.90	.40	4.77	2.87	1.44	.53	5.29	3.99	1.99	2.87
12	.64	.54	.45	0.00	1.36	2.28	.72	.96	3.74	1.16	.68	1.78
13	0.00	.69	2.22	1.26	1.17	1.45	1.33	0.00	2.55	1.99	0.00	0.00
14	1.81	3.26	2.20	1.89	.69	1.90	1.65	4.01	2.61	0.00	1.16	1.96
15	3.94	4.71	2.84	4.37	0.00	2.43	4.27	10.47	2.96	.24	2.95	.46
16	5.89	7.20	5.30	7.14	1.74	3.75	9.00	14.72	5.66	3.12	5.45	4.79
17	7.65	9.94	11.67	9.17	3.54	6.39	14.88	18.33	6.19	5.17	7.41	7.84
18	8.16	12.33	14.16	12.67	5.39	9.02	14.83	24.71	7.98	5.82	9.74	12.23
19	9.38	14.00	14.05	11.35	5.89	10.41	17.45	24.59	9.93	6.22	12.18	13.52

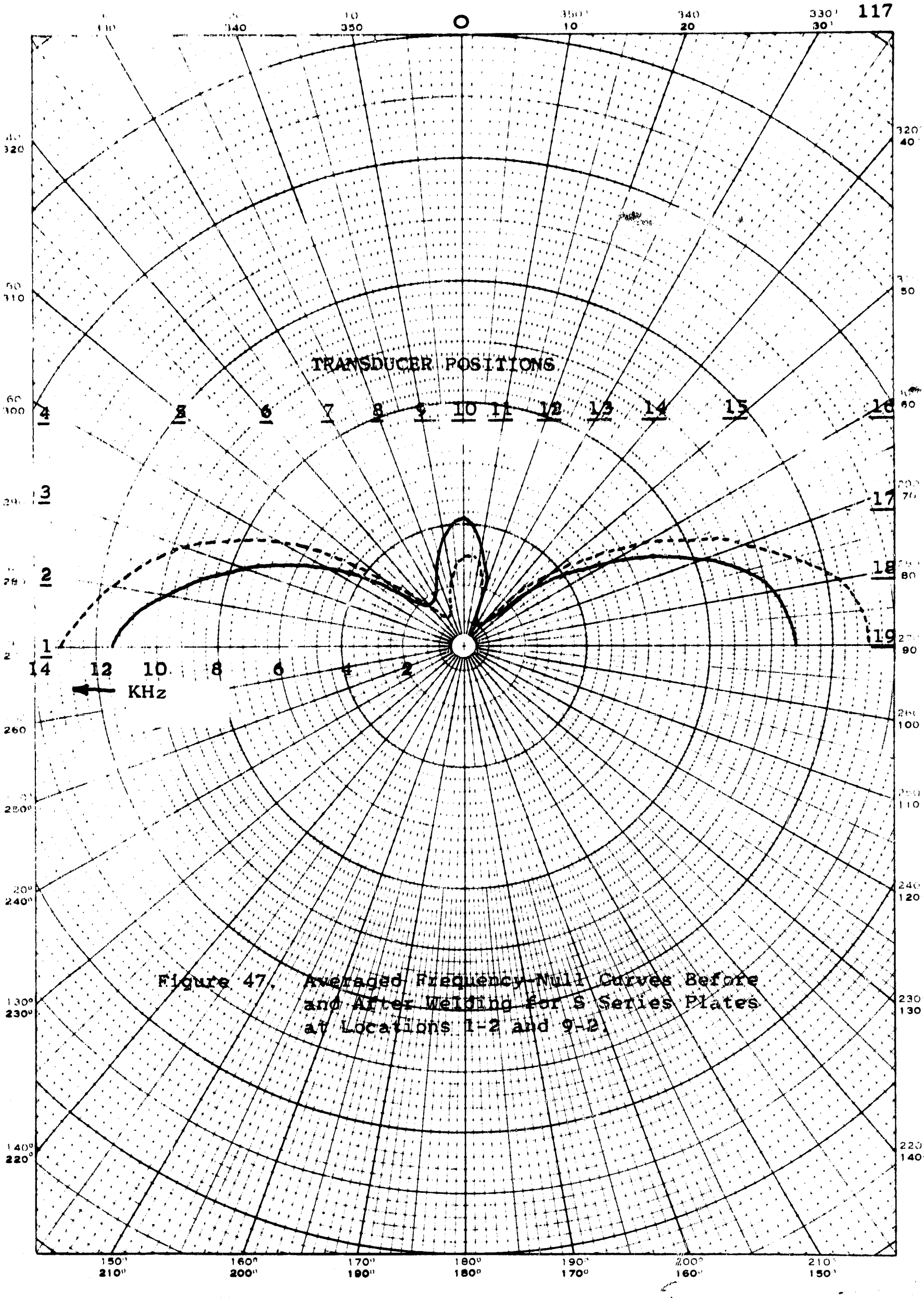

Figure 47. Averaged Frequency-Null Curves Before and After Welding for S Series Plates at Locations 1-2 and 9-2.

TABLE XVIII

FREQUENCY - NULL SURFACE WAVE DATA

S Series (Alloy 2219-T87; Thickness 0.5 Inches)

(Frequency in KHz
Location 5-3
Before Welding

Plate No.	S-1		S-2		S-3		S-4		S-5		S-6	
Side No.	S_1	S_2	S_1	S_2	S_1	S_2	S_1	S_2	S_1	S_2	S_1	S_2
Position												
1	13.66	12.96	6.10	15.45	8.44	15.10	14.86	15.27	15.03	18.94	4.91	7.64
2	12.55	11.75	5.27	15.08	8.43	13.20	12.04	12.52	14.57	13.32	3.51	6.15
3	10.62	9.19	3.93	10.31	6.45	9.84	8.58	11.22	13.06	11.32	2.94	3.49
4	8.35	6.41	2.40	5.87	5.10	6.20	6.85	6.42	9.99	9.00	.66	1.60
5	5.35	2.95	.98	2.60	3.39	3.38	4.34	4.46	7.71	6.69	.12	.02
6	3.31	3.29	1.00	.12	2.72	3.40	2.04	2.02	0.00	3.97	.67	.04
7	1.77	3.25	1.40	0.00	2.14	4.95	0.00	.62	6.41	2.89	1.47	0.00
8	0.00	2.25	3.34	1.78	1.55	7.62	5.90	0.00	6.28	2.50	2.88	1.29
9	.88	1.49	4.93	3.79	1.54	9.32	1.86	1.26	5.37	3.67	4.47	3.06
10	.14	3.69	5.78	4.75	3.54	10.85	3.87	1.18	5.84	4.81	5.19	3.63
11	1.11	1.63	4.86	3.13	1.45	9.37	5.01	5.20	7.60	3.31	5.47	3.40
12	1.89	1.47	3.43	2.49	1.44	5.92	3.08	2.27	7.54	0.00	3.59	1.97
13	2.76	0.00	1.58	1.47	.63	2.19	2.27	.96	7.33	2.00	1.22	1.02
14	3.34	.50	.41	1.57	.71	0.00	2.96	1.34	7.51	2.08	0.00	.35
15	4.54	1.60	0.00	3.64	0.00	1.20	5.16	1.70	10.36	6.20	.56	1.59
16	7.87	4.29	1.84	7.80	2.03	4.85	7.32	6.53	9.98	7.49	2.25	3.64
17	10.61	7.76	3.73	11.21	4.32	9.34	9.66	10.57	10.02	11.72	4.07	5.94
18	12.78	9.92	4.64	13.60	8.04	12.75	12.35	13.88	12.19	11.66	5.11	7.55
19	13.04	11.16	5.94	15.25	8.13	14.19	12.41	15.62	12.87	15.86	5.43	8.50

TABLE XIX

FREQUENCY - NULL SURFACE WAVE DATA

S Series (Alloy 2219-T87: Thickness 0.5 Inches)

(Frequency in KHz
Location 5-3
After Welding

Plate No.	S-1		S-2		S-3		S-4		S-5		S-6	
Side No.	S_1	S_2	S_1	S_2	S_1	S_2	S_1	S_2	S_1	S_2	S_1	S_2
Position												
1	14.40	13.57	9.92	14.76	11.37	10.25	13.22	10.60	6.30	17.84	7.28	9.91
2	14.06	12.74	8.16	15.81	12.71	9.57	12.47	9.93	5.58	13.45	4.93	9.56
3	12.22	10.51	4.15	11.11	6.93	6.30	8.89	7.02	4.90	11.97	2.43	4.49
4	7.80	6.65	1.78	8.20	8.27	2.91	5.72	3.29	2.38	10.04	2.46	0.00
5	5.75	2.87	0.00	4.77	6.68	.68	2.49	.30	1.02	5.77	1.21	.80
6	3.09	1.49	1.00	1.39	4.24	3.34	.06	0.00	0.00	2.99	1.52	1.42
7	2.47	1.31	2.20	0.00	3.00	3.29	.26	.42	.77	.39	1.63	1.19
8	.38	.36	3.87	.92	3.16	5.68	0.00	.22	4.01	0.00	3.71	1.64
9	1.59	3.48	4.51	1.97	3.74	6.25	1.72	.32	3.83	2.72	3.98	3.09
10	2.35	3.08	5.96	3.29	3.94	8.67	2.46	.23	7.26	2.67	3.53	3.26
11	.78	0.00	5.03	2.62	2.61	6.01	2.24	2.96	5.47	3.61	5.30	3.20
12	.09	.41	4.09	1.26	2.00	4.63	4.77	2.58	5.09	1.87	3.54	2.60
13	0.00	1.15	3.22	1.54	0.00	1.20	2.19	2.05	2.85	2.65	.77	2.73
14	1.78	1.45	2.91	2.43	.62	0.00	3.11	2.23	1.65	3.08	.55	2.95
15	4.59	3.84	4.77	3.37	2.60	1.07	6.67	1.69	1.03	5.94	0.00	3.09
16	6.01	6.40	5.35	6.74	4.17	3.44	7.47	3.85	2.46	9.12	2.82	4.95
17	8.77	9.94	8.02	10.87	6.66	5.57	11.02	6.27	2.89	11.47	4.65	9.05
18	11.86	13.11	9.46	12.96	11.46	9.07	13.54	7.39	5.65	14.72	5.59	8.63
19	13.68	13.57	10.95	15.23	11.53	9.85	13.45	10.16	7.48	16.58	6.40	9.70

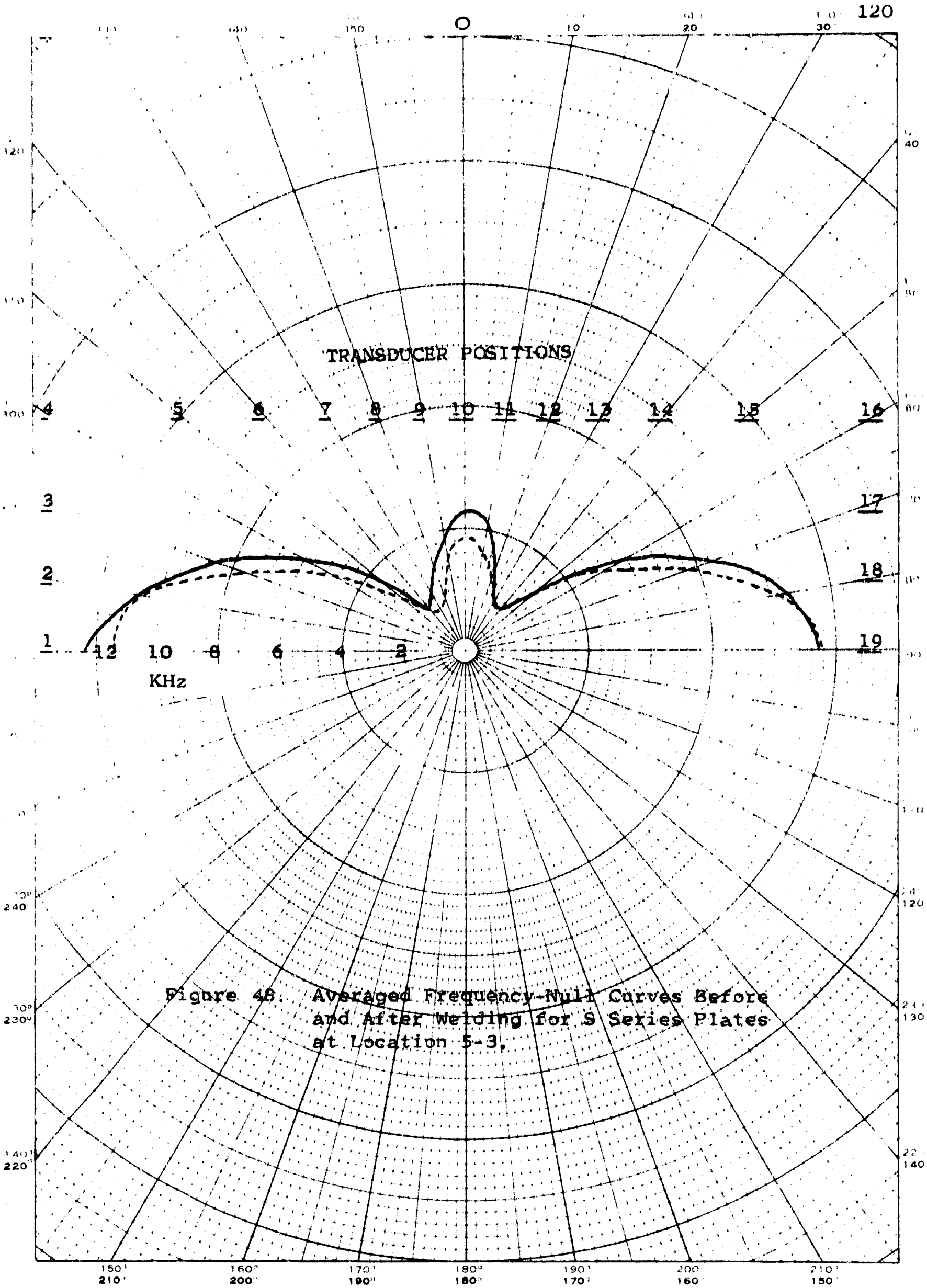

Figure 48. Averaged Frequency-Null Curves Before and After Welding for S Series Plates at Location 5-3.

welding at position 1 for locations 1-2 and 9-2 than at location 5-3. This fact could also be derived from the destructive tests performed on welded plates and is consistent with the time of flight measurements.

The same type of changes in velocity after welding were observed in both the "P" and "S" series. It should be pointed out that the pattern of frequency change versus orientation for the "P" series is rotated by 90^{o} with respect to that of the "S" series. In other words, the initial state of the "P" series shows that there is a higher apparent compression in the direction perpendicular to the side to be welded than in the parallel direction. The converse is true in the "S" series of plates. Here again, this is consistent with the time of flight measurements. The effect resulting from welding, shown by the destructive tests discussed earlier is to add a tensile stress perpendicular to the weldment and a compressive stress parallel to the weldment. With the initial pattern shown for the "P" series such a condition of added stress would tend to shrink the area under the curve. Observing Figure 45, it is seen that this is indeed the case. In the case of the initial pattern observed in the "S" series, the effect of the weldment would be to increase the area under the curve. Here again, this is true as can be seen in Figure 47.

Quantitatively speaking, the added stress can be calculated from the curves by referring to Table I to obtain the proper stress coefficients. For example, in Figure 45, it is seen that the change in the difference in frequency, which corresponds to subtracting the frequency of the dashed curve from the solid curve at position 10, is 2.1 KHz. Table I gives the stress acoustic coefficient for the frequency null system for Alloy 2014-T6 to be 1.00 KHz for 10^{3} pounds per square inch. Therefore, the change in stress would be 2,100 pounds per square inch. It is important to emphasize that this is the average change in stress and that also it is the stress change only at the surface. In addition to being the average over the 12 positions of the 6 plates, the stress change at any one location presented in Table VII is the average stress change seen over the path length covered by the transducer assembly. The transducer assembly employed has a surface wave path length of approximately 2 inches compared to

the 1.125 inches of the two knife edge assembly used in the modified time of flight measurements. Therefore, it can be seen that the nanosecond readings obtained with the time of flight measurement will not necessarily correlate with the frequency null measurement at a given location due to the fact that both transducer assemblies average the surface stress over different path lengths. In other words, if the stress distribution over a path length is other than a constant value, transducer assemblies of different path lengths read a different average stress. This is indeed the case in a welded plate where the stress goes from regions to compression.

IX. APPLICATION TECHNIQUE CONSIDERATIONS

To apply the knowledge and techniques learned from this investigation to specific applications requires careful consideration of all factors involved. It has been demonstrated that both ultrasonic surface and shear waves may be used to measure the stress resulting from an applied load. For residual stresses it is possible to determine the magnitude and major axes of the stress, however, it is difficult to determine whether one axis is in compression or the other axis is in tension. For example, the solid curve of Figure 45 shows that the average magnitude of the apparent stress in the plates at location 1-2 and 9-2 is approximately 14,000 pounds per square inch. The question still remains of whether a uniaxial compressive stress exists transverse to the welded side or a uniaxial tensile stress parallel to the weldment side. Another possibility would be a biaxial type of loading along these axes. This question cannot be resolved without a standard of comparison.

In measurements such as those made concerning the welded plates where the effect of welding was studied, the destructive tests furnished the necessary standard of comparison. Applications using surface and shear waves, where before and after type measurements are not made need an absolute standard. Such a standard would have to be found for each alloy and would carry the requirement of being stress free. Grain orientation, temperature effects, and inconsistencies in the alloy surface composition are a few of the factors which would effect the absolute velocity of every sample tested.

The application of stress analysis with the shear wave technique offers a method of determining the tensile versus compressive direction providing both before and after measurements are possible. This requirement is similar for strain gages, but has the additional merit that stress is measured directly and the element may be removed during processing of the material. The key to the solution of this problem is the ultrasonic longitudinal wave. Since the longitudinal wave is insensitive to stress, it can be used as a reference in the sample.

Consider the transducer assembly shown in Figure 49. Here the X-cut crystal is placed on top of a Y-cut crystal. Each of the crystals are fed from two diode switches in conjunction with the modified time of flight system. The ultrasonic waves will then be generated and received by separate crystals. Note that the longitudinal velocity in aluminum is approximately twice that of the shear wave. Therefore, the shear wave can be phase compared to the second received longitudinal pulse. In making the actual stress measurement the same procedure described earlier is used. The absolute numbers read from the delayed trigger dial of the oscilloscope are recorded. As before the difference between these numbers gives the stress magnitude. The sample under investigation is then subjected to the particular process to be studied, for example, welding.

The ultrasonic measurements are again repeated. Since the absolute numbers were recorded during the first measurement, it can now be determined as to how the shear wave velocity along each axis has changed relative to the longitudinal velocity. As an example, suppose that it is found that both of the velocities along the major stress axes increase due to a biaxial load. The higher velocity for each shear wave component indicates that both axes have been placed in more compression. Furthermore, by knowing the exact amount of the travel time change along each of the axes, the induced stress can be calculated using the stress acoustic coefficients of Table I. It should be pointed out that any strain changes due to the induced stress causes the same change in path length for the longitudinal wave and both components of the shear wave. By comparing each shear wave component to the longitudinal

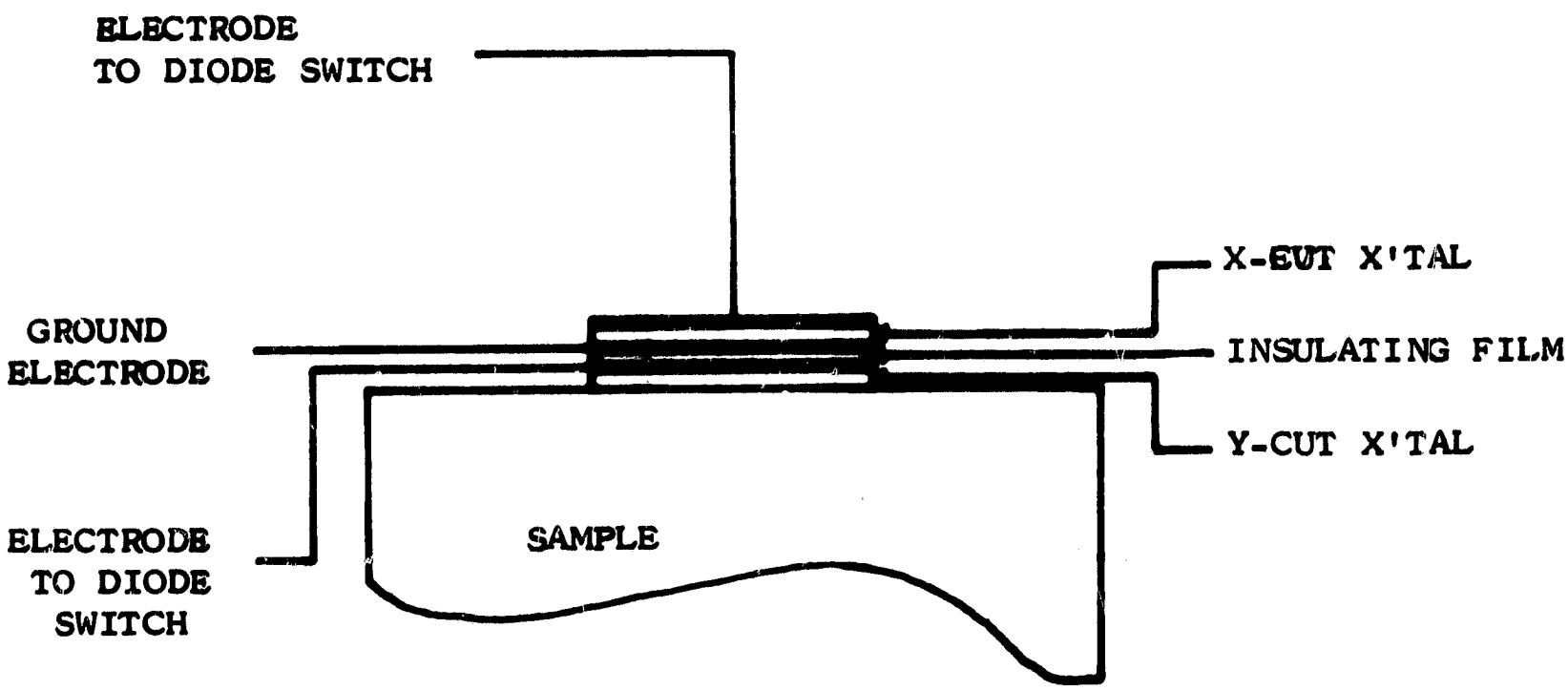

Figure 49. Piggyback Transducer Assembly Configuration.

wave velocity, the measurement is insensitive to strain and solely a function of the stress. Furthermore, this procedure minimizes any variation that might be noted due to temperature changes or changes in the composition of the material.

Another particular problem was noted when applying the shear wave stress analysis technique. In some cases it was very difficult to determine which of the two velocities along the major axes was greater. The basic reason for this problem concerns the fact that the amplitude of the shear wave varies as the lucite-backed transducer assembly is rotated from one major axis to the other. In fact, it can completely disappear if the polarization of the first received pulse is 90^{o} to the polarization of the Y-cut crystal. When the signal appears after rotation of the transducer assembly, it is impossible to immediately determine if the received pulse is advanced of retarded in time, however, a technique was developed to solve this problem.

Consider the fact that the change in velocity of the shear wave is independent of frequency. At the yield stress of aluminum alloys the change in time of propagation can be as much as $\pm$ 263 x 10^{-9} seconds for an inch path length. Knowing that the period of a 7 MHz signal is 143 x 10^{-9} seconds, it is possible that the relative phase change between the sample and reference signals can be as high as $\pm$ 664^{o} at 7 MHz which is almost 2 cycles. If the measurements are made at 1 MHz the propagation time change is still $\pm$ 263 x 10^{-9} seconds, but at this frequency the period is 1000 x 10^{-9} seconds. The relative phase shift between the sample and reference signal is only $\pm$ 94.5^{o}. There is no question at this frequency whether the wave velocity increased or decreased since the time of a period is greater than the possible change in propagation time. Although it might seem wise at this point to use 1 MHz as an operating frequency, this is not the case. The modified time of flight system loses resolution at lower frequencies.

One thing is evident, however, from the above discussion. In order to positively determine the increase or decrease in velocities along a major stress axis, measurements made at two frequencies are necessary. Fortunately, the lucite-backed transducer assembly is able to generate a shear wave over a bandwidth of approximately 1 MHz centered around 7 MHz.

To see how a dual frequency technique can be used in the modified time of flight measurements, consider the following experimental procedure. The transducer assembly is first placed on one of the major axes of stress and the sample signal is brought into phase with the reference signal as usual. The value read from the internal trigger delay dial on the oscilloscope is recorded. Next, the transducer assembly is rotated 90^{o} to the other major axis. The sample signal is again brought into phase with the nearest cycle of the reference signal and the value from the trigger dial is recorded. Once this is accomplished, the sample signal is shifted with respect to the delay by $\pm$ 2 cycles by means of the internal trigger control. Therefore, five readings from the trigger dial are recorded. Each of these five readings are subtracted from the first dial readings obtained on the other major axis. The transducer assembly is again rotated 90^{o} back to the original axis. At this time the frequency of the pulsed oscillator is changed to a new arbitrary value approximately 0.5 MHz either side of the initial frequency. The same procedure is again followed. It is noted that for each frequency there are five numerical differences obtained, however,there are only two of these differences out of the ten which are identical. This difference is the correct indication for the change in travel time.

As a numerical example, suppose that the change in travel time between two major axes is actually 150×10^{-9} seconds and that the two frequencies used in the measurement are arbitrarily chosen as 7 and 6.5 MHz. Furthermore, assume that the velocity along the second axis is greater than along the first. This simply means that if it was possible to observe the signal from the transducer assembly on the oscilloscope during the first 90^{o} rotation, the signal would advance from left to right. Let the first axis reading at 7 MHz on the vernier dial of the internal trigger read 400. This number is arbitrary since it depends largely on the setting of the delay trigger. In order to bring the sample and reference signals into phase with the nearest cycle the vernier dial would have to be set to 393. Other readings for the $\pm$ 2 cycles would then be 250, 107, 536 and 679 yielding differences of +7, +150, +293, -136, and =279 respectively. After the transducer assembly is rotated back to the original position, the frequency of the

pulsed oscillator is lowered to 6.5 MHz. Assume that at this frequency the initial reading on the vernier dial is 450. To bring the sample and reference signals in phase with the nearest cycle at this frequency when the 90° rotation is performed requires the vernier dial to read 454. The other readings then obtained for the ± 2 cycles are 300, 146, 608, and 762 yielding the respective difference of +150, +304, -158 and -312. It is seen that out of the ten differences there are two that are identical. Therefore, since the sign of difference is positive, the second major axis is in compression relative to the first. The magnitude of the stress is now calculated from the coefficients given in Table I.

X. FATIGUE DETECTION AT MICROWAVE FREQUENCIES

A. Fatigue Damage as a Surface Phenomenon

It is a well known fact that materials subjected to a cyclically varying stress may fail even though the calculated unit stress is always less than the static proportional limit. Such fatigue failure is gradual and progressive and is not accompanied by yielding. The endurance limit of a material, sometimes called the fatigue limit, is defined as the stress which may be applied and released, or reversed, an indefinite number of times without causing the material to fail. The endurance limit so defined is arrived at, for a particular material cycling a number of samples, at different maximum stress levels, to failure. The maximum stress, S, is plotted against the number of cycles to failure, N. The resulting S-N curve becomes more-or-less assymptotic to the value of stress called the endurance limit. Such a value arrived at statistically is not only dependent upon the nature of the material, i.e., the alloy, etc., but is strongly influenced by the condition of the surface of the material. For instance, the roughness of the surface may cause a variation of as much as 18 per cent in the endurance limit between a sample, rough machined and one highly polished. It has been shown also that an exceedingly small amount of corrosion present with cyclic stress will cause a considerable reduction in the endurance limit.

An examination of the literature concerning the statistical evaluation of fatigue failure in metals emphasizes the importance of the surface of the material to its failure in fatigue. Fatigue failure begins at the surface of a metal and it is, therefore, the surface of the metal which must be examined for early evidences of fatigue damage.

Fatigue damage is though of as being a progressive phenomenon beginning with the microscopic scratches and deformations that are present in even the most highly polished surfaces. These minute scratches may gradually deepen and propagate under cyclic stress due to stress concentration induced around them and assisted by any corrosion which may be present.

B. Electromagnetic Measurement of Surface Properties

The fact that the electrical surface resistivity of a metal increases with increasing surface roughness is illustrated in Figure 50. The formation of micro-cracks due to fatigue damage at the surface of a metal may be thought of as a localized increase in surface roughness and hence, should be measureable as an increase in surface resistivity. An experiment to measure the increase in surface resistivity must be designed in such a manner that surface resistance is measured without also measuring the bulk properties of the material. By taking advantage of the skin effect of high frequency propagation, the depth to which the surface is measured may be controlled by selecting the frequency at which measurements will be made.

Preliminary experiments to relate corrosion and fatigue damage to an increase in surface resistivity were made using a sample in the form of a half wave linear resonator operated at frequencies near 1 GHz. This choice of frequency represents a compromise among depth of surface measurement, economy and availability of equipment, and geometrical compatibility of the sample with the ultrasonic techniques in use in this laboratory.

The sample consists of a rod 7 inches long and usually 1/4 inch in diameter. The sample was supported at voltage nodes with low loss teflon insulators within and coaxial with

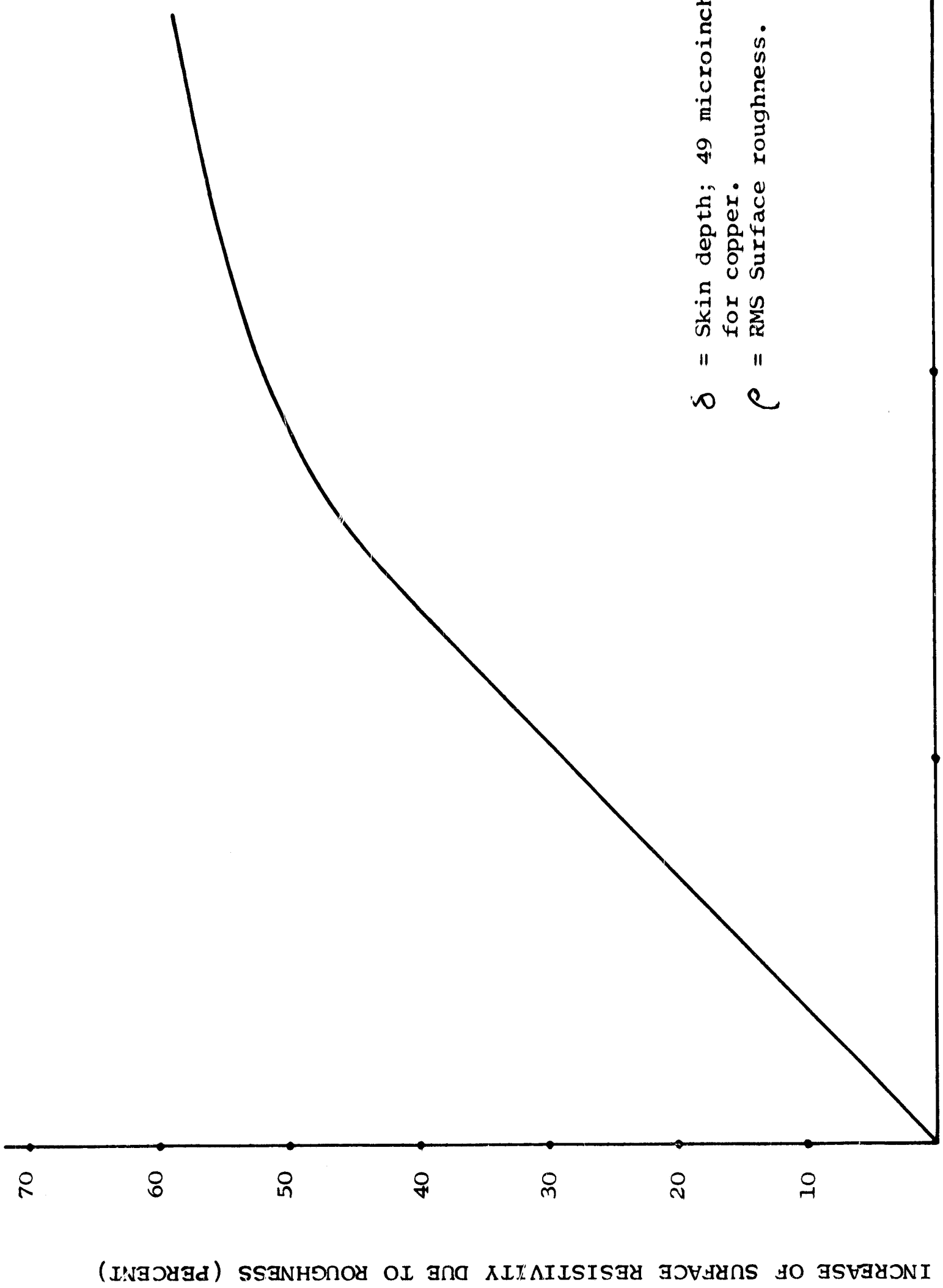

Figure 50. Surface Roughness versus R
s Resistance at 3GHz.

an outer cylinder of polished, silver plated copper to form a low loss coaxial resonator. Increased surface resistivity of the sample results in an increase in bandwidth of the resonator when considered as a bandpass filter. Instrumentation for these measurements is shown in Figure 51.

A number of samples were prepared from a variety of aluminum alloys and were highly polished. Some of these samples were subjected to torsional fatigue while others were exposed to a 3 per cent salt water bath for ten minutes out of every hour.

The change in electrical surface loss was monitored hourly for the torsional fatigue experiment and every ten hours for the corrosion experiment. The composite results of these experiments are presented as Figures 52 and 53.

In the case of the corrosion experiment, the damage was more or less uniform over the surface of the sample and the technique for measuring electrical surface resistivity over relatively large percentages of the sample surface was quite effective. The fatigue damage, however, tended to be quite localized which resulted in the measured relation between fatigue damage and surface resistivity being much less apparent.

Since early fatigue damage is, in general, quite localized, it is apparent that nondestructive testing techniques must be a compromise between speed of search and sensitivity. A system of sufficient sensitivity to detect fatigue damage in its early stages must necessarily examine a very thin section of a very small area of surface. The experiments conducted at 1 GHz using the linear resonator examined a large percentage of the sample surface to a depth of approximately 1×10^{-4} inch. Raising the frequency of measurement by a factor of ten will result in measuring the surface resistivity to a depth of approximately 3.5×10^{-5} inches.

White awaiting delivery of suitable equipment for use at the higher frequency, experiments were conducted to develop coupling and instrumentation techniques for examining smaller areas of surface. A microwave stripline bridge was designed

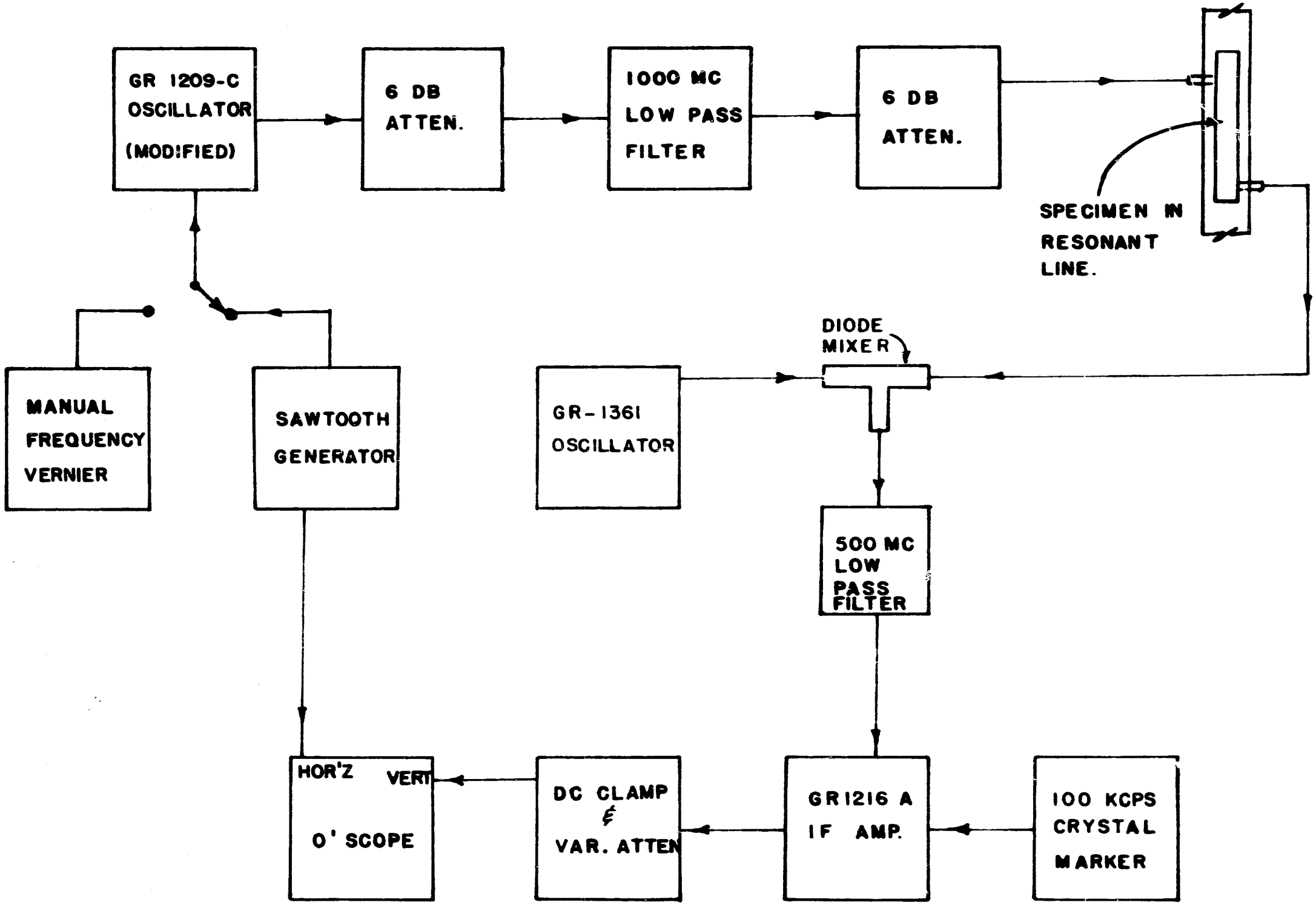

Figure 51. Block Diagram of Linear Resonator System for Surface Resistivity Measurements at 800 MHz.

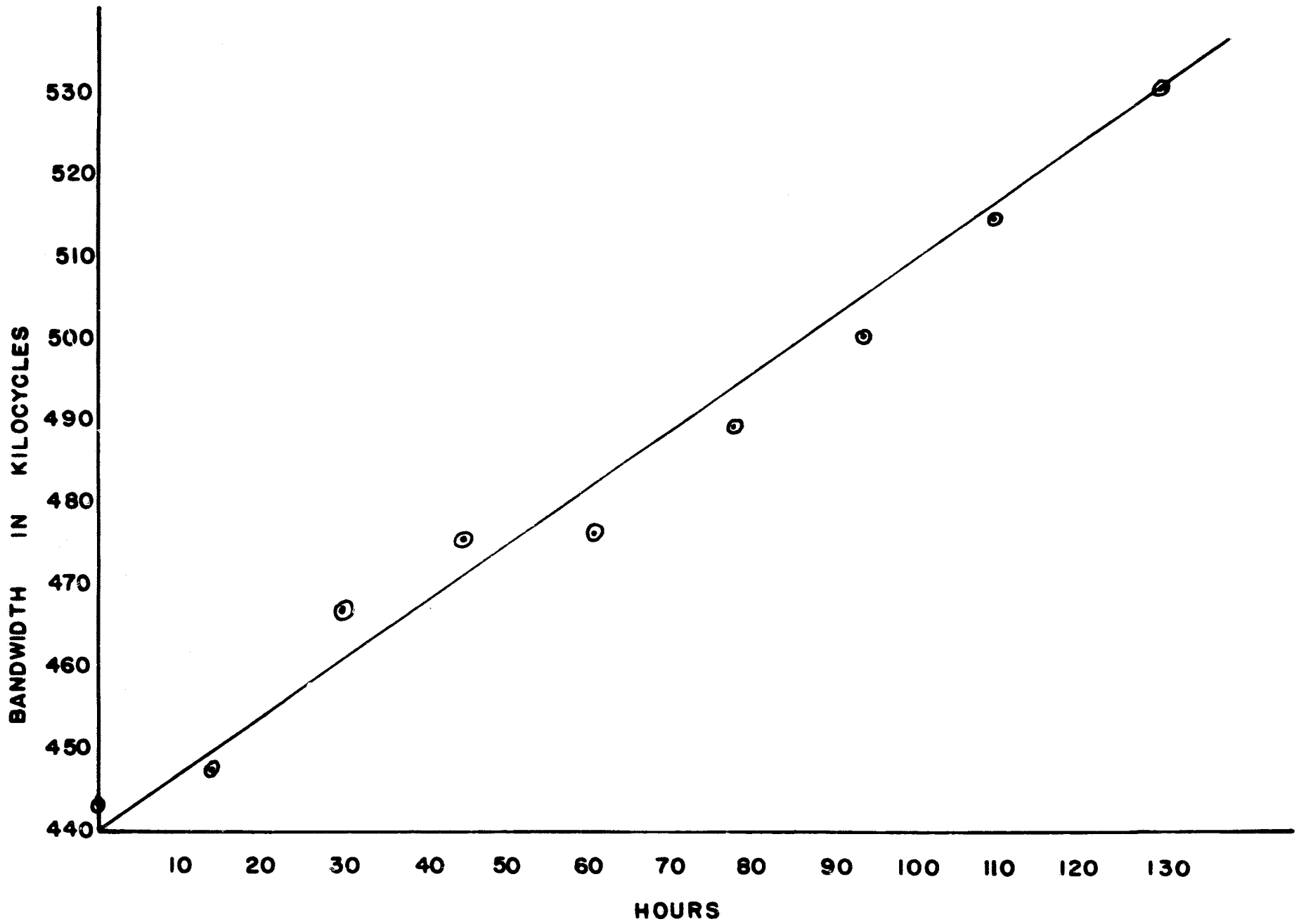

Figure 52. Electrical Bandwidth of a Linear Resonator Incorporating An Aluminum Sample Versus Time Subjected to a Corrosive Bath.

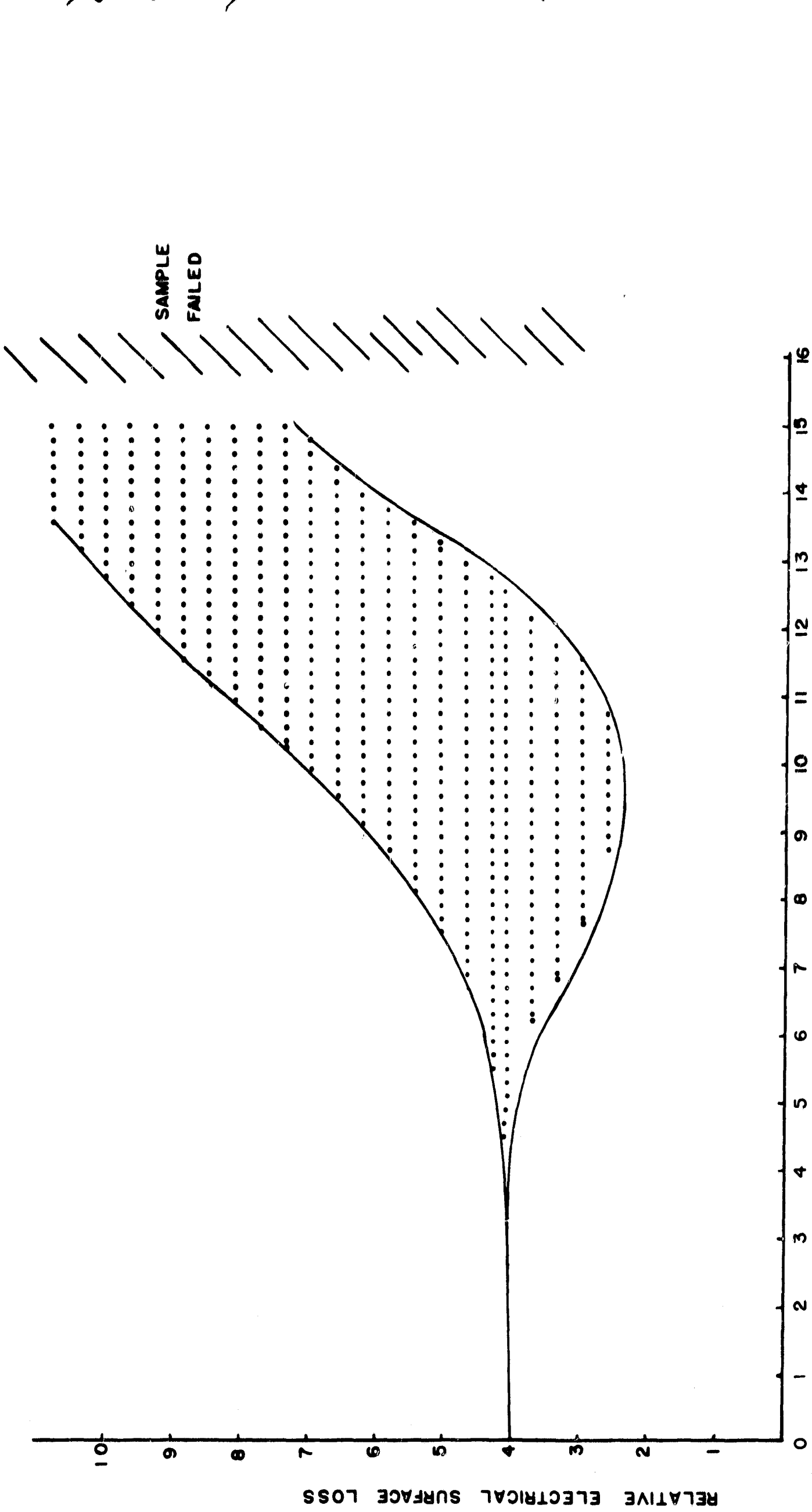

Figure 53. Relative Electrical Surface Loss Versus Hours Subjected to Torsional Fatigue.

and built for use at 1 GHz. Measurements with this equipment showed that differences in materials were easily detected and gross changes in surface finish were detectable. Although it remained insufficiently sensitive for the detection of early fatigue damage, the technique appears to be promising for future work at higher frequencies.

If a transmission line of characteristic impedance, Z_o, is terminated in a load, Z_1, where Z_1 is not equal to Z_o, a portion of the incident wave is reflected. The voltage reflection factor given by

$$\rho = \frac{z_1 - z_o}{z_1 + z_o}$$

is a complex quantity whose magnitude is equal to the ratio of the amplitudes of the reflected and incident voltages at the load and whose argument is the advance in phase of the voltage accompanying the reflection. In addition, if the load is anisotropic, the reflected wave may contain eigenmodes not present in the incident wave. If the terminating load of the waveguide consists of a sample containing micro-cracks, the real component of Z_1, i.e., its resistance, should increase resulting in a change in the reflection factor. If the micro-cracks are caused by fatigue, they may be oriented in such a manner as to contribute sufficient anisotropy to cause the generation of different eigenmodes which should be detectable in a properly designed waveguide system.

The approach taken in this laboratory was to measure the change in termination impedance by measuring the reflection factor. This was done by setting up a suitable waveguide bridge to compare the sample with a reference termination. The sample was coupled to the waveguide through appropriate choke flanges in order that no current need flow across the waveguide-sample junction. In practice, the reference termination of the form R+ jX was made by connecting a variable shorting stub in series with a matched termination. This adjustable termination was changed so that the reflections from the sample and the termination alternately added and subtracted. Using the measured change in output of the bridge

as a measure of reflection factor appears to be considerably more sensitive to change in sample surface resistivity than using a fixed termination for the bridge reference. An even greater sensitivity to small changes in the surface resistivity of a sample may be had by incorporating it as a part of a low loss cavity resonator. The Q of such a cavity resonator is defined as

$$Q = 2\pi \frac{\text{energy stored}}{\text{energy lost per cycle}}$$

and may be made quite high; typically 20,000. If the geometry of the cavity is selected to have a high Q and if the construction of the cavity is such that the losses, though small, occur mainly in the sample, then small changes in the surface resistivity of the sample should cause detectable changes in the Q.

The cavity resonator must be designed to have a high Q and must provide for the introduction of the sample as a current carrying portion of the resonator. Since the energy is stored in the volume of the cavity and lost largely in its bounding surfaces, the ratio of the volume to the surface area must be kept high. These factors suggest a cylindrical cavity with the sample forming one end. The choice of the mode at which to operate the cavity is important. It should provide a well defined current flow pattern in the sample with no current flow between the sample and the cavity since the sample must be repeatedly and repeatably removed and replaced during the course of the experiment. A cylindrical cavity operated in the JE_{011} mode provides a high operating Q, reasonable size at the chosen operating frequency and the required current distribution on the surface of the cavity and on the sample.

The free space resonant wave length of a right cylindrical cavity is given as

$$\lambda_o = \frac{2}{\sqrt{\left(\frac{2\chi_{1m}}{\pi D}\right)^2 + \left(\frac{n}{L}\right)^2}}$$

where L = axial length
D = diameter
$X_{\ell m}$ = m^{th} root of $J'_\ell(x)$ = o for TE modes
$X_{\ell m}$ = m^{th} root of $J_\ell(x)$ = o for TM modes

Since $J_o(x) = -J'_1(x)$ for we have $X_{11} = X_{o\ell}$ and the TE_{o1n} modes have the same resonant wave length as the TM_{11n} modes. This degeneracy may be resolved by introducing a variety of small perturbations which have a greater effect on one mode than on the other. A small axially mounted rod 0.125" in diameter and 0.312" long was used for this purpose. The purity of the TE_{011} mode was demonstrated by observing a negligible change in Q when the sample was tilted slightly with respect to the cavity. For maximum Q, a cavity operating in the TE_{011} mode should have a diameter to length ratio of 1.6 to one. The cavity, illustrated in Figure 54, has a diameter of 1.955 inches and a length of 1.21 inches and is resonant at 8.8 GHz. Its inner surfaces were highly polished and silver plated.

A microwave system was set up as shown in Figure 55 for the determination of surface resistance changes by observing the changes in the bandwidth of the cavity resonator as the sample, which formed one of its ends, was subjected to fatigue damage induced by bending stress. Samples were prepared from 1/4 inch thick aluminum strip 4 inches wide and of 2024-T3511 Alloy and temper. The samples were approximately 10 inches long and one side of each was carefully flattened and polished with successively finer grits of abrasive paper through number 600. The samples were subjected to a bending stress by being placed against rigid supports 8 inches apart and having the center of the sample deflected cyclically by 1/4 inch. The samples were carefully cleaned with a solvent, and dried prior to each microwave measurement. Although these measurements generally indicated an increasing bandwidth and, therefore, an increasing surface loss with increasing fatigue damage, experimental uncertainities were too large to permit definitive results.

Experimental variables were reduced and repeatability was greatly increased by use of the technique illustrated in Figure 56. The experimental set up is similar to that used for the bandwidth measurements with the exception that the transmission loss of the cavity is measured. This is done by

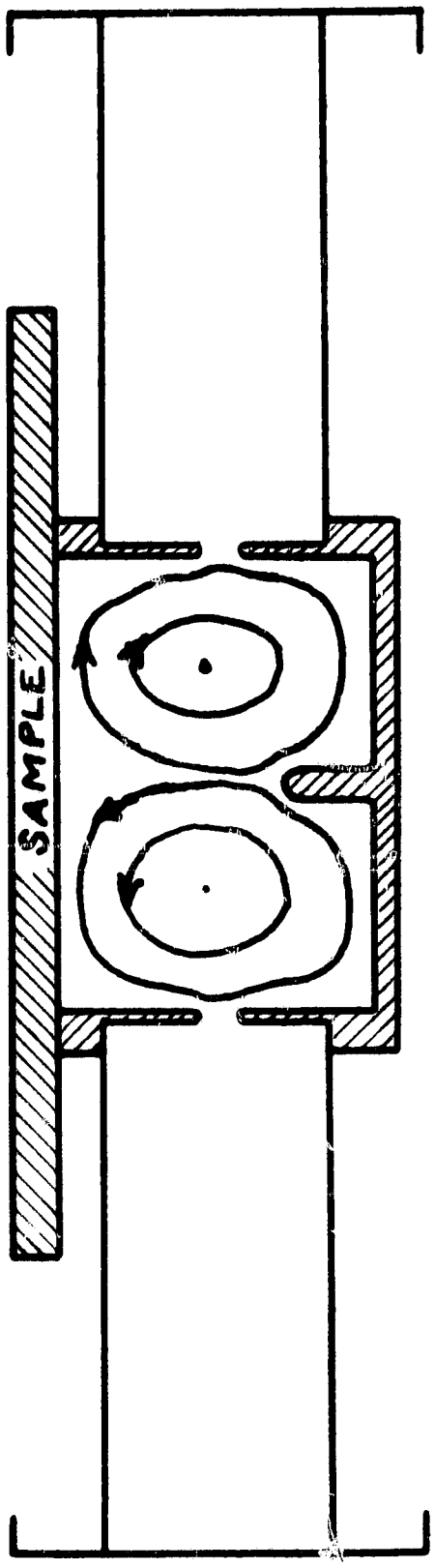

Figure 54. Cavity Resonator for use at 9 KMHz. The Pin for Splitting the Degeneracy of the TE_{011} and TM_{111} Modes is Shown and the Approximate TE_{011} Magnetic Lines are Sketched.

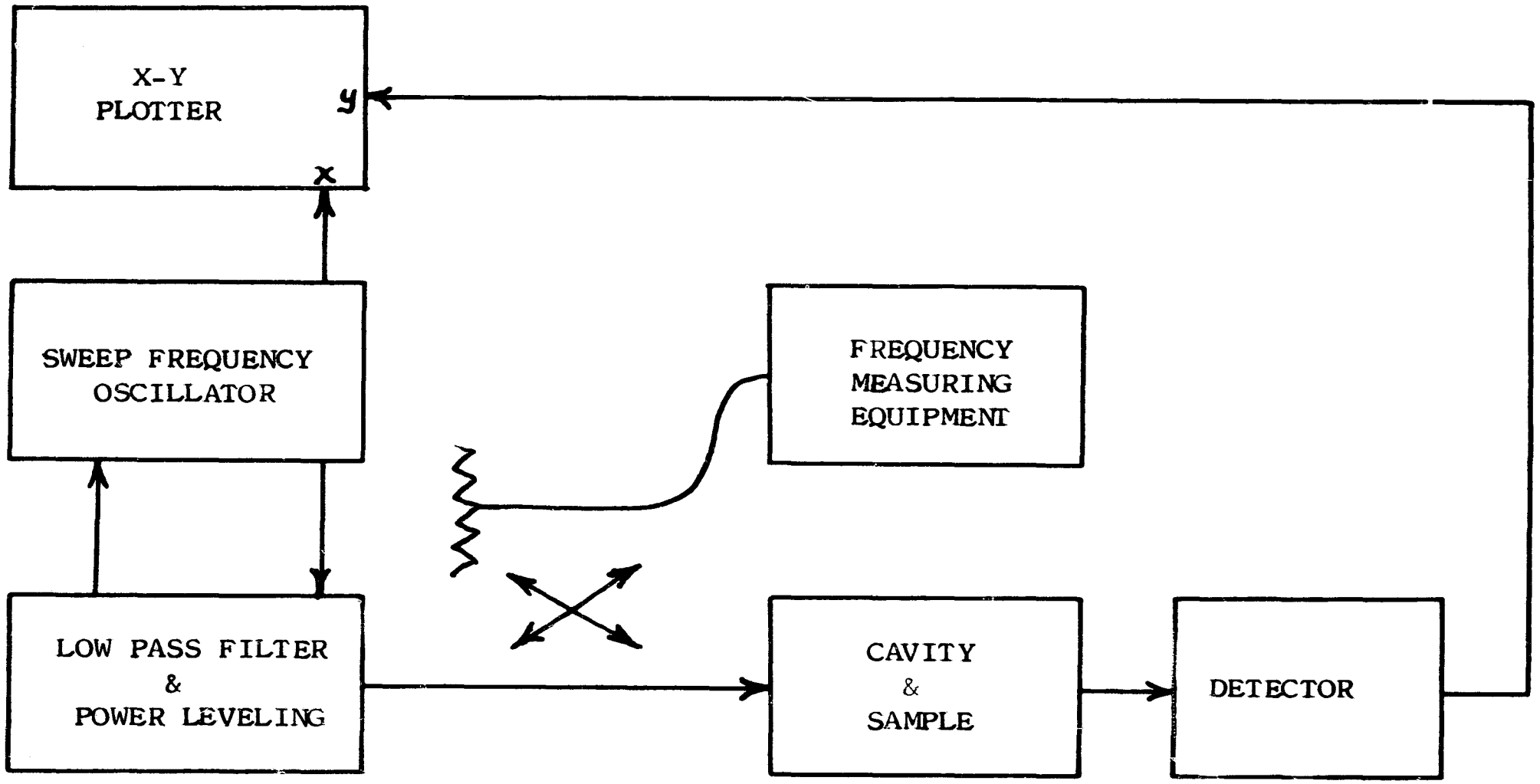

Figure 55. Microwave Equipment for Measurement of Resonator Losses by Bandwidth Determination.

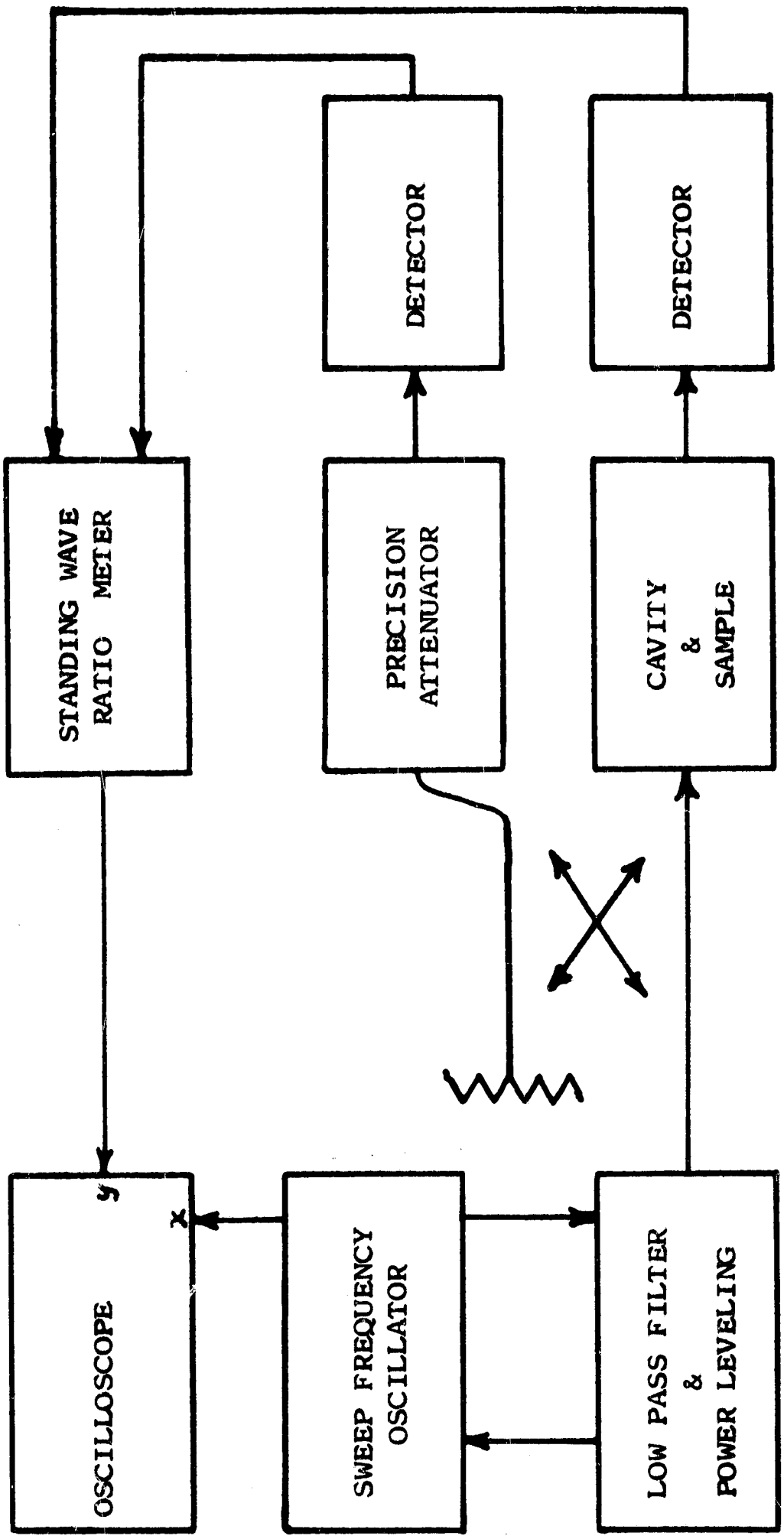

Figure 56. Microwave Equipment for Measurement of Resonator Losses by Measuring Transmission Loss.

adjusting the precision variable attenuator to make the magnitude of the signal at detector A equal to that at detector B. For the magnitude of the signal transmitted through the cavity to be meaningful in this comparison, the system must always be operated at the exact resonant frequency of the cavity. A narrow band, swept frequency technique was employed to avoid the possibility of making invalid amplitude comparisons at frequencies other than of resonance. Relative amplitude measurements were made as the frequency swept through the resonant frequency of the cavity. In this manner, minor drifts in signal generator frequency and amplitude could not affect the accuracy of the measurement. At no time during the experiment was it necessary to make significant equipment adjustments. The measurements were consistently repeatable.

Measurements of cavity transmission loss were made using three locations on the sample as an end plate for the cavity resonator. One of these test locations was at the center of the sample where the bending stress was a maximum and the other two locations were in areas of minimum stress near the ends of the sample. The samples were marked in such a way that these test locations could be accurately relocated. The transmission loss for the center location was divided by the average transmission loss of the two end locations and the results for a typical sample plotted against cycles of bending stress in Figure 57.

It should be noted that there is little change in the relative loss until the curve breaks rather sharply upward at approximately 80 per cent of the fatigue life of the sample. Before each measurement the sample was cleaned as described before and carefully examined under thirty power magnification and oblique lighting for visual evidences of fatigue was visually detected. This visual evidence usually occurred after a change of approximately 5 per cent in relative transmission loss. Changes in relative transmission loss of 1 per cent are detectable.

XI. RECOMMENDATIONS FOR FATIGUE MEASUREMENTS

The final techniques which have been described concerning

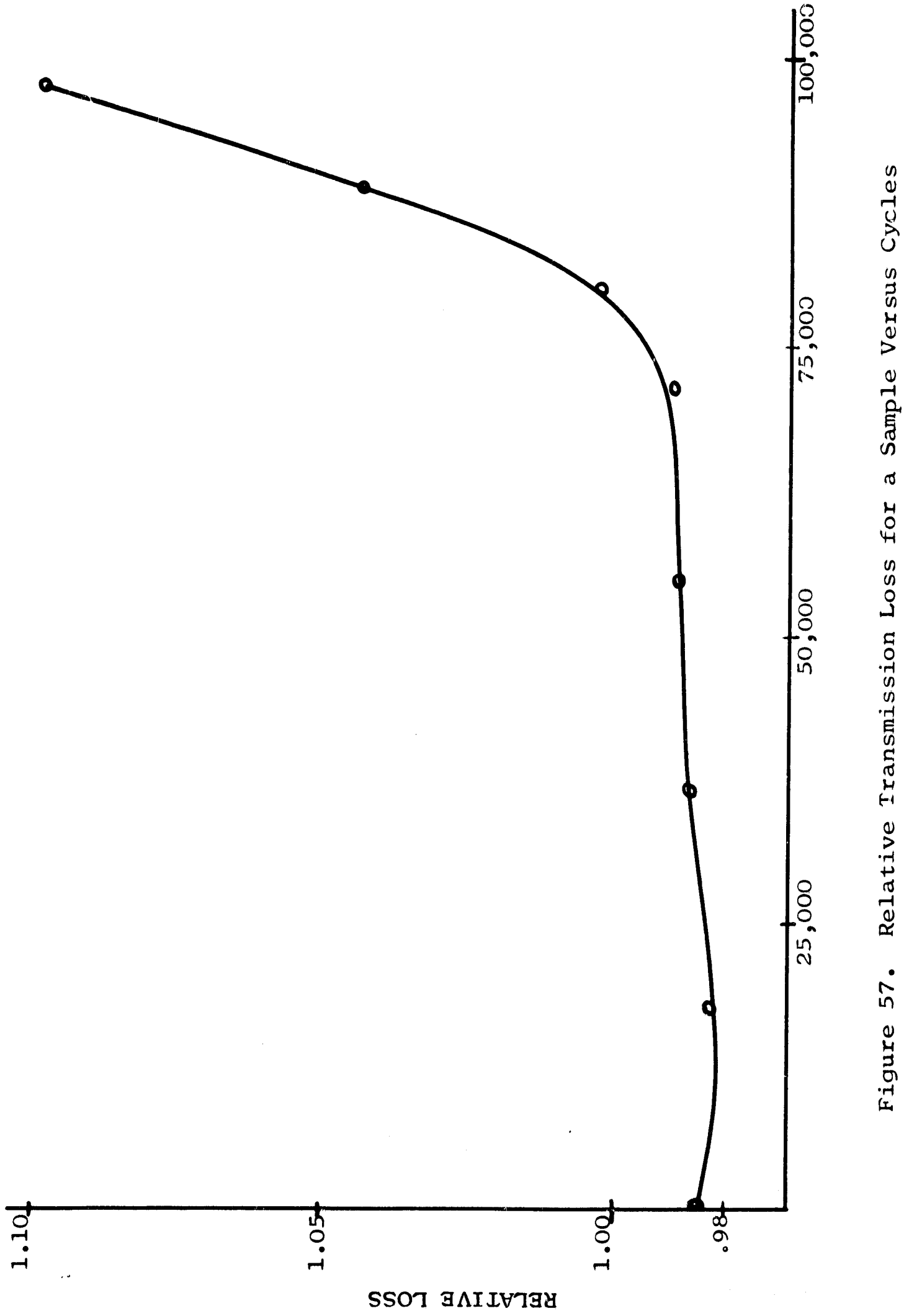

Figure 57. Relative Transmission Loss for a Sample Versus Cycles of Bending Stress.

the measurement of the state of fatigue of a metallic surface are extremely encouraging and should result in the development of field techniques. The measurements reported have been made under idealized laboratory conditions, however, a variation of the techniques should allow for measurements being made under more adverse conditions. A relatively large area of the sample was incorporated with the cavity used for the measurement. The area which first showed visible signs of fatigue damage was an extrememly small fraction of the surface area being examined. Some compromise must be made between the speed of measurement and sensitivity of detection. A smaller area cavity would increase the sensitivity of detection but would require more time for the study of a given surface. With the present cavity size, it has been demonstrated that fatigue damage can be detected at approximately 80 per cent of the life of the structure. Below this value the measurements are independent of the life and the structure. For this reason, it should be possible to compare a measurement of the surface resistivity at one location versus the resistivity at another location on the same portion of the structure. Although the number of cycles for all parts of the structure should be the same. The stress distribution is most likely to be different so that failure will occur at one location before another. It is therefore suggested that a technique which would compare the surface resistivity at two locations on the same surface would result in a satisfactorily method of detecting the onset of fatigue failure by the measurement of the surface resistivity. It should again be emphasized that the measurements under laboratory conditions indicated the onset of a minute crack in the surface before any visible signs of cracking occurred even when the surface was observed under magnification.

XII. SUMMARY

Ultrasonic methods of stress analysis have been developed for the determination of stresses through the thickness of a metallic structure and the stress near the surface of a structure. Two methods of measurement have been used including a "modified time of flight method" and a "frequency null method." The modified time of flight method uses commercially available instrumentation assembled in a manner for which the propagation time for an ultrasonic wave is compared to a referenced delay

time. The relative propagation time for two components of a wave may be measured to an accuracy of one nanosecond corresponding to a sensitivity of less than 1000 pounds per square inch.

The frequency null technique required the use of a continuous oscillator so that the frequency of the ultrasonic wave could be determined accurately. For this purpose a special instrument was constructed utilizing a gated amplifier. The continuous wave oscillator is gated to produce short duration pulses suitable for separating the multiple reflections that occur. The methods of measurement involves the determination of the frequency at which a fixed path length is an integer number of ultrasonic wave lengths. If path length is known, then the frequency corresponding to a known number of wave lengths allows for the determination of the velocity of propagation. Since stress is related to velocity of propagation, the stress may be determined using this method.

Quarts crystals are used for the generation of the ultrasonic waves. A Y-cut crystal vibrates predominately in shear and is used for the determination of the bulk stress in a material. The relative velocities along the two major axes of stress are measured. For each alloy of a material, the relationship between the velocities is established and correlated with stress. It is found that stress is linearly related to the relative change in velocity along the principal axes of stress producing a stress-acoustic constant. The stress-acoustic constant is used to convert the relative velocity measured to stress. The major axes of stress may be determined by an observation of the decay pattern of the multiple reflections for the ultrasonic shear wave.

Surface stresses are determined in a similar manner, however, it is necessary to define a fixed path length in order to accomplish a measurement. Two types of transducers have been used for this purpose. The first consists of two wedge shaped structures which contact the surface along a "knife edge." The ultrasonic signal is generated at one knife edge and detected at the second knife edge which is parallel to the first. The relative velocity of propagation versus orientation

on a flat plate allows for a determination of the stress near the surface of the material. Similarly, lucite wedges are used with a fixed separation using the angle of refraction to produce and detect surface waves. Both types of transducers are coupled to the surface by the use of a static force. No couplant is used since it would affect the path length.

A study of the stress distribution in plates containing a weldment was used to illustrate the practical application of the methods. The magnitude of the stresses as determined ultrasonically was correlated against destructive measurements. Agreement was obtained when the stress was averaged over the length of sample included in the destructive tests. The ultrasonic measurements indicated that the maximum stresses occurred near the weld and furthermore the stresses were greatest near the start and stop of the weldment.

It was further determined that grain orientation imposes limitations on the ultrasonic methods of stress analysis. The ultrasonic waves are sensitive to grain orientation producing effects corresponding to as much as 15,000 pounds per square inch of equivalent stress. For this reason it is necessary to make measurements both before and after processing in a similar manner to that used with strain gages. For this method, it is possible to remove the transducer while the material is being processed.

Although the methods have been developed to a useful state for application to practical problems of stress analysis, further study is warranted to improve the spatial resolution of the measurements as well as to further define the effects of grain orientation. The ultrasonic methods of stress analysis can be a valuable addition to the methods of analysis already available.